GSK3β-mediated DNA damage repair in pancreatic cancer

Dissertation

for the award of the degree
”Doctor rerum naturalium”

of the Georg-August Universität Göttingen
within the doctoral program
Molecular Medicine
of the Georg-August University School of Science (GAUSS)

Faculty of Medicine

submitted by
Geske Elisabeth Schmidt

from Heide, Germany

Göttingen, 2020

Thesis Committee

Prof. Dr. Volker Ellenrieder, Department of Gastroenterology, Gastrointestinal Oncology and Endocrinology, University Medical Center Göttingen

Prof. Dr. Argyris Papantonis, Institute of Pathology, University Medical Center Göttingen

Prof. Dr. Bernd Wollnik, Institute of Human Genetics, University Medical Center Göttingen

Members of the Examination Board

1st Referee: Prof. Dr. Volker Ellenrieder, Department of Gastroenterology, Gastrointestinal Oncology and Endocrinology, University Medical Center Göttingen

2nd Referee: Prof. Dr. Argyris Papantonis, Institute of Pathology, University Medical Center Göttingen

Further members of the Examination Board

Prof. Dr. Bernd Wollnik, Institute of Human Genetics, University Medical Center Göttingen

Prof. Dr. Steven A. Johnsen, Division of Gastroenterology and Hepatology, Mayo Clinic, Rochester, MN, USA

Dr. Nico Posnien, Department of Developmental Biology, University of Göttingen

Prof. Dr. Michael Zeisberg, Department of Nephrology and Rheumatology, University Medical Center Göttingen

Date of submission: 30.09.2020

Date of oral examination: 25.11.2020

Content

Abbreviations

53BP1	p53-Binding Protein 1
5-FU	5-fluorouracil
ADEX	Aberrantly differentiated endocrine exocrine
AKT	Protein kinase B
AP-1	Activating Protein-1
AR-A	AR-A 014418
ATF-2	Activating Transcription Factor 2
ATM	Ataxia Telangiectasia Mutated
ATR	Ataxia Telangiectasia And Rad3-Related Protein
BER	Base excision repair
BET	Bromodomain and extra-terminal domain
BRCA1	Breast cancer 1
BRCA2	Breast cancer 2
BSA	Bovine serum albumin
CDKN2A	Cyclin dependent kinase inhibitor 2A
CDX	PDX derived cell line
ChIP	Chromatin Immunoprecipitation
ChIP seq	ChIP sequencing
CK1	Casein kinase 1
CsA	Cyclosporin A
CtBP	C-terminal binding protein
CtIP	CtBP interacting protein
DAPI	4,6-Diamidin-2-phenylindol
DDIAS	DNA Damage Induced Apoptosis Suppressor
DDR	DNA damage response
DDT	Dichlorodiphenyltrichloroethane
D-loop	Displacement loop
DMEM	Dulbecco's Modified Eagle Medium
DNA	Deoxyribonucleic acid
DNA-PKcs	DNA- dependent protein kinase catalytic subunit
DNMT	DNA methyltransferases
DSB	Double strand break
DTT	Dithiothreitol
DYRK	Dual-specificity tyrosine-phosphorylation-regulated kinase
E. coli	Escherichia coli
EDTA	Ethylenediaminetetraacetic acid
EGTA	Ethylene glycol bis(β-aminoethylether) tetraacetic acid
EtOH	Ethanol
FBS	Fetal Bovin Serum
g	Gravity
GS	Glycogen Synthase
GSK3α	Glycogen Synthase Kinase 3α

GSK3β	Glycogen Synthase Kinase 3β
GSK3βi	GSK3β inhibition
HAT	Histone Acetyl Transferases
HCl	Hydrochloride
HDAC	Histone Deacetylases
HEPES	N-(2-Hydroxyethyl)piperazine-N′-(2-ethanesulfonic acid)
HMT	Histone methyltransferases
HR	Homologous recombination
IF	Immunofluorescence
IHC	Immunohistochemistry
IP	Immunoprecipitation
KCl	Potassium chloride
KDM1A	Lysine (K)-Specific Demethylase 1A
KDM5B	Lysine (K)-Specific Demethylase 5B
MAPK	Mitogen-activated protein kinase
MEM	Minimum Essential Medium
min	Minutes
mTOR	Mammalian target of rapamycin complex 1
MTT	3-(4,5-dimethylthiazol-2-yl)-2,5-diphenyltetrazolium bromide
NaCl	Sodium chloride
NaF	Sodium fluoride
NEAA	Non-Essential Amino Acid
NFAT	Nuclear factor of activated T-cells
NF-κB	Nuclear Factor κ-light-chain-enhancer of activated B cells
NGS	Normal goat serum
NHEJ	Non-homologous end joining
PALB2	Partner and localizer of BRCA2
PanIN	Pancreatic intraepithelial neoplasms
PARP	Poly (ADP-ribose) polymerase 1
PB	Phosphate buffer
PBS	Phosphate buffered saline
PCR	Polymerase chain reaction
PDAC	Pancreatic ductal adenocarcinoma
PDX	Patient derived xenografts
Pen	Penicillin
PFA	Paraformaldehyde
PI3K	Phosphatidylinositol 3-kinase
PKC	Protein kinase C
Pol	Polymerase
QM	Quasimesenchymal
QRT-PCR	Quantitative realtime-PCR
RNA	Ribonucleic acid
RNA seq	RNA sequencing
RPA	Replication protein A
rpm	Revolutions per minute
RT	Room temperature
SDS	Sodium dodecyl sulfate

SDS-PAGE	Sodium dodecyl sulfate polyacrylamide gel electrophoresis
Seq	Sequencing
sgRNA	Single guide RNA
ssDNA	single-strand DNA
STAT	Signal Transducer and Activator of Transcription
TCGA	The Caner Genome Atlas
TEMED	Tetramethylgethylenediamine
TOPBP1	DNA TOPoisomerase 2-Binding Protein 1
WCL	Whole cell lysate
XLF	XRCC4-like factor
XRCC4	X-ray repair cross-complementing protein 4
γH2AX	phosphorylation of histone 2AX

List of Figures

List of Tables

Dedicated

to my Parents

Abstract

With a 5-year survival rate of less than 8% pancreatic cancer is one of the most aggressive and lethal malignancies**.** The dismal survival rates in pancreatic cancer patients are mainly due to aggressive tumor growth, high metastatic and relapse rates as well as resistance to conventional drug therapies. Despite research effort in optimizing the therapy, the prognosis remains poor. Accordingly, there is a desperate need to develop better treatment strategies to optimize therapy of pancreatic cancer patients. Pancreatic cancer exhibits a high degree of tumor heterogeneity. Thus, research focuses on the identification of various molecular subtypes in PDAC patients based on differential gene expression profiles. However, the identified molecular subtypes remain to be translated into new therapeutic strategies. The most promising approach is based on vulnerabilities caused by variant mutations of DNA damage repair pathways.

In this study we aimed to determine a deeper mechanistic understanding of GSK3β and its influence on pancreatic cancer behavior. Specifically, we examined the effect of GSK3β on transcriptional regulation and function of pancreatic cancer cells.

Our study uncovers a previously uncharacterized role of GSK3β in regulating the transcription of DNA damage-related genes. Based on our results, we suggest that pharmacological targeting of GSK3β may represent a novel and effective strategy in the treatment of pancreatic cancer, especially in patients with induced DNA damage by variant agents. We show, that irrespective of germline or somatic mutations in BRCA genes, there is also the possibility to induce a BRCAness subtype at the transcriptional level through inactivation of GSK3β. The inhibition of GSK3β in pancreatic cancer cells can therefore cause an “inducible” BRCAness-like phenotype.

As a direct consequence a higher sensitivity towards various DNA damage-related agents, e.g. the PARP inhibitor Olaparib, cisplatin and irinotecan, is achieved. Furthermore, we unraveled the mechanistic link between GSK3β inhibition and “BRCAness” induction and identified NFATc1 as a key transcriptional driver of this central pathway in DNA damage regulation. This is in line with our observation, that NFTAc1 loss recapitulates the same phenotype as GSK3β inhibition.

1. Introduction

1.1. Pancreatic Cancer

With a 5-year survival rate of less than 8% pancreatic cancer is one of the most aggressive and lethal malignancies. It is projected to be the second leading cause of cancer-related deaths in the upcoming years.[1] The dismal survival rates in pancreatic cancer patients are mainly due to its aggressive tumor growth with early metastasis, the high relapse rate and the remarkable resistance to conventional drug therapies. The majority of pancreatic cancer cases are diagnosed at late tumor stages, often due to the late onset of clinical symptoms. Thus, only few patients are eligible for resection, which is the only curative treatment option so far.[2,3] Accordingly, there is a desperate need to develop better and more effective therapeutic strategies in the treatment of pancreatic cancer patients. At the histological level, around 90% of all cases are classified as Pancreatic Ductal Adeno Carcinoma (PDAC), originating from the exocrine part of the pancreas. PDAC development is preceded by well-defined pre-malignant lesion, called Pancreatic Intraepithelial Neoplasms (PanIN), and is most frequently associated with mutational activation of the *KRAS* oncogene (Kirsten RAt Sarcoma virus). [4–7] In fact, mutations of *KRAS* are found in early PanIN lesions and in approximately 90-95% of all patients with pancreatic cancer.[8,9] Mutations of Tumor Protein P53 (*TP53*) and Deleted in Pancreatic Cancer-4 (*SMAD4*) are also signature mutations of pancreatic cancer and are found in about 50-60% of all pancreatic cancer patients.[7,10] Importantly, about 10-15% of all pancreatic cancer patients show a familiar background with mutations related to DNA damage repair pathways, such as BReast CAncer 1 and 2 (*BRCA1*/*BRCA2)*, Partner And Localizer of BRCA2 (*PALB2)* or Ataxia Telangiectasia Mutated *(ATM)*.[11–13] Other risk factors of pancreatic cancer development include smoking, obesity, and the presence of chronic pancreatitis.[14] Recently, numerous genome wide genetic and transcriptional analysis not only reaffirmed the signature mutations *KRAS*, *TP53* and *SMAD4*

but also demonstrated a high degree of molecular heterogeneity in pancreatic cancer. Importantly, these recent studies also showed that pancreatic cancer can be classified into distinct subtypes based on their molecular profiles. These current findings open up a new and very attractive field in pancreatic cancer research, which aims at a better understanding of the subtypes in tumor biology and should reveal new therapeutic strategies.[15–17]

1.1.1. PDAC Subtypes

Recent transcriptional profiling uncovered the presence of distinct molecular subtypes in pancreatic cancer patients.[18] The foundation of this exciting new field was laid in 2011 by Collisson et al.[19], who defined three different subtypes based on gene expression analysis in microdissected PDAC tissue. Based on the identified gene signatures, subtypes were classified as quasi-mesenchymal (QM), classical (CL) and exocrine-like PDAC. Among the three subtypes, quasi-mesenchymal tumors reflected a particularly aggressive phenotype with the lowest survival of all patients.[19] Consistently, Moffitt and colleagues[20] defined the classical and basal-like subtypes with the latter showing poor survival rates.[20] In a similar study Bailey et al.[21] identified four subtypes, which were classified as squamous, immunogenic, pancreatic progenitor and Aberrantly Differentiated Endocrine eXocrine (ADEX).[21] Importantly, further studies (Puleo et al.[22]) described a significant transcriptional overlap between the basal-like phenotype and the quasi-mesenchymal and squamous subtype, respectively.[22] Taken together, there is strong evidence for different molecularly defined tumor subtypes in pancreatic cancer. In addition, recent evidence strongly supports the idea of subtype-specific tumor biology and phenotypic behavior in pancreatic cancer. Accordingly, recent evidence from metabolic profiling studies supported subtype-specific differences and emphasized a close association between the squamous subtype and a glycolytic profile, while the classical phenotype

displayed a lipogenic cell metabolism. Furthermore, it has been shown that pancreatic cancer exerts subtype-specific responses to drugs targeting metabolic features.[23] For instance, a recent study showed a strong impact of Glycogen Synthase Kinase 3β (GSK3β) on glycolysis in the squamous subtype.[24] This finding is of particular interest, as recent studies have shown that GSK3β is often induced in PDAC with mutant Ras signaling activation, where the kinase in turn activates NF-κB signaling[25], or drives glycolysis[24] to promote tumorigenesis. Moreover, several of those pathways have been reported by Bailey et al.[21] to be deregulated pathways in PDAC (Fig. 1). These interesting findings highly suggest a critical role of this kinase in Kras driven carcinogenesis of the pancreas, although the underlying mechanisms remain elusive.[26]

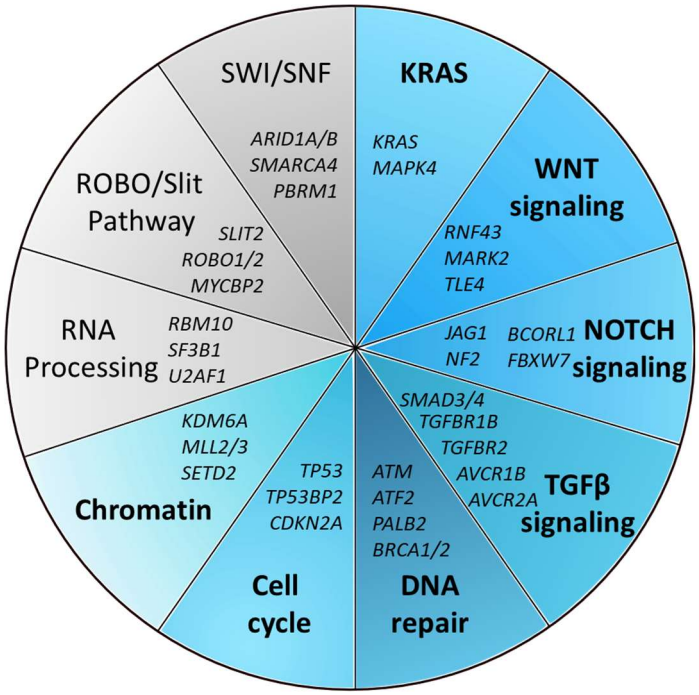

Figure 1: Major pathways altered in pancreatic cancer. Pie graph displaying the majorly deregulated pathways in pancreatic cancer with their most important key players. The blue color indicates pathways which are affected by GSK3β. Modified from Bailey et al. (2016).

1.2. Glycogen Synthase Kinase 3β (GSK3β)

1.2.1. Function and regulation

In general, Glycogen Synthase Kinase 3β (GSK3β) is a ubiquitously expressed serine/threonine kinase. Two isoforms, termed GSK3α and GSK3β are known so far which are encoded by different genes.[27] Although the isoforms share a highly conserved catalytic domain they target different sets of cell proteins for posttranslational modification.[28] GSK3 was first discovered as a kinase for glycogen synthase, hence its name.[29,30] GSK3β is constitutively active in the cell and its targets are mostly pre-phosphorylated proteins (primed).[31–33] Its activity is inhibited by several cellular signaling networks and kinases, including p70 S6, p90Rsk, protein kinase A, protein kinase B (AKT) and Protein Kinase C (PKC), through phosphorylation at serine 9 (Fig. 2).[34] Importantly, these kinases themselves are often regulated by more than one signaling cascade (e.g. the Mitogen-Activated Protein Kinase (MAPK) pathway, Wnt signaling, mammalian Target Of Rapamycin Complex 1 (mTORC1) and PhosphatIdylinositol 3-Kinase (PI3K)). The remarkable number of kinases with inhibitory functions on GSK3β emphasize the complexity of GSK3β regulation in a cell.[35–44] In fact, GSK3β activity is tightly controlled by these kinases through a complex network of extra- and intracellular signals, including insulin, growth factors, cytokines and chemokines as well as Wnt signaling and inducers of apoptosis.[44–47] The back reaction is induced by protein phosphatase 1 and protein phosphatase 2A. These enzymes remove the inhibitory phosphorylation in order to restore the function of GSK3β.[48–50] Phosphorylation can also cause an enhanced GSK3β function, when occurring at tyrosine 216 via autophosphorylation or other kinases.[51–53] Furthermore, the localization of GSK3β determines its downstream factors and the complex formation and thus its effects.[54,55] The targets of GSK3β are numerous and can variably lead to stabilization, inactivation or priming for their degradation.[52,56] For example phosphorylation of β-catenin, a part of Wnt-signaling, leads to its degradation.[57] Other targets include Nuclear Factor of

Activated T cells (NFAT), c-Jun, c-myc and cyclin D1. Their phosphorylation leads to nuclear export and subsequent their degradation.[58–63] GSK3β-mediated phosphorylation of Tau results in decreased microtubule stabilization. [49,52,64] As several target proteins of GSK3β are also known to be deregulated in different diseases, GSK3β is often a major player in disease related pathways, either as a promoting or suppressive factor.

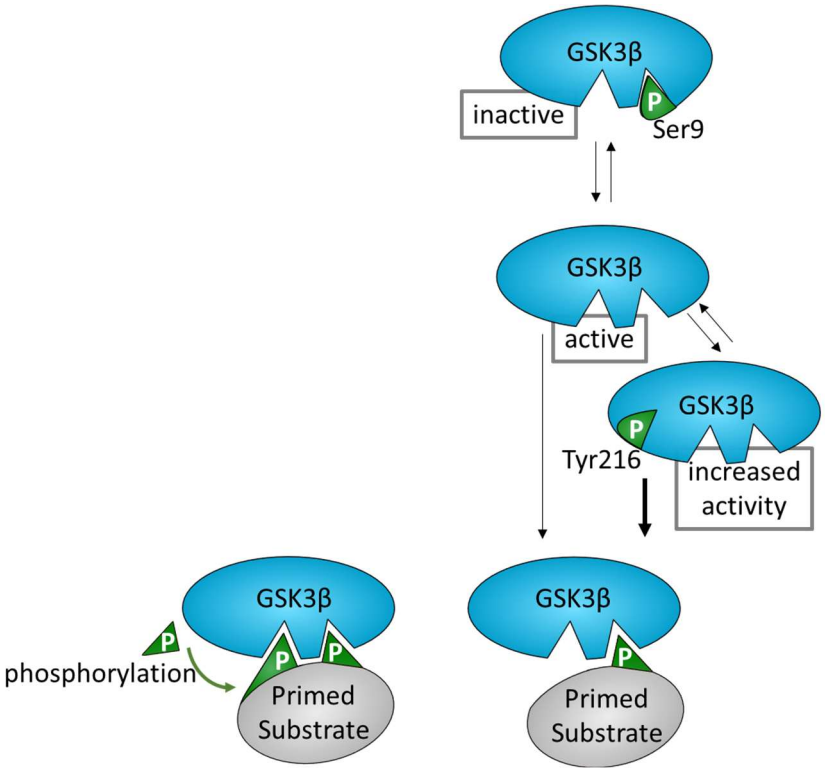

Figure 2: Regulation of GSK3β activity. GSK3β is constitutively active and can be enhanced in its activity by phosphorylation at tyrosine 216 (Tyr216). It has major affinity to primed (already phosphorylated) substrates, which are located 4 residues beside the phosphorylation side for GSK3β. Its function can be inhibited via phosphorylation at serine 9 (Ser9).

1.2.2. GSK3β in disease

1.2.2.1. GSK3β in cancer

GSK3β plays a key role in several diseases like neurological and metabolic disorders, inflammatory or cardiovascular diseases as well as cancer.[33] In neurological diseases, namely Alzheimer's disease, GSK3β affects the destabilization of tau, the formation of β-Amyloid plaques as well as the impairment of synaptic plasticity and memory formation.[65] GSK3β regulates important inflammatory transcription factors as Nuclear Factor κ-light-chain-enhancer of activated B cells (NF-κB), Signal Transducer and Activator of Transcription (STAT) or NFAT by controlling the transcription of cytokines and the T-cell response. [33,66–68]

GSK3β has a rather ambiguous role in cancer as it can act as a tumor suppressor or tumor promoter depending on the tumor identity. GSK3β leads to the destabilization of proteins with important oncogenic functions, like c-Myc, c-Jun or β-catenin, thereby playing a tumor suppressive role in various malignant contexts.[69,70] Its tumor suppressive role was described in skin cancer and mammary carcinoma where it suppresses the Wnt/β-catenin pathway and decelerates cell cycle progression. It has been shown that during disease progression, GSK3β is usually transcriptionally downregulated or inhibited via serine 9 phosphorylation.[49,71–74] In other contexts like triple negative breast cancer, GSK3β promotes tumor growth and drives the acquisition of cancer stemness and therapy resistance. Moreover it mediates therapy resistance in several tumor entities such as glioma, colorectal and lung cancer as well as pancreatic cancer. [75,76] In pancreatic cancer it has been shown that nuclear accumulation of GSK3β is associated with a higher grade of dedifferentiation displayed as an enhanced tumor aggressiveness.[77] This tumor promoting function of nuclear GSK3β was also observed in glioblastoma, where it promotes stemness through stabilization of the histone demethylase KDM1A.[78] Related studies demonstrated that the combination of GSK3β inhibition with

chemotherapeutic agents decreased tumor cell survival.[79,80] Another important chemo-sensitization mechanism of GSK3β inhibition is induction of DNA damage, which has been shown in ovarian cancer, glioblastoma and pancreatic cancer.[75] In ovarian cancer, GSK3β inhibition has been found to destabilize Uracil N-Glycosylase (UNG2), a protein needed for the initiation of Base Excision Repair (BER), causing sensitization to 5-fluorouracil.[81] Another DNA repair mechanism which is influenced by GSK3β, is DNA double strand break repair via phosphorylation of p53-Binding Protein 1 (53BP1) in glioblastoma.[82] In pancreatic cancer, GSK3β stabilizes DNA TOPoisomerase 2-Binding Protein 1 (TOPBP1), a protein involved in the Ataxia Telangiectasia and Rad3-related protein (ATR) signaling response upon DNA damage. Thus, the inhibition of GSK3β sensitizes cells to the DNA damaging gemcitabine treatment.[83] Other oncogenic properties contributing to resistance including Epithelial-Mesenchymal Transition (EMT), cancer stemness and migration can also be diminished by GSK3β inhibition.[76] Other effects of GSK3β inhibition are the induction of NF-κB-mediated apoptosis [25,84], causing transcriptional regulation of cell cycle proteins and the induction of caspase activity in several cancer identies.[85–87] GSK3β also afflicts cell proliferation in pancreatic cancer by the stabilization of NFATc2.[59,60] NFATc2 belongs to the family of NFAT proteins which has been shown to be an important oncogenic regulator in pancreatic cancer.[88,89]

1.3. Nuclear Factor of Activated T Cells (NFAT)

Nuclear Factor of Activated T Cells (NFAT) is a ubiquitously expressed group of transcription factors, which are involved in several cellular functions such as immune response and ER stress. It also plays a major role in human malignancies, as it affects processes as proliferation or tumor microenvironment.[90,91] NFAT proteins comprise four major members, namely

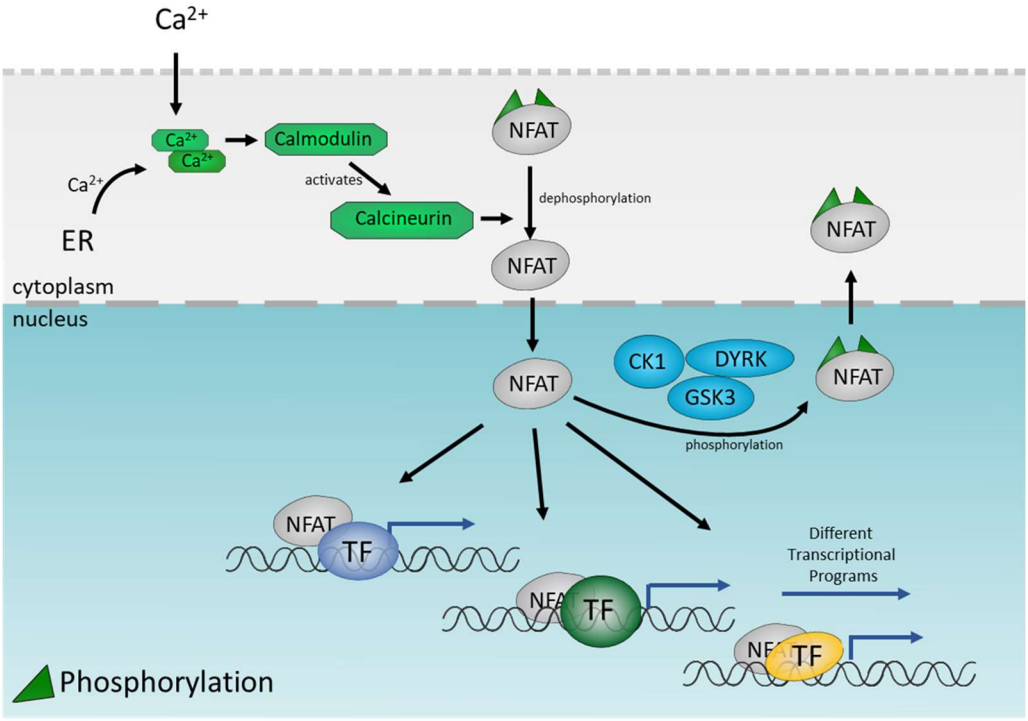

Figure 3: Regulation of NFAT signaling. NFAT is activated through calcium signaling, as the Ca^{2+} causes the activation of calcineurin by calmodulin. Calcineurin causes the dephosphorylation of NFAT. NFAT can shuttle in the nucleus afterwords and interact with different transcription factors (TF) and depending on those induce gene expression. A phosphorylation in the nucleus by GSK3, CK1 or DYRK cause a translocation back into the cytosol.

NFATC1, NFATC2, NFATC3 and NFATC4 .[92] The location of NFAT (cytoplasm or nucleus) is dependent on its phosphorylation status (Fig. 3).[93] When inactive, NFAT is hyperphosphorylated and present in the cytoplasm. Upon cell activation and increased Ca^{2+} influx, calmodulin activates the phosphatase calcineurin, which in turn dephosphorylates NFAT and thus promots its transition into the nucleus.[94] Following inactivation via rephosphorylation, NFAT is shuttled to the

cytosol. Several NFAT targeting kinases have been described like GSK3, Casein Kinase 1 (CK1) and Dual-specificity Tyrosine-phosphorylation-Regulated Kinase (DYRK).[95] An interaction of NFAT proteins with other transcription factors and chromatin regulatory proteins, like Activator Protein 1 (AP-1), GATA, forkhead box P-family proteins or SOX2, is very prominent in the nucleus. These interactions determine substrate specificity and regulate gene transcription. Another aspect of NFAT regulated signatures is the high dependence on the cell type and the nuclear composition of these interacting partner proteins.[94,96] Beside its role in regulating the innate immune response and inflammation, NFAT can regulate apoptosis or cell cycle propagation. Thereby, isoform and cell type dependent NFAT can regulate genes that induce or repress cell cycle progression as p21, p15, cyclins or cyclin dependent kinases.[97] Another aspect is the regulation of the transcription of pro- as well as anti-apoptotic genes by NFAT isoforms.[97] Taking the various mechanisms involving NFAT into account, it is only evident that numerous diseases and processes have been shown to be affected by NFAT, importantly also cancer.[92,98]

1.3.1. NFAT in cancer

The deregulation of NFAT plays a major role in oncogenic processes such as carcinogenesis, proliferation, metastasis and chemoresistance. These effects depend on specific isoforms expression, activation status and interaction partners.[91,92,95] NFAT is overexpressed or strongly activated in several cancer types. Prominent examples are lymphoma, breast or pancreatic cancer. In breast cancer NFAT promotes cancer cell invasion via CycloOXygenase 2 (COX2)[99,100], while in pancreatic cancer NFAT proteins foster tumor growth and survival at least in part by inducing c-Myc expression. This process is further facilitated due the recruitment of the histone acetylase p300 leading to enhanced binding of ETS domain-containing protein Elk1. In addition, silencing of NFAT dramatically reduces tumor growth *in vivo* and *in vitro*.[101,102] Moreover, c-Jun was identified as an interaction partner of NFAT involved in acinar cell dedifferentiation.[103] The

NFATc1/STAT3 complex has been found to be crucial for driving pancreatic carcinogenesis.[104] In addition to interacting partners, factors regulating NFAT can strongly modulate its functions. For example, GSK3β stabilizes NFATc2 in pancreatic cancer cells by protecting it from proteasomal degradation.[60,105] Despite its prominent role in PDAC, targeting of NFAT remains challenging, due to the broad effects caused to its general inhibition.[91,106]

1.4. Therapy of PDAC

Despite tremendous effort in defining molecular subtypes in pancreatic cancer and translating the results to therapy strategies, molecular-based new therapy approaches remain to be developed. The current standard care for pancreatic cancer was slightly improved by introducing new chemotherapeutic regimens next to gemcitabine.[107] Combining gemcitabine with nab-paclitaxel increases the median survival for nearly two months up to 8.5 comparing to gemcitabine monotherapy.[108] Further improvement in survival was accomplished by introducing FOLFIRINOX treatment, which enhanced the survival from 6.8 months of gemcitabine treated patients up to 11.1 months. FOLFRINOX consists of four different chemotherapeutics, namely oxaliplatin, irinotecan, fluorouracil, and leucovorin. The treatment is limited to patients with a good performance status, due to major side effects.[109] Even though these extensions of chemotherapeutic treatment improved survival, their minimal effects could be caused by disregarding the tumor heterogeneity in pancreatic cancer. The only clinically established subclassification that had beneficial effects on treatment, is combining DNA damage treatment in tumors with vulnerabilities in DNA damage repair.[110]

1.5. DNA Damage Repair

DNA damage repair mechanisms are an important response to prevent genomic instability and apoptosis. Subsequently, different repair mechanisms are present in the cell to repair damage. DNA Damage Response (DDR) includes detection followed by response and repair to maintain the integrity of the genome.[111] DNA damage can be caused by endogenous events occurring in a regular manner in the cell during replication, hydrolytic reactions or by reactive oxygen species[112,113] Exogenous stimuli like toxins, irradiation, or UV light can induce DNA damage as well.[114]

1.5.1. Types of DNA damage and repair

The mechanisms of DNA damage repair are highly dependent on the type of DNA damage. Various chemotherapeutic agents act via induction of DNA damage resulting in cell death. The standard chemotherapeutic agent gemcitabine, which is incorporated in the DNA, evokes the termination of replication.[115] This leads to stalled replication forks and single strand breaks of the DNA, causing apoptosis.[116] Another nucleoside analog in PDAC therapy is fluorouracil (5-FU), which is an analog of uracil and has a similar mode of action as gemcitabine.[117] The folinic acid leucovorin enhances the effects of 5-FU by inhibiting the thymidylate synthase.[118] Another component of FOLFIRINOX is irinotecan, which is an inhibitor of topoisomerase 1. Topoisomerase 1 is required for relaxing the DNA during DNA replication and transcription. Therefore, its inhibition leads to the formation of DNA double-strand breaks.[119,120] The fourth component of FOLFIRINOX is oxaliplatin, which induces stress on ribosome biogenesis.[121] Another treatment option is cisplatin. It displays a high affinity to DNA and binds to the nucleophilic N7-sites of purine bases. This process causes intra- and inter-strand crosslinks.[122,123] Repair mechanisms for these crosslinks are nucleotide-

excision repair and homologous recombination as well as mismatch repair and non-homologous end joining .[123,124]

1.5.1.1. Repair of DNA strand breaks

Two major repair mechanisms for DNA strand breaks are Homologous Recombination (HR) and Non-Homologous End Joining (NHEJ). NHEJ can be performed during every point of the cell cycle and is not restricted to the S and G2 phase, which applies for HR.[125]

During NHEJ (Fig. 4) the ends of the DSB are bound by a heterodimer of KU70 and KU80, which form a complex at the DNA ends. This is followed by binding of the DNA-dependent Protein Kinase catalytic subunit (DNA-PKcs), leading to its activation via autophosphorylation and the recruitment of Artemis. Artemis is a nuclease that prepares the DNA ends for adding nucleotides and ligation of strands. This process is affected by the compatibility of the DNA strand ends and their modification. Multiple Polymerases (Pol) can implement nucleotides e.g. Pol μ or Pol λ. Subsequently, the ends are ligated by the DNA ligase IV. While this process does not require a template and is fast, it is very error prone. Inappropriate repair can lead to genomic instability resulting in apoptosis and cell death.[125–128]

A more accurate way to repair DSBs is HR (Fig. 4), which requires a template from the sister chromatid.[129] The general mechanism involves the initial binding of the MRN complex, consisting of MRE11, RAD50 and NBS1 (Nibirn), to the DSB ends. Its binding causes the induction of cell cycle regulation, as G2/M arrest via ATM signaling, as well as the phosphorylation of histone 2AX and altering of the chromatin. A central protein in HR is BRCA1, which is interacting with the MRN complex and a plethora of other factors, reflecting its importance in efficient HR repair. The CtBP (C-terminal Binding Protein) Interacting Protein (CtIP) then binds to the MRN complex. This supports the resection at DSBs as endonuclease, as well as it is involved in the recruitment of other DNA repair

factors, which also contributes to the resection process.[130–132] The binding of the Replication Protein A (RPA) to the arisen single-stranded DNA (ssDNA) is the first step of the resection process. RAD51 promoted by BRCA2 then replaces RPA. This interaction is crucial to promote the strand exchange. The formed nucleoprotein filament is crucial for the recognition of the homologic region on the template. With the help of cofactors it promotes the strand invasion to the template and forming the Displacement loop (D-loop).[111,125,133–135] Some major proteins being involved in HR disturb the repair network and make a cell susceptible for agents requiring HR for damage clearance, as it is shown for BRCAness.[136]

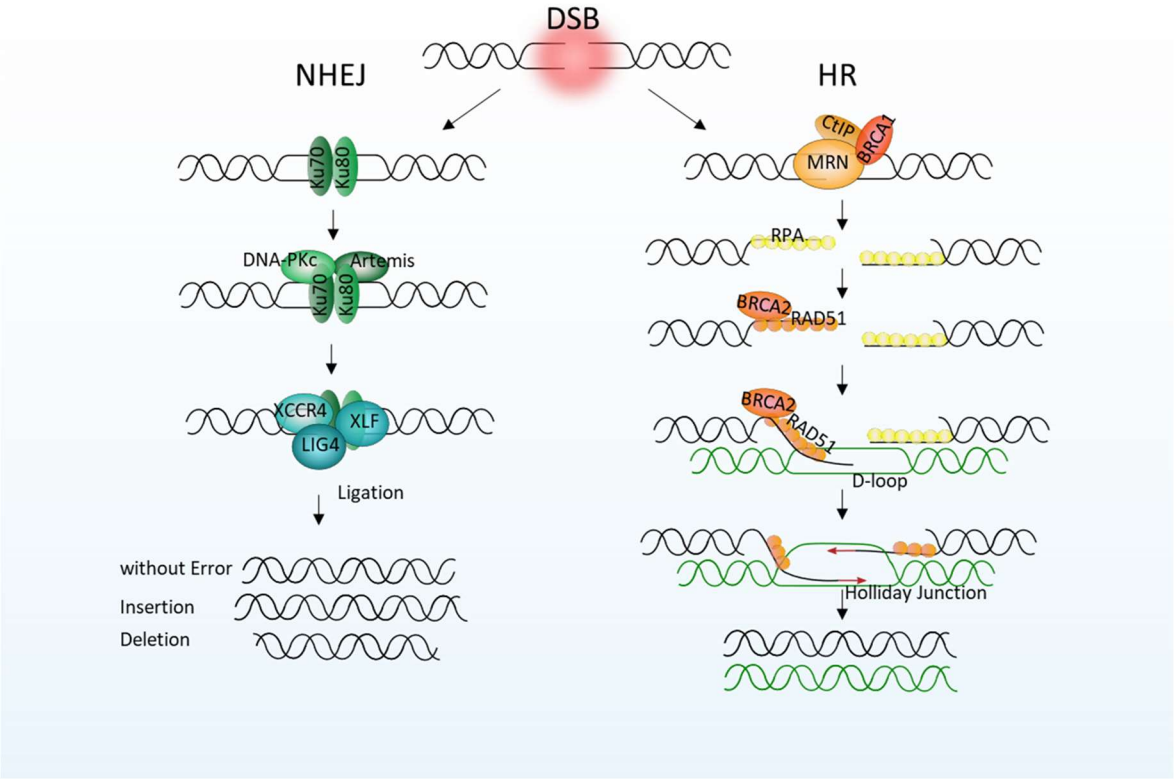

Figure 4: DNA double strand repair by the major pathways NHEJ and HR. Simplified scheme of the DSB repair pathways. During NHEJ the heterodimers of KU70 and KU80 are binding, which leads to binding of DNA-PKcs and recruitment of Artemis, preparing DNA strands for ligation. Polymerases like Pol μ or Pol λ can add nucleotide, followed by the ligation of DNA strand ends via the complex of the DNA ligase IV (LIG4), XRCC4 and XLF. The process is error prone, thus it can come to insertion of extra nucleotides or deletion. HR is using a template of a sister chromatid to avoid mistakes during repair. During the initial step, the MRN complex, CtIP and BRCA1 are binding and process the resection of the DNA strand. RPA is binding to the ssDNA, which is replaced by RAD51 promoted by BRCA2. The nucleoprotein filament is recognizing the homologic region, promotes the invasion and formation of the d-loop. It comes to the formation of a Holliday junction and copying and repair of the DNA strand break.

1.5.2. BRCAness

BRCA mutations are well known for increasing the risk of developing various malignancies like breast, ovarian, colon, and pancreatic cancer. Due to a recent study by Golan et al. (2019)[110], Poly [ADP-ribose] polymerase (PARP) inhibitors were introduced into clinical guidelines in the United States[137].

This was the result of patients with a BRCA mutated tumor showing better survival rates, when treated with the PARP inhibitor Olaparib. PARP is an important protein involved in the repair of single strand breaks. The inhibition of PARP therefore increases double strand breaks formation. Cell death will result from accumulating DNA damage, when double strand breaks were not repaired by homologous recombination.[138] "BRCAness" can also be mediated by mutation defects in HR genes other than BRCAs. This is an important factor in mediating the same treatment vulnerabilities.[138] In PDAC about 24% of patients have a deficiency in DNA damage repair and might benefit of a PARP inhibitor or platinum-based therapy.[18,139]

1.6. Aim of the project

Recent studies propose an oncogenic function of GSK3β in pancreatic cancer, although the underlying mechanisms remain to be determined. It also remains unclear whether and how GSK3β targeting offers a promising strategy in pancreatic cancer treatment. In this study we aimed to determine a deeper mechanistic understanding of its role in the regulation of pancreatic cancer behavior. Specifically, we examined the effect of GSK3β on transcriptional regulation and function of pancreatic cancer cells. The comprehension of important transcription factors being involved in the effects of GSK3β is a promising approach in improving stratification of patients, who might benefit from a combination therapy of chemotherapeutics with GSK3β inhibitors. Thus, the key novelty of this work is to evaluate the potential of GSK3β-related treatments in combination with other therapeutics to improve therapy outcome, based on a prior stratification.

2. Materials and Methods

2.1. Materials

2.1.1. Buffers

Table 1. Composition of buffers and solutions.

Buffer/Solution	Composition
Blocking solution	5 % (w/v) milk powder in TBS-T
BSA blocking solution	5 % (w/v) BSA in TBS-T
Buffer A	10 mM Hepes pH 7.9, 10 mM KCl, 0,1 mM EDTA, 0,1 mM EGTA, 0.1 M DTT, 1x cOmpelte
Buffer C	20 mM Hepes pH 7.9, 0.4 M NaCl, 1 mM EDTA, 1 mM EGTA, 0.1 M DTT, 1x cOmpelte
Citrate buffer	10 mM citric acid monohydrate, pH 6.0
Crystal violet solution	0.1 % (w/v) crystal violett, 20 % (v/v) EtOH in H_2O
Gomes lysis buffer	150 mM NaCl, 1 % (v/v) NP-40, 0.5 % (w/v) sodium deoxycholate, 50 mM Tris-HCl (pH 8.0), 20 mM EDTA, 20 mM NaF
Gomes wash buffer	100 mM Tris-HCl (pH 8.5), 500 mM LiCl, 1 % (v/v) NP-40, 1 % (w/v) sodium deoxycholate, 20 mM EDTA, 20 mM NaF
5x Laemmli buffer	225 mM Tris pH 6.8, 50 % (v/v) glycerol, 5 % (w/v) SDS, 100 mM DTT, 0,02 % (w/v) bromophenol blue, 5 % (v/v) 2-mercaptoethanol
MTT solubilization solution	100 mM HCl, 10 % (v/v) Triton X-100 in isopropyl alcohol
Nuclear preparation buffer	150 mM NaCl, 20 mM EDTA (pH 8.0), 50 mM Tris (pH 7.5), 0.5 % (v/v) NP-40, 1 % (v/v) Triton X-100, 20 mM NaF
PB	17 mM monobasic sodium phosphate, 60 mM dibasic sodium phosphate, adjust to pH 7.4
PBS	137 mM NaCl, 2.7 mM KCl, 1.8 mM KH_2PO_4,10 mM Na_2HPO_4, adjust to pH 7.2-7.4
PBS-T buffer	PBS, 0.01 % (v/v) Triton X-100

Running buffer	25 mM Tris, 190 mM glycine, 0.1 % (w/v) SDS
SDS separating gel (x %):	x % (v/v) Acrylamide, 375 mM Tris (pH 8.8), 0.1 % (w/v) SDS, 0.1 % (w/v) APS, 0.04 % (v/v) TEMED
SDS stacking gel	5 % (v/v) acrylamide, 125.5 mM Tris (pH 6.8), 0.1 % (w/v) SDS, 0.1 % (w/v) APS, 0.1 % (v/v) TEMED
TBE buffer	0.13 M Tris, 45 mM boric acid, 2.5 mM EDTA
TBS-T buffer	0.2 M Tris base, 1.5 M NaCl, 0.05 % (v/v) Tween 20
TE buffer	10 mM Tris-HCl (pH 8.0), 1 mM EDTA (pH 8.0)
Weinmann buffer	50 mM Tris-HCl (pH 8.0), 10 mM EDTA, 1 % (v/v) SDS
Whole cell lysis buffer	50 mM HEPES pH 7.5-7.9, 150 mM NaCl, 1 mM EGTA, 10 % (v/v) Glycerin, 1 % (v/v) Triton X-100, 100 mM NaF,10 mM $Na_4P_2O_7$ x 10 H_2O, 1x cOmpelte

2.1.2. Chemicals and reagents

Table 2. Chemicals and reagents.

Chemicals/Reagents	Company
2-mercaptoethanol	Carl Roth, Karlsruhe, Germany
Aceton	AppliChem GmbH, Darmstadt, Germany
Acrylamide	Carl Roth, Karlsruhe, Germany
Agarose	Nippon Genetics, Tokyo, Japan
Agarose A/G Beads	Merck, Darmstadt, Germany
Ampicilin	Merck, Darmstadt, Germany
AMPure XP beads	Thermo Fisher Scientific, Waltham, Massachusetts, USA
APS	Carl Roth, Karlsruhe, Germany
ATP	Thermo Fisher Scientific, Waltham, Massachusetts, USA
Boric acid	Merck, Darmstadt, Germany
Bromophenol blue	Merck, Darmstadt, Germany
BSA	Merck, Darmstadt, Germany
Buffer O	Thermo Fisher Scientific, Waltham, Massachusetts, USA

Chloroform	AppliChem GmbH, Darmstadt, Germany
Citrtic acid	Carl Roth, Karlsruhe, Germany
Competent E. coli 10beta	New England Biolab, Ipswich, USA
cOmplete	Roche, Rotkreuz, Switzerland
Crystal violet	Carl Roth, Karlsruhe, Germany
DAPI	Merck, Darmstadt, Germany
DMEM, Gibco	Thermo Fisher Scientific, Waltham, Massachusetts, USA
DMSO	Merck, Darmstadt, Germany
DNA Marker Plus 1kb	Nippon Genetics, Tokyo, Japan
DTT	Merck, Darmstadt, Germany
EDTA	Thermo Fisher Scientific, Waltham, Massachusetts, USA
EGTA	Merck, Darmstadt, Germany
Ethanol	Carl Roth, Karlsruhe, Germany
Fast Digest BBsI	Thermo Fisher Scientific, Waltham, Massachusetts, USA
FBS	BIOWEST SAS, Nuaillé, France
Formaldehyde	Merck, Darmstadt, Germany
Glycerol	Merck, Darmstadt, Germany
Glycine	Carl Roth, Karlsruhe, Germany
H_2O_2	AppliChem GmbH, Darmstadt, Germany
HCl	AppliChem GmbH, Darmstadt, Germany
Heamatoxilin	Merck, Darmstadt, Germany
HEPES	Carl Roth, Karlsruhe, Germany
High range protein ladder	Thermo Fisher Scientific, Waltham, Massachusetts, USA
Hoechst	Merck, Darmstadt, Germany
ImmoMount	Thermo Fisher Scientific, Waltham, Massachusetts, USA
Isopropanol	AppliChem GmbH, Darmstadt, Germany
KCl	Merck, Darmstadt, Germany
LB Agarose	Merck, Darmstadt, Germany
LB Media	Merck, Darmstadt, Germany
LiCl	Merck, Darmstadt, Germany
Linear acrylamide	BIORON, Römerberg, Germany
Lipofectamin 2000	Bio-Rad, Hercules, USA
Mastermix for Syber Green	Bio-Rad, Hercules, USA
MEM NEAA (100x), Gibco	Thermo Fisher Scientific, Waltham, Massachusetts, USA
MEM, Gibco	Thermo Fisher Scientific, Waltham, Massachusetts, USA
Methanol	Carl Roth, Karlsruhe, Germany
Midori Green	Nippon Genetics, Tokyo, Japan
Milk powder	Carl Roth, Karlsruhe, Germany

monobasic potassium phosphate	Merck, Darmstadt, Germany
MTT	Biomol, Hamburg, Germany
NaCl	Merck, Darmstadt, Germany
NaF	Merck, Darmstadt, Germany
Nitrocellulose membrane	Bio-Rad, Hercules, USA
Normal Goat Serum	Abcam
NP-40	Merck, Darmstadt, Germany
Page Ruler™ prestained ladder (26616)	Thermo Fisher Scientific, Waltham, Massachusetts, USA
Pen/Strep, Gibco®	Thermo Fisher Scientific, Waltham, Massachusetts, USA
PFA	AppliChem GmbH, Darmstadt, Germany
Phenol/Chloroform/Isoamyl alcohol	Carl Roth, Karlsruhe, Germany
Primer/sgRNA	Merck, Darmstadt, Germany
Protein assay dye reagent concentrate	Bio-Rad, Hercules, USA
Proteinase K	AppliChem GmbH, Darmstadt, Germany
RNaseA	Merck, Darmstadt, Germany
Roti Mount	Carl Roth, Karlsruhe, Germany
ROTIclear	Carl Roth, Karlsruhe, Germany
RPMI, Gibco	Thermo Fisher Scientific, Waltham, Massachusetts, USA
SDS	Carl Roth, Karlsruhe, Germany
siLentFect	Bio-Rad, Hercules, USA
SOC outgrowth media	New England Biolab, Ipswich, USA
Sodium deoxycholate	Merck, Darmstadt, Germany
sodium phosphate dibasic	Carl Roth, Karlsruhe, Germany
Spectra Mulitcolor High Range Protein Ladder (26625)	Thermo Fisher Scientific, Waltham, Massachusetts, USA
Super Script II Reverse Transcriptase	Thermo Fisher Scientific, Waltham, Massachusetts, USA
T4 Ligase	Thermo Fisher Scientific, Waltham, Massachusetts, USA
Tango Buffer	Thermo Fisher Scientific, Waltham, Massachusetts, USA
TEMED	Carl Roth, Karlsruhe, Germany
Trans-Blot Turbo RTA Transfer Kit	Bio-Rad, Hercules, USA
Tris	AppliChem GmbH, Darmstadt, Germany
Tris-HCl	Carl Roth, Karlsruhe, Germany
Triton X-100	Carl Roth, Karlsruhe, Germany
TRIzol Reagent	Thermo Fisher Scientific, Waltham, Massachusetts, USA

Trypsin 10x, Gibco	Thermo Fisher Scientific, Waltham, Massachusetts, USA
Tween-20	Merck, Darmstadt, Germany
Western Lightening Plus ECL	Perkin-Elmar, Waltham, USA
Western Lightening Ultra	Perkin-Elmar, Waltham, USA
Xylol	AppliChem GmbH, Darmstadt, Germany

2.1.3. Equipment and consumables

Table 3. Equipment and consumables.

Equipment/Consumables	Company
Ariumpro ultrapure water system	Sartorius, Göttingen, Germany
Benchtop Automated Tissue Processor	Leica Biosystems, Wetzlar, Germany
Biorupter Pico	Diagenode, Denville, USA
Cell Culture 6-well plate	Sarstedt, Nümbrecht, Germany
Cell Culture 96-well plates	Greiner Bio One, Kremsmünster, Austria
Cell Culture Flask	Sarstedt, Nümbrecht, Germany
Cell Scraper	Sarstedt, Nümbrecht, Germany
Cell strainer, 50 µM	BD Bioscience, Franklin Lakes, USA
ChemoStar ECL Imager	INTAS Science Imaging Instruments, Göttingen, Germany
Combitips advanced	Eppendorf, Hamburg, Germany
Combitips advanced, Biopur	Eppendorf, Hamburg, Germany
Cryopure vial	Sarstedt, Nümbrecht, Germany
FACS CantoII	BD Bioscience, Franklin Lakes, USA
Falcon Tube 15 mL/ 50 mL	Sarstedt, Nümbrecht, Germany
Fluorescence Microscope System for Advanced Imaging Widefield Systems	Leica Camera, Wetzlar, Germany
HERAcell 240i CO_2 incubator	Thermo Fischer Scientific, Waltham, USA
HistoCore Arcadia C cooling plate	Leica Biosystems, Wetzlar, Germany

IKAMAG Magnetic Stirrer RCT	IKA, Staufen, Germany
Light microscope "BX43"	Olympus, Tokyo, Japan
Light microscope "BX43"	Olympus, Tokio, Japan
Low binding micro tubes	Sarstedt, Nümbrecht, Germany
Mettler Toledo FE20 FiveEasy Benchtop pH meter	Thermo Fischer Scientific, Waltham, USA
MicroAmp Fast Optical 96-Well Reaction Plate	Thermo Fischer Scientific, Waltham, USA
MicroAmp Optical Adhesive Films	Thermo Fischer Scientific, Waltham, USA
Micropipette tips TipOne	Starlab, Hamburg, Germany
Microplate reader "PHOMO"	Autobio, Zhengzhou, China
Microscope – BX43F/ CKX53	Olympus Corporation, Tokyo, Japan
Microtome (Leica RM2265)	Leica Biosystems, Wetzlar, Germany
Mini-PROTEAN Tetra handcast system	Bio-Rad Laboratories, Hercules, USA
Mini-PROTEAN Tetra Vertical Electrophoresis Cell	Bio-Rad Laboratories, Hercules, USA
Multifuge X1 Centrifuge Series	Thermo Fisher Scientific, Waltham, USA
Multipette plus	Eppendorf, Hamburg, Germany
NanoPhotometer P-330	INTAS Science Imaging Instruments, Göttingen, Germany
Neubauer chamber	Assistant, Sondheim/Rhön, Germany
Nitrocellulose membrane	Bio-Rad Laboratories, Hercules, USA
Paraffin Tissue embedder (EG1150H)	Leica Biosystems, Wetzlar, Germany
PerfectSpin 24R Refrigerated Microcentrifuge	Peqlab, Erlangen, Germany
Pipetboy acu 2	INTEGRA Biosciences, Biebertal, Germany
Pipetboy acu 2	INTEGRA Biosciences, Biebertal, Germany
Pipettes, Research Plus	Eppendorff, Hamburg, Germany
Polystyrene Tube with Screw Cap	Greiner Bio One, Kremsmünster, Austria

PowerPac Basic Power Supply	Bio-Rad Laboratories, Hercules, USA
Precision balance PCB	Kern & Sohn, Balingen, Germany
PSU-20i Orbital Shaking Platform	Grant Instruments, Shepreth, UK
Qubit Fluorometer 3	Thermo Fisher Scientific, Waltham, USA
Reactions Cups 0.5 mL, 1.5 mL, 2 mL	Sarstedt, Nümbrecht, Germany
Safe 2020 Class II Biological Safety Cabinets	Thermo Fischer Scientific, Waltham, USA
Scotsman AF80 Ice Flaker	Hubbard Systems, Suffolk, UK
Serological pipettes	Sarstedt, Nümbrecht, Germany
Shadon Sequenza System	Thermo Fisher Scientific, Waltham, USA
Sprout Minicentrifuge	Biozym Scientific, Hessisch Oldendorf, Germany
StepOnePlus Real-Time PCR System	Thermo Fisher Scientific, Waltham, USA
Superfrost glass slides	Thermo Fischer Scientific, Waltham, USA
ThermoMixer	Eppendorf, Hamburg, Germany
TipOne filtertips	Starlab, Hamburg, Germany
Trans-Blot Turbo Transfer System	Bio-Rad Laboratories, Hercules, USA
VacuuHandControl VHC^{pro}	Vacuubrand, Wertheim, Germany
Vacuum pump: BVC Control	Vacuubrand, Wertheim, Germany
Water bath (WNB14)	Memmert, Schwabach, Germany
Weighing balance	Sartorius, Göttingen, Germany

2.1.4.Kits

Table 4. Kits.

Kit	Company
Cell Proliferation ELISA, BrdU, colorimetric (11647229001)	Merck, Darmstadt, Germany
Bioanalyzer High Sensitivity DNA Analysis (5067-4626)	Agilent, Santa Clara, USA
DAB ImmPACT	Vector Laboratories, Burlingame, USA
iscript cDNA Synthesis Kit	Bio-Rad, Hercules, USA
iscript Universal SYBR Green Supermix	Bio-Rad, Hercules, USA
Macherey-Nagel NucleoBond Xtra	Thermo Fisher Scientific, Waltham, Massachusetts, USA
MycoAlert Mycoplasma Detection Kit	Lonza Group, Basel, Switzerland
Peroxidase Rabbit IgG Vectastain ABC Kit	Vector Laboratories, Burlingame, USA
Peroxidase Mouse IgG Vectastain ABC Kit	Vector Laboratories, Burlingame, USA
Qubit dsDNA HS Assaykit	Thermo Fisher Scientific, Waltham, Massachusetts, USA
DNeasy Blood & Tissue Kit	Qiagen, Venlo, Neatherlands
Trans-Blot Turbo RTA Midi Nitrocellulose Transfer Kit	Bio-Rad, Hercules, USA
TruSeq RNA Library Prep Kit v2 Set A,B	Illumina, San Diego, USA

2.1.5.Therapeutic drugs

Table 5. Therapeutic drugs.

Drug	Company
9-Ing-41	Aobious, Gloucester, MA, USA
AR-A014418	Abmole Bioscience Inc., Houston, USA
Cisplatin	Merck, Darmstadt, Germany
Olaparib	Selleckchem, Houston, USA
SN-38	Selleckchem, Houston, USA

2.1.6.Software

Table 6. Software.

Software	Version	Company
ChemoStar	0.3.28.0	Intas Science Imaging Instruments, Göttingen, Germany
DESeq2	1.22.1	[140]
FASTQC	0.65	[141]
FASTQ Trimmer	1.0.0	[142]
GraphPad Prism	7.05	GraphPad, San Diego, USA
htseq-count	0.6.1p1	[143]
Image Lab	5.2.1	Bio-Rad, Hercules, USA
Inkscape	1.0	
PVC Viewer	1.5.3.1	Implen, München, Germany
SortSam	2.18.2.1	[144]
TopHat	v2.1.1	[145]
CellSens Entry	1.12	Olympus Corporation, Tokyo, Japan
FlowJo	10.1r1	FlowJo, Oregon, USA

2.2. Methods

2.2.1.Cell culture

For *in vitro* studies, established human and murine pancreatic cancer cell lines as well as primary murine pancreatic cancer cells isolated from the KPC (K-ras$^{LSL.G12D/+}$; Trp53$^{R172H/+}$; Pdx-1-Cre) model[146] and the KNPC (K-ras$^{LSL.G12D/+}$; NFATc1 c.a.; Trp53$^{R172H/+}$; P48-Cre/+)[96] model were used. Further, cell lines isolated from patient derived xenografts (PDX) and provided by CP1 of the Clinical Research Unit 5002 were analyzed. In brief, PDX derived cell lines (CDX) were isolated from patient tumor material which have been cultivated for several generations in mice. CDX indicated with “Bo” as well as PDX material, were kindly provided by the collaboration with Prof. S. Hahn (Ruhr-Universität Bochum) and Prof. J. Siveke (University Hospital Essen). Chemotherapeutic agents and inhibitors used in this study are displayed in table 5. The inhibitors were solved in DMSO. Control conditions were treated with the same solvent content as treatment samples.

Table 7. Media compositions of cell lines.

Cell line	Origin	Media composition
KPCbl6	murine	DMEM, 10 % (v/v) FCS, 1 % (v/v) NEAA
KPCbl6 – ctr Klone	murine	DMEM, 10 % (v/v) FCS, 1 % (v/v) NEAA
KPCbl6 – NFATc1 k.o. #1	murine	DMEM, 10 % (v/v) FCS, 1 % (v/v) NEAA
KPCbl6 – NFATc1 k.o. #2	murine	DMEM, 10 % (v/v) FCS, 1 % (v/v) NEAA
KPCbl6 – NFATc1 k.o. #3	murine	DMEM, 10 % (v/v) FCS, 1 % (v/v) NEAA
KNPC	murine	DMEM, 10 % (v/v) FCS, 1 % (v/v) NEAA
L3.6	human	MEM, 10 % (v/v) FCS
Capan1	human	RPMI, 10 % (v/v) FCS
Capan2	human	RPMI, 10 % (v/v) FCS
CDX-5	human	RPMI, 10 % (v/v) FCS
CDX-7	human	RPMI, 10 % (v/v) FCS
CDX-62-Bo	human	RPMI, 10 % (v/v) FCS

CDX-80-Bo	human	RPMI, 10 % (v/v) FCS
CDX-85-Bo	human	RPMI, 10 % (v/v) FCS
CDX-57-Bo	human	RPMI, 10 % (v/v) FCS
CDX-13	human	RPMI, 10 % (v/v) FCS
CDX-103-Bo	human	RPMI, 10 % (v/v) FCS

2.2.2.CRISPR/Cas9-mediated knockout

To generate knock-out cells for NFATc1 in KPCbl6 cells, we used the CRISPR/Cas9 system. The protocol was kindly provided by Feda Hamdan. Single guide RNAs (sgRNA) targeting exon 3 kindly provided and designed by Marie Hasselluhn (AG Hessmann) were used. Oligomers were annealed, by mixing 20 µL of the upper and lower oligo [100 µM] with 10 µL of Buffer O and 50 µL of H_2O. The mix was incubated for 10 min at 95 °C in a water bath (600 mL), followed by cooling down in the water bath (transfer to 4 °C) for two hours. The product was diluted 1:400 for subsequent cloning into the PX-458 vector. The vector includes a Cas9 endonuclease, a green fluorescent protein (GFP)-tag for sorting purposes and an ampicillin resistance for selection. For ligation the reaction mix (100 ng PX-458 plasmid, 2 µL annealed oligos, 2 µL Tango Buffer, 1 µL DTT (10 mM), 1 µL ATP (10mM), 1 µL Fast Digest BBsI, 0.5 µL T4 Ligase, filled up with H_2O for a final volume of 20 µL) was incubated in a thermocycler for six cycles (each 5 min at 37 °C followed by 5 min at 21 °C). For the transformation into *Escherichia coli* (*E. coli*), competent cells were incubated with 2 µL of the ligation product for 35 s at 42 °C, followed by 5 min on ice. The cells were then mixed with 400 µL of SOC media, incubated for 1 h at 37 °C. Afterwards, bacteria were plated onto Ampicillin (50 µg/mL)-containing LB agarose plates. Single colonies were picked, cultivated/cultured and subsequently plasmids isolated. The successful implementation of the oligos was confirmed by sequencing (Microsynth Seqlab, Göttingen). For the transfection, 5 µg of the plasmid were

mixed with 1 mL of OptiMEM and 25 µL of Lipofectamin 2000, followed by an incubation for 10 min at room temperature (RT). Cells were supplemented with fresh media before adding the transfection reagents mix. For the generation of single cell clones, cells were trypsinized after 48 h, washed with PBS and resuspended in PBS prior to cell sorting. Additionally, cells were filtered (50 µm cell strainer) to remove non single cells beforehand. Sorting and separation of successfully transfected cells (GFP-positive) was performed by the central service unit for cell sorting of the UMG (S. Becker, Department of Hematology and Oncology, University Medical Center Göttingen). To avoid cell lines originating from multiple clones, wells were observed in a regularly manner and wells containing more than one primary colony were excluded. Confirmation of NFATc1 knockout was performed by PCR, Western blot and qRT-PCR. RNA and proteins were isolated as described in 1.2.7. and 1.2.9. DNA was isolated following the instructions of the DNeasy Blood & Tissue Kit. After a positive result by PCR, indicated by a change of the fragment size, clones were sequenced (Microsynth Seqlab, Göttingen) to confirm the knockout of NFATc1 in KPCbl6 cells.

Table 8. Oligonucleotides for generation of NFATc1 knockout cells in murine KPCbl6 cells.

Target	Sequence
NFATc1 Exon3	5'GACCGGCTGTAGCTCGGCACTGCAG
NFATc1 Exon3	5'AAACCTGCAGTGCCGAGCTACAGCC

2.2.3. Polymerase chain reaction (PCR)

To validate the NFATc1 knockout in KPCbl6 cells, isolated genomic DNA (gDNA) was used for the PCR, using primers flanking the putative region in which the sequence had been edited. The PCR reaction mix (2.5 µL 10x buffer, 1.25 µL Primer rev/for, 0.5 µL JumpStart Polymerase, 0.5 µL dNTPs, 100 ng DNA, final volume 25 µL) was run on a thermocycler. The settings are shown in table 9. The

PCR product was supplemented with 6x loading dye and loaded on a 1 % agarose gel supplemented with Midori Green (in TBE buffer). Bands were visualized using the Gel Doc.

Table 9. PCR program for CRISPR/Cas9 validation.

Temp. [°C]	Time [min]	
95	3	
95	0:30	
63	0:30	34 cycles
72	0:30	
72	10	

Table 10. Primer to validate CRISPR/Cas9 mediated NFATc1 knock-out.

Target		Sequence
Primer 1	forward	5'ATCTGCCTGTCTGTCTGTGC
	reverse	5'TCATAACCCGCTCCCTCAGA
Primer 2	forward	5'TGCTGGGTAGATGCAGACAC
	reverse	5'AGCCATTCCCTCTGTGAGGA

2.2.4.Transfection of cells

2.2.4.1. siRNA-mediated knock-down

For a temporary knock-down, cells were seeded in a 6-well plate. The media was removed after 24 h and 1.5 mL of fresh growth media were added. For one reaction, 500 µL of Opti-MEM were mixed with 6 µL siRNA and 6 µL of siLentFect. The mix was incubated for 20 min at RT and then supplemented to the normal growth media. Depending on the experiment, cells were harvested after 24-72 h.

Table 11. siRNAs.

Target	Target species	Catalog number	Company
GSK3β	murine	185671	Thermo Fisher Scientific, Waltham, Massachusetts, USA
GSK3β	human	S6240	Thermo Fisher Scientific, Waltham, Massachusetts, USA
NFATc1	murine	288360	Thermo Fisher Scientific, Waltham, Massachusetts, USA
Control siRNA		AM4611	Thermo Fisher Scientific, Waltham, Massachusetts, USA

2.2.4.2. Plasmid transfection

For the transfection of plasmids, cells were seeded in a 6-well plate and cultured until the required confluency was reached. Before the transfection, media was removed, and 1.5 mL of normal growth media added. For the reaction, 1 µg of the needed plasmid and Lipofectamine2000 (2.5 µL for 1 µg of DNA) were added to 500 µL of Opti-MEM. The mix was incubated for 10 min at RT prior transfection. As control, an empty vector was transfected. Cells were harvested as indicated in the corresponding experiment.

Table 12. Plasmids.

Plasmid	Specifications	provided by
pSpCas9(BB)-2A-GFP PX458	Vector for sgRNAs	Kindly provided by Steven Johnsen
GSK3β wt-HA tag	pcDNA3, Amp	was a gift from Jim Woodgett (Addgene plasmid # 14753)[147]
Vector control	pCMV2C	Stratagene
NFATc1 c.a.- HA tag	MSCV, Amp	was a gift from Neil A. Clipstone

2.2.5.Flow cytometry

Cell cycle analysis

Cells were cultivated and treated as indicated in the corresponding experiment. After the treatment, cells were trypsinized, counted and up to 1,000,000 cells transferred into a (15 mL/50 mL) falcon. For fixation, cells were centrifuged at 1200 rpm for 3 min (RT) and the pellet resuspended in 600 µL PBS. While vortexing the sample, 1.4 mL of ice-cold ethanol (100 %) was added dropwise. Samples were incubated for 30 min at 4 °C, followed by a centrifugation (1,200 rpm, 3 min, RT). The supernatant was discarded and the pellet washed two times with 1 mL of washing solution (PBS + RNase A (5 µg/mL)). After the last centrifugation and discarding the washing solution, cells were resuspended in 100 µL of PBS supplemented with 5 µL Hoechst. The sample was incubated for 30 min at 37 °C, followed by measurement (FACS CantoII, BD Biosciences), wherefore it was diluted with 400 µL of PBS. Analysis was performed using FlowJo.

2.2.6.Functional assays

MTT assay

Cells were seeded depending on their proliferation rate and the treatment duration in a corresponding density. The control cells were seeded so that they did not reach 100 % confluency at the endpoint of treatment. For a treatment of 72 h, 1,200 KPCbl6 cells, 2,000 L3.6 cells and 5,000-8,000 cells of CDX cells were seeded as quintuplicates in a 96-well plate. Cell viability and metabolic activity were measured by adding thiazolyl blue tetrazolium bromide (MTT, 5 mg/mL in H_2O) for a final concentration of 0.5 mg/mL to the culturing media of the cells and incubated for 2 h. CDX were incubated for 4 h. After incubation, media was removed and cells were dissolved in solubilization solution for 20 min at RT. The amount of metabolized MTT was measured at 595 nm using a photometer.

BrdU assay

For evaluation of the proliferation rate, cells were seeded in 96-well plates as indicated for the MTT assay and incubated as required for the corresponding experiments. For the BrdU assay, the manufacturer's protocol of the Colorimetric cell proliferation ELISA kit was followed. Treatments were performed in technical and biological triplicates.

Crystal violet assay

For the crystal violet staining, cells were seeded in 24-well or 96-well plates and incubated as shown in the corresponding experiments. At the endpoint, cells were fixed by adding 4 % PFA in PBS for 10 min. After incubation, PFA was removed and cells were incubated for 10 min covered in crystal violet solution (0.1 % (w/v) crystal violet, 20 % (v/v) EtOH in H_2O). After the removal of the solution, cells were washed with H_2O to remove unbound crystal violet. Staining was documented by pictures and quantified by dissolving in MTT solubilization solution and measurement at 595 nm with a photometer.

2.2.7.Extraction of RNA

For RNA extraction from cell culture experiments, cells were washed twice with PBS. Subsequently, cells were dissolved in TRIzol (0.5 mL/ well/ 6-well plate). Chloroform (200 µL per 500 µL of TRIzol) was added, samples vortexed and centrifuged (13,000 rpm, 30 min, 4 °C). The aqueous phase was collected and an equal amount of isopropanol added. Samples were mixed and incubated at -80 °C for 1 h. Sample were centrifuged for 30 min at 13,000 rpm, 4 °C and the supernatant removed. The pellet was washed twice with 500 µL of 70 % (v/v) EtOH. After EtOH removal, the pellet was dried, resuspended in nuclease-free water and stored at -80 °C. The quality of RNA was controlled by measuring the photometric values.

2.2.8. Quantitative real time polymerase chain reaction (qRT-PCR)

The cDNA synthesis for the qRT-PCR was carried out by using 1 µg of RNA and following the manufacturer's instructions of the BioRad cDNA synthesis kit. The final product was diluted 1:5 in nuclease-free H_2O. Samples were run in technical and biological triplicates. For relative Ct values, values were normalized to Ct values of *RPLP0*. For running qRT-PCR, the iTaq Universal SYBR Green Supermix was utilized. One reaction was composed of 3.9 µL H_2O, 0.05 µL of each primer (10 pmol), 5 µl iTaq Universal SYBR Green Supermix and 1 µL of the template cDNA. Primers are listed in table 13. The qRT-PCR program specifications are shown in table 14. qRT-PCR was performed using the software StepOne v2.3.

Table 13. Human primer sequences for qRT-PCR.

Target		Sequence
BRCA1	forward	5' GCCTTCTAACAGCTACCCTTC
	reverse	5' CTTCTGGATTCTGGCTTATAGGG
BRCA2	forward	5'TGCTGGGTAGATGCAGACAC
	reverse	5'AGCCATTCCCTCTGTGAGGA
ATM	forward	5'ATTCCGACTTTGTTCCCTCTG
	reverser	5'CATCTTGGTCCCCATTCTAGC
ATR	forward	5'GAAAGAGGCTCCTACCAACG
	reverse	5'CATTTCTAGTCGAGCTACCCAG
RPLP0	forward	5'TGGGCAAGAACACCATGATG
	reverse	5'AGTTTCTCCAGAGCTGGGTTGT

Table 14. Program for qRT-PCR.

Temp. [°C]	Time [min]	
95	10:00	
95	0:15	40 cycles (qRT-PCR)
60	1:00	50 cycles (ChIP-qRT-PCR)
Melt Curve		
60 to 95, increment 0.5	0:15	

Table 15. Primer for ChIP-qRT-PCR.

Target		Sequence
BRCA2	forward	5' GCCAGTCGACCTCCTTCAC
	reverse	5' AGCCGAGACACACACGTTAG
BRCA1	forward	5'CCAGACAGCATGGAACCACA
	reverse	5'ACTGAGAAACAGAACAAAGCGG

2.2.9.Protein extraction

Isolation of whole cell lysate (WCL)

For extraction of whole cell lysate, cells were washed twice with ice-cold PBS, followed by lysis in WCL buffer. Subsequently, cells were scraped in lysis buffer and collected. After an incubation of 30 min on ice, samples were centrifuged at full speed for 20 min. The supernatant was used for Western blot analysis.

The protein concentration was measured using the Bio-Rad Protein Assay, following the manufacturer's manual. Samples and standard were measured in duplicates on a microtiter plate. As standard increasing concentrations of bovine serum albumin (BSA) solved in WCL buffer were used. To measure the absorbance at 595 nm using a photometer, 200 µL of the Bio-Rad Protein Assay

Reagent were mixed with 1 µL of the sample or the different standard solutions. Based on the standard curve, the concentration of the sample was calculated.

2.2.10. Western blot

For Western blot analysis, 20-30 µg protein in Laemmli Buffer [1x] were heated up to 95 °C for 5 min and loaded on a sodium dodecyl sulfate polyacrylamide gel electrophoresis (SDS-PAGE). For size indication, corresponding protein ladders were applied. After separation, proteins were transferred via the Trans-Blot Turbo Transfer system onto a nitrocellulose membrane for 15 to 35 min. After the transfer, membranes were blocked in blocking solution or BSA blocking solution (table 1) for 1 h at RT. The primary antibody was incubated over night at 4 °C in 5 % (w/v) milk/BSA in TBS-T. After washing the membrane in TBS-T (3x 10 min), the membrane was incubated with a secondary antibody (coupled with horseradish peroxidase (HRP)) diluted in 5 % milk (w/v) in TBS-T for 1 h at RT. After incubation, the membrane was washed again in TBS-T (3x 10 min), followed by detection via Chemocam Imager, using Western Lightening ECL/Ultra reagent.

Table 16. Antibody dilutions for Western blot.

Target	Species	Dilution/ Diluted in	Catalog Number	Company
β-actin – HRP coupled	mouse	1:40,000/ milk	A3854	Merck, Darmstadt, Germany
GSK3β	rabbit	1:1,000/ milk	9315	Cell Signaling Technology, Inc., Danvers, United States
NFATc1	mouse	1:500/ BSA	sc-7294	Santa Cruz Biotechnology, Dallas, United States
γH2AX	mouse	1:1,000/ BSA	80312	Cell Signaling Technology, Inc., Danvers, United States
HA	rabbit	1:1,000/ milk	3724	Cell Signaling Technology, Inc., Danvers, United States

Anti-rabbit IgG-HRP	goat	1:10,000/ milk	7074	Cell Signaling Technology, Inc., Danvers, United States
Anti-mouse IgG-HRP	horse	1:10,000/ milk	7076	Cell Signaling Technology, Inc., Danvers, United States

2.2.11. Immunofluorescence (IF)

Immunofluorescent stainings were performed on KPCbl6 cells seeded on coverslips. Cells were seeded, allowed to grow for 24 h, followed by treatment with cisplatin. After treatment, cells were fixed with 4 % PFA in PB for 10 min. After fixation, PFA was removed and cells washed twice with PB. Cells were permeabilized using 0.4 % Triton-X100 in PB for 10 min. Prior to the primary antibody, cells were blocked with 5 % normal goat serum (NGS) in PB for 1 h at RT. The primary antibody was incubated in 5 % NGS in PB (concentration indicated in table 17) over night at 4 °C. Cells were washed three times for 10 min with PB and incubated for 1 h with the secondary antibody (diluted in 5 % NGS in PB) at RT, washed again for three times, incubated for 3 min with DAPI (0.2 mg/mL), followed by three times washing. Cells were mounted on glass slides using Immomount.

Table 17: Antibody dilutions used for IF.

Target	Species	Dilution	Catalog number	Company
Alexa Flour 568-	Donkey	1:500	A10042	Thermo Fisher Scientific, Waltham, USA
GSK3β	mouse	1:500	GTX83315	GeneTex, Irvine, USA

2.2.12. Immunohistochemistry (IHC)

Tumor tissue of cisplatin-treated C57BL6 mice orthotopically transplanted with KPCbl6 cells was kindly provided by the group of Prof. Dr. Matthias Dobbelstein within the cooperation of KFO 5002. Furthermore, patient biopsies were a kind gift of Prof. Dr. Phillip Ströbel and the Department of Pathology. The TMA staining of NFATc1 were performed and graded by Nai-Ming Chen (AG Ellenrieder). The GSK3β TMA staining was kindly stained by the Department of Pathology by Hanibal Bohnenberger and graded by Nai-Ming Chen.

Tissue preparation

In brief, tissue was fixed in 4 % PFA (in PBS) at RT overnight followed by the dehydration in EtOH using a tissue processor. The tissue was transferred stepwise to increasing EtOH concentrations (55 %, 85 %, 96 %, 100 %, 100 %, 100 %, 1 h incubation each). Finally, the tissue was transferred to xylol three times (1 h each) and finally transferred to paraffin until embedding. Cooled blocks (4 °C, overnight) were cut in sections of 4 µm using a microtome. Sections were dried at 37 °C overnight.

Staining

The tissue sections were deparaffinized twice for 10 min in Roticlear, followed by rehydration in decreasing EtOH concentrations, (99 %, 99 %, 96 %, 80 %, 70 % and 50 %, 3 min incubation each). After three washes in tab water, slides were boiled in citrate buffer for 20 min and allowed to cool down for 30 min on ice. Followed by washing three times in tab water, slides were incubated in 3 % of H_2O_2 (in deionized H_2O) for 10 min. For blocking and antibody incubation, slides were fixed in the Shadon Sequenza system. After washing with PBS containing either 0.1 % (v/v) Tween-20 or Triton X-100 (PBS-T), non-specific antigens were blocked with 10 % (w/v) BSA in PBS-T for 1 h at RT. Antibody dilutions are indicated in table 17. The primary antibody was diluted in PBS-T containing 1 %

(w/v) BSA and incubated over night at 4 °C. Unbound antibody was removed by washing three times with PBS-T. The slides were incubated for 1 h with the corresponding biotinylated secondary antibody (Vectastain ABC kit). The secondary antibody was diluted 1:200 in PBS-T containing 1 % (w/v) BSA. After incubation, slides were washed three times with PBS-T and then incubated for 1 h with the AB-mix that was prepared half an hour before usage. For one slide, 1 µL of solution A and 1 µL of solution B were mixed with 200 µL of PBS-T. Subsequently, the slides were washed three times with PBS-T. The DAB Substrate Kit was used for signal detection after manufacturer's protocol. The reaction was stopped by transferring the slides into tab water. Afterwards, slides were stained for 3 min in hematoxylin and washed for 5 min in tab water. Before mounting, sections were dehydrated by increasing EtOH concentrations (70 %, 80 %, 96 %, 99 %, 2 min incubation each), followed by incubation in Roticlear (four times, 10 min each). Finally, sections were mounted with Rotimount and coverslips.

Table 18. Antibody dilutions for IHC.

Target	Species	Dilution/ Buffer	Catalog number	Company
GSK3β	rabbit	1:400/ Triton	12456	Cell Signaling Technology, Inc., Danvers, United States
γH2AX	mouse	1:100/ Triton	80312	Cell Signaling Technology, Inc., Danvers, United States

2.2.13. Chromatin immunoprecipitation (ChIP)

The ChIP protocol was adapted from Najafova et al.[148]. Cells were fixed with 1 % formaldehyde (in PBS) at RT for 20 min and quenched by adding glycerol (final concentration of 125 mM) for 5 min at RT. Plates were washed twice with ice-

cold PBS and 1.5 mL (for a 15 cm plate) of nuclear preparation buffer (containing 1x cOmplete). Cells were scraped, collected and centrifuged (2 min, 12,000 g, 4 °C). The nuclear pellet was washed with 1 mL of nuclear preparation buffer and centrifuged again. The remaining pellet was resuspended in 200-600 µL of Gomes Lysis Buffer (with 0.1 % (v/v) SDS) and incubated on a rotating wheel for 15 min at 4 °C. Samples were split in 200 µL fractions and sonicated for 20-30 cycles (30 s On/Off) with the Bioruptor Pico. Samples were pooled, centrifuged (10 min, 12,000 g, 4 °C) and the supernatant was collected. From each sample, 10 µL were used for the shearing check. Therefore, 1 µL Proteinase K (20mg/mL) and 0.3 µL of RNase (30 µg/µL) were added to the sample and incubated for 3 h at 55 °C and overnight at 65 °C. DNA fragments supplemented with 6x DNA loading dye were separated on a 1.5 % agarose gel (supplemented with Midori green). If the fragments had reached the required size, it was proceeded with the samples or samples sonicated a second time. Therefore, samples were diluted up to 500 µL with Gomes Lysis buffer (containing 1x cOmplete) and 100 µL of sepharose beads (50 % slurry in Gomes Lysis Buffer) were added and incubated (1 h, 4 °C, on a rotating wheel). After centrifugation (2 min, 12,000 g, 4°C), the supernatant was collected. The precleared sample was split for the different IPs, IgG control and input (control?). The aliquots were filled up with Gomes Lysis buffer (containing protease inhibitors) to a final volume of 500 µL and incubated with the antibody (1-2 µg/IP) overnight at 4 °C while rotating. The input was frozen until further processing. Sepharose beads were blocked with 1 mg/mL BSA in Gomes Lysis Buffer at 4 °C while rotating overnight. Beads were washed three times with Gomes Lysis Buffer and centrifuged for 2 min at 1,000 g. After the final removal of the lysis buffer, lysis buffer was added in a 1:1 ratio to the beads for a 50 % slurry. To each IP,30 µL of blocked beads were added and incubated for 2 h (rotating, 4 °C). The complexes were washed once with Gomes Lysis Buffer (1 mL), twice with Gomes Wash, once again with Gomes Lysis Buffer and twice with TE buffer. For isolation of the DNA, 50 µL Tris (10 mM, pH 8.0) with RNase (0.2 µL) were added to the samples and incubated for 30 min at 55 °C. Then, 50 µL 2x Weinmann Buffer and 1 µL Proteinase K (20 mg/mL) were added and the samples incubated overnight at 65 °C. The samples were centrifuged (2,000 g, 2

min) and the supernatant was collected. 100 µL Tris (10 mM, pH 8.0) were added to the beads, incubated (10 min, 65 °C, 800 rpm) and centrifuged (5,000 g, 2 min). The supernatant was added to the first fraction and supplemented with 10 µL LiCl (8 M), 4 µL linear acrylamide and 200 µL phenol/chloroform/isoamyl mix (25:24:1), vortexed for 30 s and centrifuged for 2 min at full speed. The aqueous phase was collected. To the phenolic phase, 200 µL Tris (10 mM, pH 8.0) and 0.4 M LiCl were added, vortexed for 30 s and centrifuged for 2 min at full speed. The aqueous phase was added to the first fraction. 1 mL 100 % EtOH was added and the mixture incubated for at least 2 h at -80 °C. After centrifugation (15,000 g, 30 min, 4°C), the supernatant was removed, the pellet washed once with 70 % EtOH and centrifuged again (15,000 g, 30 min, 4°C). The pellet was allowed to dry and finally resuspended in 80 µL nuclease free H_2O. The samples were further analyzed via qRT-PCR.

Table 19: Antibody dilutions for ChIP.

Target	Species	Dilution	Number	Company
NFATc1	rabbit	8 µL	ab25916	Abcam, Cambridge, Great Brittan
Rabbit IgG	rabbit	1 µg	C15410206	Diagenode Inc., Denville, United States

2.2.14. RNA sequencing

Sequencing of mRNA (non-stranded) was performed in triplicates of L3.6 cells with knock-down of GSK3β, control treatment and treatment with the GSK3β inhibitor AR-A 014418 (10 µM) for 48 h. RNA was isolated as described in 1.2.7. and its quality checked via an RNA gel. Therefore, samples were loaded on a 1 % agarose gel (containing Midori Green Advance) to determine RNA integrity. Bands were visualized using the GelDoc. Library preparation was performed by using the TruSeq RNA Library Prep Kits and following the manufacturer's protocol. The final product concentration was measured via Qubit. Further, the fragment sizes and purity were analyzed by using the Agilent Bioanalyzer 2100 (high sensitivity DNA analysis kit, Agilent 5067-4626). Samples were pooled in

an equal ratio and sequenced by the NGS Integrative Genomics Core Unit, University Medical Center Göttingen, Germany.

Sequencing data analysis

The provided FastQ files were analyzed on usegalaxy.org[149]. For quality control, the FASTQC (version 0.65)[141] was used. The sequences were trimmed by 11 bases at the 5' end using the FASTQ trimmer (version 1.0.0)[142]. TopHat tool (version 2.1.1)[145] was employed for mapping to the human transcriptome (hg19) under very sensitive bowtie2 settings, followed by SortSAM (version 2.18.2.1)[150]. Read counts were obtained by HTSeq (version 0.6.1p1; -f bam -r pos -s reverse -a 10 -t exon -m union)[143]. Differential gene expression was analyzed via DESeq2 (version 2.11.40.6)[140]. For subsequent pathway analysis, genes with log2fold values ≥ 0.5 and ≤ -0.5, padjusted ≤ 0.05, were used. Differential gene set analysis was performed using GSEA (version 4.0.3)[151,152] as well as gene ontology analysis (geneontology.org) via Panther overexpression test (version 15.0, Fisher's exact test, false discovery rate (FDR)) with GO database or Reactome pathway database. Heatmaps of selected genes were generated with GraphPad Prim7 using log2fold changes.

2.2.15. Data analysis

Statistical analysis was performed with Graph Pad Prism7 using the unpaired student t-test and indicating significances with * $p < 0.05$, ** $p < 0.01$, and *** $p < 0.001$. Graphs show the mean of three biological replicates and standard deviation (SD) if not indicated differently.

3. Results

In this study, we investigate the oncogenic role of GSK3β in the context of pancreatic cancer. GSK 3β is known to be highly expressed in dedifferentiated tumors of PDAC and involved in regulating cell growth and chemoresistance.[60,77,83,105] However, a deeper understanding of the molecular mechanisms underlying these effects is necessary to develop better targeted therapies. This study aims to uncover these mechanisms with the overall goal of defining subgroups of pancreatic cancer patients that will benefit from therapy with GSK3β inhibitors.

3.1. GSK3β is associated with poor survival in PDAC patients

GSK3β was reported to either have tumor promoting or suppressive role depending on the origin of the tumor and the cellular context. GSK3β was reported to mainly play an oncogenic role in the case of pancreatic cancer.[60,77,79] To validate this, we analyzed the expression and protein levels in three different cohorts, composed the publicly available TCGA (Cancer Genome Atlas Database) database, a cohort of tissue microarrays, and tumors of patient derived xenografts. The TCGA database consists of 172 pancreatic cancer patients from which we selected for the survival analysis the 25% percentile with the highest and lowest expression values (OncoLnc.org). This revealed that high mRNA expression of GSK3β correlates with worse overall survival rates in PDAC patients (Fig.5A).

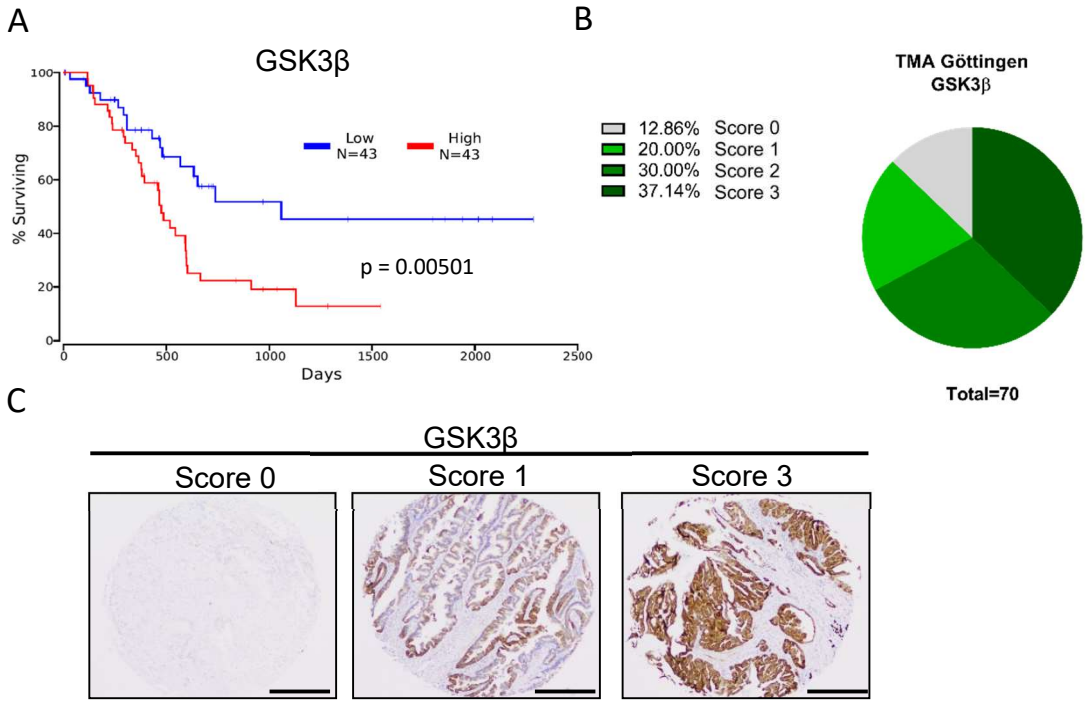

Figure 5: GSK3β expression correlates with survival in human pancreatic cancer samples. A) TCGA analysis by OncoLnc (Anyada et al., 2016) shows a significant correlation between the expression of GSK3β and the survival of patients as depicted in the Kaplan Meyer plot. The survival of the low and high GSK3β expression, displaying the 25 % of the upper and lower percentile of GSK3β expression among the patient cohort. B) GSK3β staining of TMA showing different expression levels in pancreatic cancer patients of the Göttingen cohort. Patients were scored into four different groups (0-3) based on their expression. The score represents negative staining as 0 and gradually increases to 3 as the highest intensity of GSK3β signal. C) Representative pictures of the GSK3β scores, displaying the intensity of GSK3β in PDAC tumor tissue. Scale bar indicates 100 µm.

An independent cohort of 70 PDAC patients was dissected in regard of the tumor composition in cooperation with Dr. Hanibal Bohnenberger (Institute of Pathology, Göttingen) and Dr. Nai-Ming Chen. Consistently, evaluation of the human tissue microarrays (TMA) from the obtained patient samples showed a high expression of GSK3β in almost two thirds of the analyzed tumors (Fig. 5B). Representative pictures of the TMA display the differences in GSK3β levels (Fig. 5C). Furthermore, we analyzed the GSK3β expression in a cohort of patient-derived xenografts (PDX) (n=29). Our findings in PDX tissue were consistent with the TMA as we similarly observed high expression of GSK3β in various PDXs (Fig. 6A). Moreover, nuclear GSK3β was seen in about 10% of all tumors.

Nuclear localization of GSK3β has been shown to be indicative for a particular aggressive phenotype in pancreatic cancer[77]. In addition, cells isolated from PDX tumor tissue (CDX) were tested for their GSK3β expression levels in comparison to the well-established murine KPCbl6 cell line. Interestingly, differences observed in the PDX tissue can also be displayed by protein levels in the CDX (Fig. 6B). Therefore, testing in CDX cell lines provides a platform which enables us to test our findings in cell lines derived of tumors, representing different subtypes of PDAC, prior to *in vivo* verification.

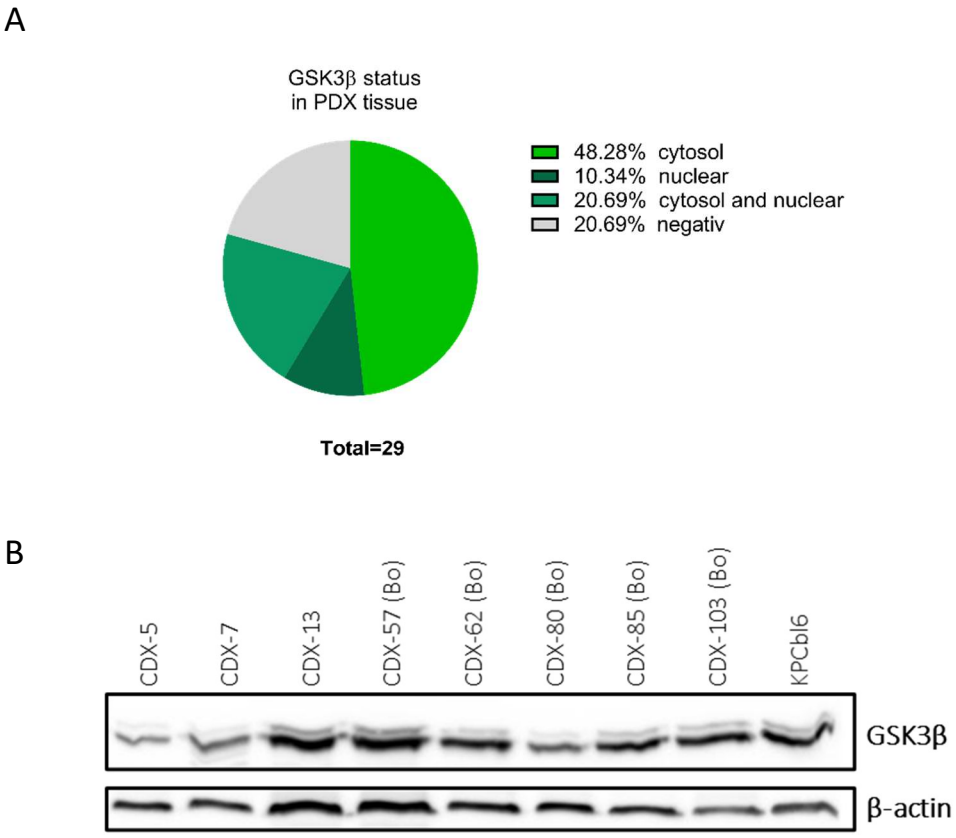

Figure 6: GSK3β in patient-derived xenograft (PDX) models. A) PDX tumor sections were stained for GSK3β by IHC and subsequent analyzed based on their localization. B) Whole cell protein lysates of various CDXs were tested via western-blot to evaluate their GSK3β expression levels under normal growth conditions. β-actin served as a loading control.

3.2. Inhibition of GSK3β leads to decreased proliferation and induction of cell cycle arrest

Next, we studied the functional consequences of GSK3β inhibition on pancreatic cancer cell proliferation and viability. For this purpose, we performed MTT assays in human L3.6pl cells and in metastatic KPCbl6 cells, which were derived from the KPC (K-ras$^{LSL.G12D/+}$; Trp53$^{R172H/+}$; Pdx-1-Cre) mouse model[146]. L3.6pl is a well-established cell line, representing the highly aggressive and chemotherapy resistant basal-like phenotype[153]. Both cell lines were cultured in serum-containing media and in the presence of increasing doses of AR-A 014418 (AR-A), a specific GSK3β inhibitor[154]. We were able to demonstrate a dose-dependent decrease in cell viability in both models (Fig. 7). Notably, L3.6pl cells showed a higher sensitivity towards GSK3 inhibition than KPC cells.

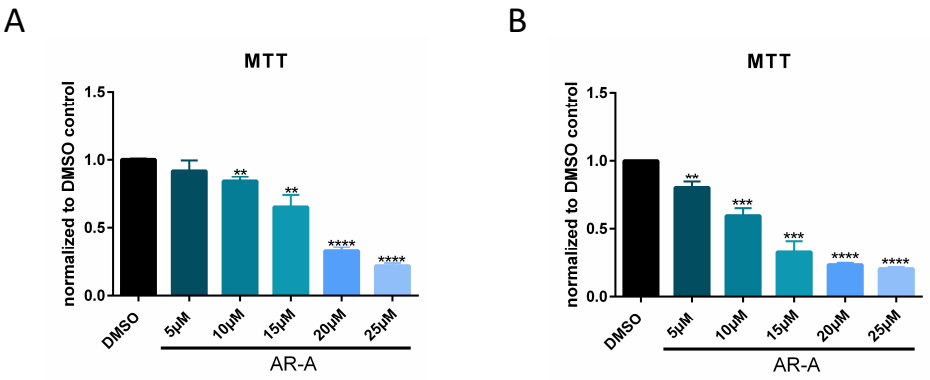

Figure 7: GSK3β leads to decreased proliferation and cell viability. MTT assays were performed after 72 h of treatment with AR-A and show a dose dependent decrease of cell proliferation and cell viability in KPCbl6 (A) and L3.6pl (B), n=3 (biological replicates with 5 technical replicates); unpaired student t-test of biological replicates; ** p≤ 0.01, *** p≤ 0.001, **** p ≤ 0.0001, mean +SD.

To confirm these findings, we extended our proliferation analysis and treated an additional set of CDXs with increased concentrations of AR-A. Interestingly, these cell lines were derived from PDXs with various localization patterns of GSK3β. PDX-13 exhibiting higher nuclear accumulation compared to the cytosolic accumulation in PDX-57 (Bo) (Fig. 8A). However, their total GSK3β expression levels do not differ on the CDX level. Interestingly, CDX-13 cells, which are derived from the PDX-13, were more sensitive to GSK3β inhibition compared to CDX-57(Bo) cells (Fig. 8B). This implies that nuclear GSK3β levels can be predictive of cells sensitivity to AR-A treatment.

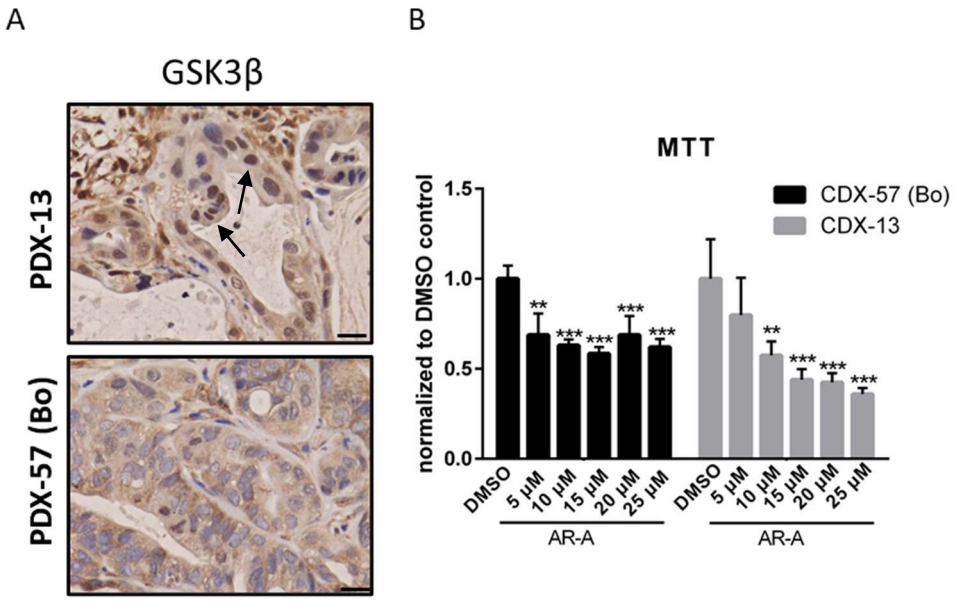

Figure 8: PDX-derived cell lines respond differently to GSK3β inhibition. A) Representative pictures of PDX13 and PDX-57 (Bo) that was used to derive cell lines (CDX), PDX-13 shows a higher nuclear localization (indicated by arrow) of GSK3β in comparison to PDX-57 (Bo). Scale bar indicates 20 µM. B) CDX cells lines were treated for 72 h with AR-A and the cell viability measured via MTT assay. CDX.13 showing a higher sensitivity towards AR-A treatment. n=3 (biological replicates with n=5 technical replicates); unpaired student t-test of biological replicates - comparison of DMSO to single treatments for each individual cell line; ** p≤ 0.01, *** p≤ 0.001, mean +SD,

Upon validation of the growth limiting effects of GSK3β inhibition, we tested its impact on cell cycle transition. Therefore, we performed flow cytometry analysis in both cell lines using increasing concentrations of the inhibitor. These studies revealed that GSK3 inhibition by AR-A treatment causes a dose-dependent G2/M cell cycle arrest in pancreatic cancer cells (Fig. 9).

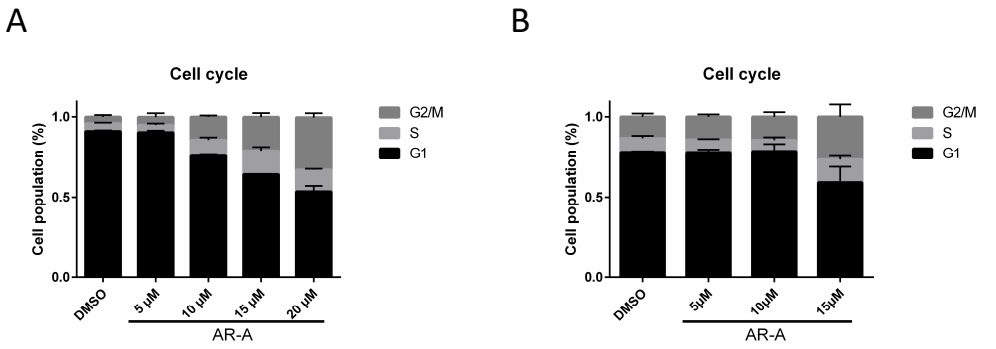

Figure 9: Cell cycle analysis in KPCbl6 and L3.6. Cell cycle analysis via flow cytometry in KPCbl6 (A) and L3.6 (B). Cells, treated with increasing concentrations of the GSK3β inhibitor AR-A for 24 h, show the induction of G2/M arrest. n=3 (biological replicates), mean +SD.

3.3. GSK3β inhibition leads to the induction of DNA damage-related gene signatures

To elucidate the molecular mechanisms underlying the oncogenic role of GSK3β in pancreatic cancer, we performed gene expression profiling by mRNA sequencing in L3.6pl cells which are highly responsive to AR-A treatment. Cells were treated with AR-A (10 µM) or DMSO as control and RNA was isolated for subsequent transcriptome-wide expression. The treatment duration of 48 hours was determined as time-point with minimal cell death while observing stable effects on the transcriptional level to ensure the uncovering of direct effects of GSK3β perturbation.

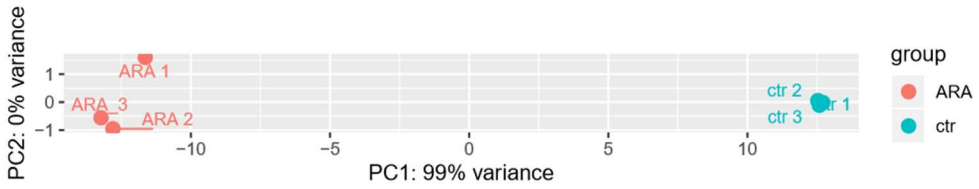

Figure 10: Principal component analysis of mRNA-seq in L3.6. PCA plot of control group and AR-A treated samples by DESeq2 analysis.

Differential genes expression analysis via DESeq2[140] revealed about 6000 regulated genes (log2fold change ≤ -0.5, ≥ 0.5; q ≤ 0.05) while 3718 genes being downregulated. Principle Component Analysis (PCA) showed clustering within the replicates but not between the conditions which supports high homogeneity between the replicates (Fig. 10). Additionally, the first principle component accounted for 99% the variability between conditions indicating that the differences between the treated and untreated cells is due to the treatment and not to any other technical factors. Furthermore, Gene Set Enrichment Analysis (GSEA) [151,152] (Fig. 11) confirmed downregulation of previously described GSK3β target genes, e.g. members of the AKT signaling pathway and genes involved in glycolysis. These results are consistent with a recent publication by Brunton et al. (2020) reporting GSK3β-mediated regulation of glycolysis, especially in squamous subtypes. In addition, our profiling analysis demonstrated a strong transcriptional repression of EMT gene signatures, indicating a role of GSK3β in

transcriptional regulation of cell plasticity and invasion and of cell cycle control genes. In addition, we observed the regulation of metabolic processes and protein transport via microtubules to be affected (Fig. 12). Thus, supporting findings of GSK3β participation in those pathways.[33,155] We found differential expression of key DNA repair mechanisms, most prominently BRCA1, and interestingly also genes involved in cisplatin responses (Fig. 11). To identify genes that are transcriptionally dependent on GSK3β, we focused our analysis on downregulated genes upon its pharmacological inhibition by AR-A. Gene ontology (GO) enrichment analysis of significantly downregulated genes upon AR-A treatment confirmed DNA double strand repair and DNA replication gene sets (Fig. 12). The revealed pathways in GSEA and GO analysis have in common to regulate different DNA damage repair mechanisms as homologous recombination, regulating signatures of important proteins of this process as BRCA1 or to modulate a general response to DNA damage. Furthermore, we observe signatures downregulated under GSK3β that are connected to a response to cisplatin. Cisplatin induced DNA damage is repaired by different pathways including HR, connecting these findings to the DNA damage repair signatures. Taken together, these pathways implicate a role of GSK3β in DNA damage repair.

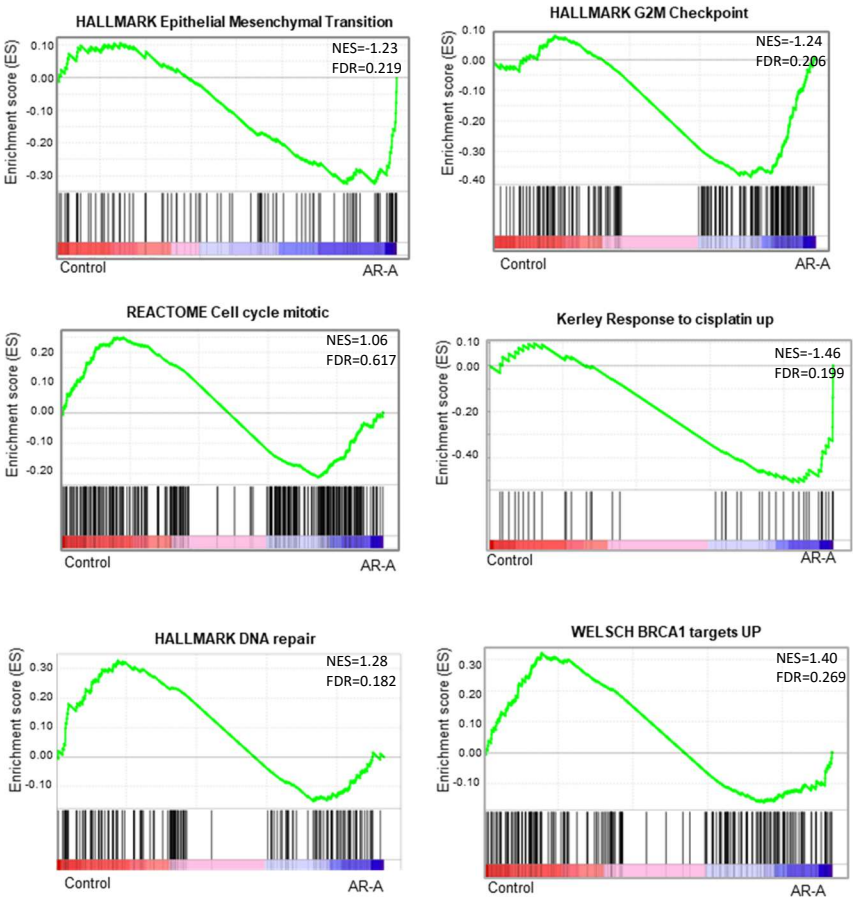

Figure 11: GSEA analysis shows downregulation of DNA repair pathways and EMT. Norm-counts of significantly regulated genes (log2fold change ≤ -0.5, ≥ 0.5; q ≤ 0.05) of DESeq2 analysis were used to perform GSEA analysis, showing the regulation of pathways related to EMT, glycolysis, cell cycle regulation and DNA repair.

Rank	GO biological process	Fold Enrichment	FDR
1	intraciliary transport involved in cilium assembly (GO:0035735)	3.58	2.49E-02
2	GPI anchor biosynthetic process (GO:0006506)	3.46	2.14E-02
3	intraciliary transport (GO:0042073)	3.38	7.54E-04
4	GPI anchor metabolic process (GO:0006505)	3.36	2.55E-02
5	mannosylation (GO:0097502)	3.17	2.75E-02
6	protein transport along microtubule (GO:0098840)	2.82	3.86E-03
7	microtubule-based protein transport (GO:0099118)	2.82	3.79E-03
8	protein localization to cilium (GO:0061512)	2.77	2.31E-02
9	recombinational repair (GO:0000725)	2.64	5.47E-04
10	double-strand break repair via homologous recombination (GO:0000724)	2.63	7.68E-04
26	double-strand break repair (GO:0006302)	2.19	2.53E-04
27	fatty acid catabolic process (GO:0009062)	2.15	4.76E-02
28	cellular amino acid catabolic process (GO:0009063)	2.05	3.68E-02
29	DNA replication (GO:0006260)	2.04	4.31E-04
30	DNA-dependent DNA replication (GO:0006261)	2	3.14E-02
42	glycosylation (GO:0070085)	1.74	1.98E-02
47	DNA repair (GO:0006281)	1.57	4.16E-03
58	DNA metabolic process (GO:0006259)	1.42	1.07E-02
59	cellular response to DNA damage stimulus (GO:0006974)	1.39	2.43E-02

Figure 12: GSK3β inhibition leads to downregulation of DNA damage-related gene signatures. Gene ontology analysis (geneontology.org) by PANTHER, using significantly downregulated genes (log2fold change ≤ -0.5; q ≤ 0.05), showing overrepresented biological processes with an FDR < 0.05.

3.3.1. Comparative analysis of genes regulated by GSK3β inhibition and knockdown

To validate the specificity of the findings under GSK3β inhibition, we next performed mRNA-seq of L3.6pl cells upon siRNA-mediated knockdown of GSK3β. DESeq2 analysis revealed a clustering of the treatment conditions (Fig. 13). However, GSK3β inhibition and knockdown conditions show differences in their profiles.

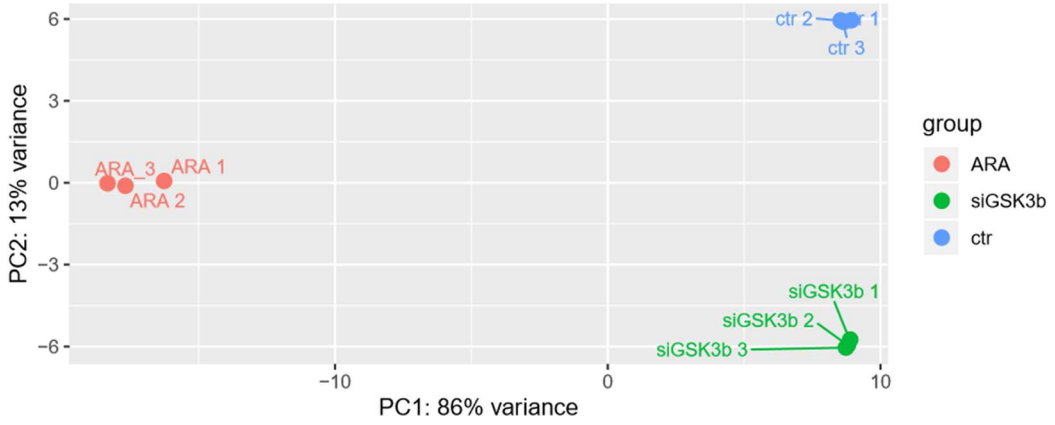

Figure 13: PCA blot of RNA-seq in L3.6pl including GSK3β knockdown. PCA plot of the control group, AR-A-treated samples and siGSK3β by DESeq2 analysis.

Subsequently, we compared up and downregulated by AR-A as well as GSK3β knockdown (log2fold change ≤ -0.5, ≥ 0.5; q ≤ 0.05). The analysis of the 640 genes which were downregulated under both conditions (Fig. 14A) confirmed the transcriptional regulation of DNA damage repair signatures involved in double-strand break repair or homologous recombination. Based on the results of the Gene Ontology and GSEA analysis a collection of genes important in the regulation of DNA damage repair and cisplatin response were selected. Those are visualized in the heatmap in Fig. 14B. Thus, important genes for DNA damage repair are downregulated upon knockdown GSK3β, although not as strong as by GSK3β inhibition.

A

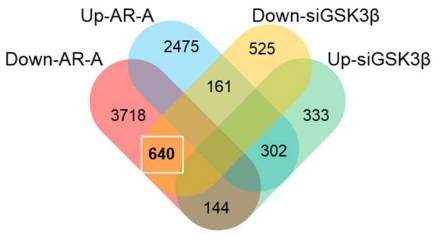

Pathway Name	Adjusted p-value
Double-Strand Break Repair	0.0730
Homologous recombination repair of replication-independent double-strand breaks	0.0852
Homologous Recombination Repair	0.0852
Recruitment of repair and signaling proteins to double-strand breaks	0.1022
serine biosynthesis	0.1022
BARD1 signaling events	0.1643
Fanconi anemia pathway	0.2190
Superpathway of serine and glycine biosynthesis I	0.2591
NADE modulates death signalling	0.2591
Unwinding of DNA	0.2591

B

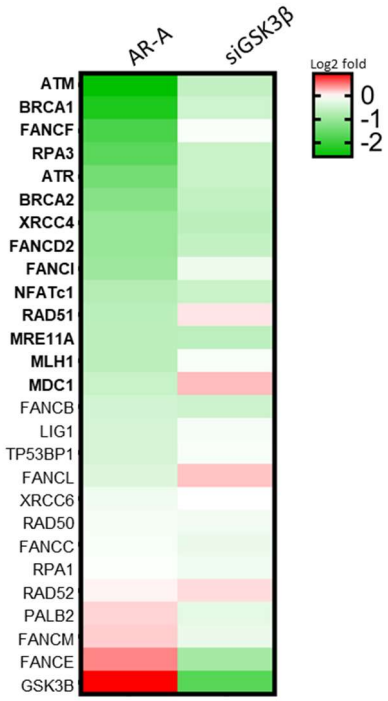

Figure 14: Downregulated gene signatures by AR-A treatment and siGSK3β. A) Number of genes regulated by AR-A treatment or siGSK3β. 650 genes are downregulated by AR-A and siGSK3β. Those were utilized for enrichment analysis (Pathway Commons analysis; webgestalt.org), showing that the top ten enrichment of pathways are related to DNA damage and DNA replication. B) Log2 fold changes of selected genes involved in DNA repair. Those genes significantly downregulated under AR-A treatment are marked in bold, displaying a difference in strength between inhibition and knockdown.

To further validate our findings, we verified the downregulation of crucial genes involved in DNA repair using qRT-PCR. Indeed, we were able to verify that genes with implications in DNA damage repair were downregulated upon AR-A treatment (Fig. 15). Mutational loss or transcriptional silencing of these genes is associated with severe defects in HR and DNA repair, increased sensitivity towards platinum-based chemotherapy and PARP inhibitors.[156] Tumor subtypes with defects in homologous recombination are defined as “BRCAness” tumors. Of note, BRCAness induced defects in HR mechanisms often compensate for repair disturbances through increased non-homologous end joining, resulting in higher chances to accumulate aberrations.[136] Thus, we hypothesize that the inhibition of GSK3β causes an “inducible” BRCAness phenotype that is initiated by transcriptional downregulation rather than genetic mutations in BRCA genes.

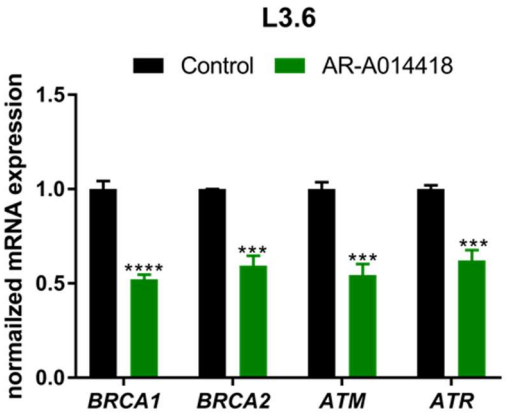

Figure 15: Representative genes related to DNA damage repair are downregulated by AR-A. L3.6 cells were treated for 48 h with 10 µM AR-A. Expression levels were normalized to the housekeeping gene RPLP0 and further normalized to the control treatment. Mean +SD, n=3 (biological replicates with 3 technical replicates), unpaired student t-test; *** p≤ 0.001, **** p ≤ 0.000.

3.4. DNA damage is induced by GSK3β inhibition

Based on the results of our mRNA-seq analysis, we aimed to further determine if the regulation of genes by GSK3β, involved in homologous recombination and in general DNA damage repair, have a biological relevance. Moreover, the strong regulation of genes like *BRCA1* or *BRCA2* suggested that co-treatment (of GSK3β inhibitors) and DNA damaging agents (e.g. cisplatin) or PARP inhibitors in pancreatic cancer cells[157] could be beneficial.

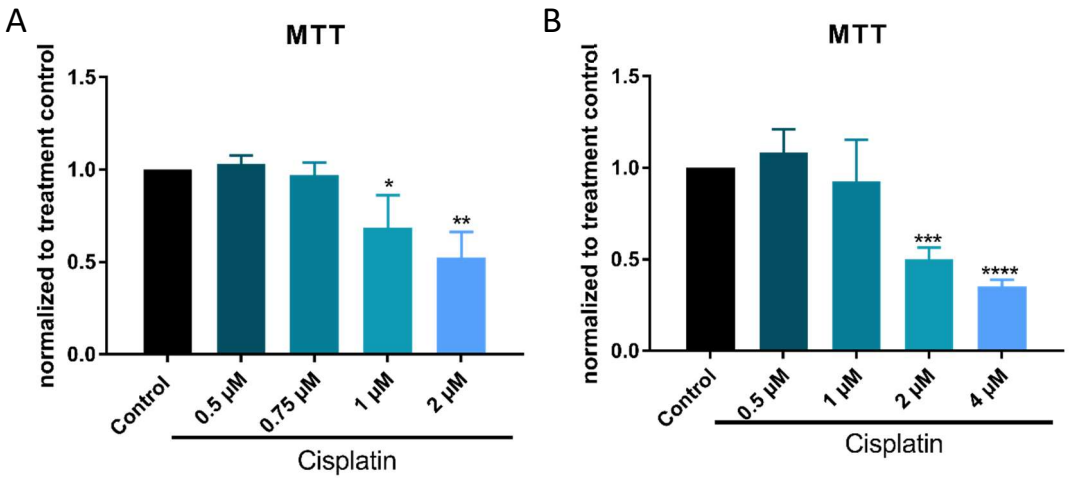

Figure 16: Cisplatin treatment in KPCbl6 and L3.6. Cells (KPCbl6 (A), L3.6pl (B)) were treated with increasing concentrations if cisplatin (solved in H_2O) for 72 h. The cell viability was evaluated by MTT assay in KPCbl6 and L3.6. Mean +SD, n=3 (biological replicates with 5 technical replicates), unpaired student t-test, * p≤ 0.05, ** p≤ 0.01, *** p≤ 0.001, **** p ≤ 0.0001.

To test our hypothesis, we first evaluated the sensitivity of KPCbl6 and L3.6pl cells to cisplatin treatment (Fig. 16) and demonstrate only moderate growth inhibition upon treatment with 1 µM cisplatin. This concentration was used for further studies. Next, we simultaneously treated KPCbl6 and L3.6pl cells with cisplatin or AR-A alone, or in combination for 24 h and stained for γH2A.X, a well-established DNA damage marker[158]. While single treatment with either cisplatin or AR-A alone already induced a moderate γH2A.X increase, the combination of both agents resulted in severe DNA damage (Fig. 17).

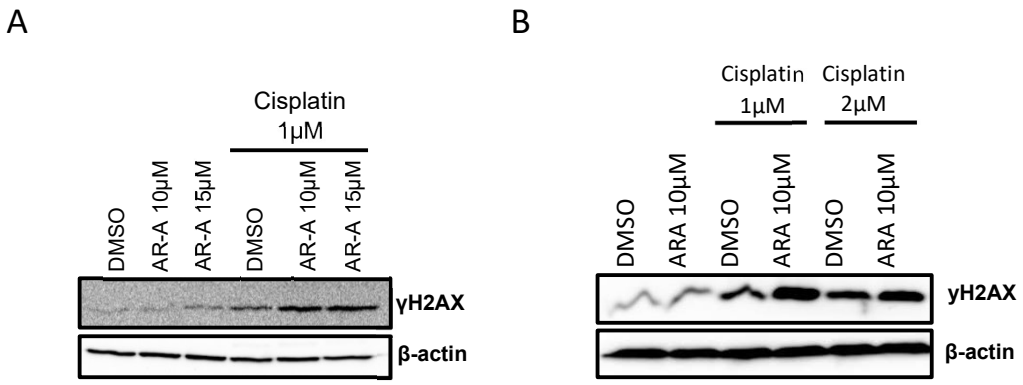

Figure 18: Simultaneous treatment of AR-A and cisplatin increased DNA damage *in vitro*. KPCbl6 (A) and L3.6 (B) cells were treated with 10µM AR-A, 1µM cisplatin and their combination for 24 h. After treatment, DNA damage was determined by detecting γH2AX. β-actin serves as loading control. β-actin serves as loading control.

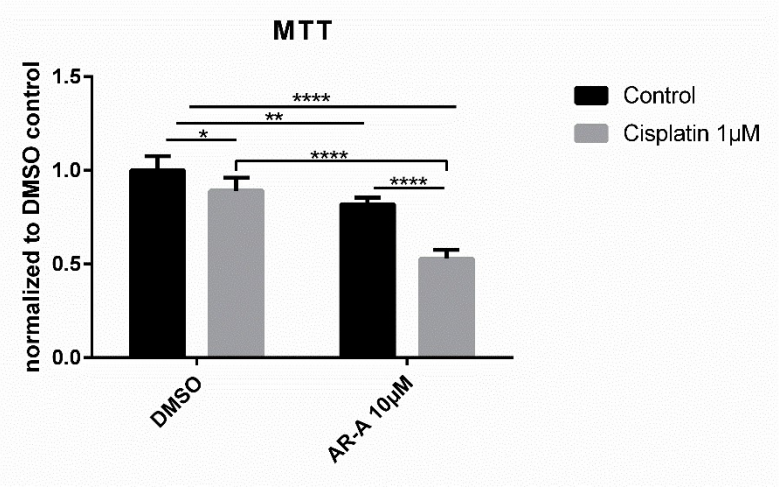

Figure 17: KPCbl6 cells show reduced proliferation under treatment of AR-A and cisplatin. MTT assay in KPCbl6 cells after 48 h treatment with 10 µM AR-A, 1µM cisplatin or their combination shows a decrease of cell viability when combining the treatments. Mean +SD, n=3 (biological replicates with 5 technical replicates), unpaired student t-test, * p≤ 0.05, ** p≤ 0.01, **** p ≤ 0.0001.

Together, these experiments suggested that inactivation of the GSK3β kinase enhances the DNA damage induced by cisplatin in pancreatic cancer cells. In line with the enhanced levels of DNA damage we induced an accentuated growth reduction via MTT assay caused by the combination of AR-A and cisplatin treatment (Fig. 18).

3.4.1.DNA damage induction is reproducible upon GSK3β knockdown and a different GSK3β inhibitor

To confirm this model, we carried out an additional set of experiments and treated pancreatic cancer cells with cisplatin in the presence and absence of endogenous GSK3β. For this purpose, we silenced GSK3β in KPCbl6 cells before treatment with cisplatin for 24 hours (Fig. 19A).

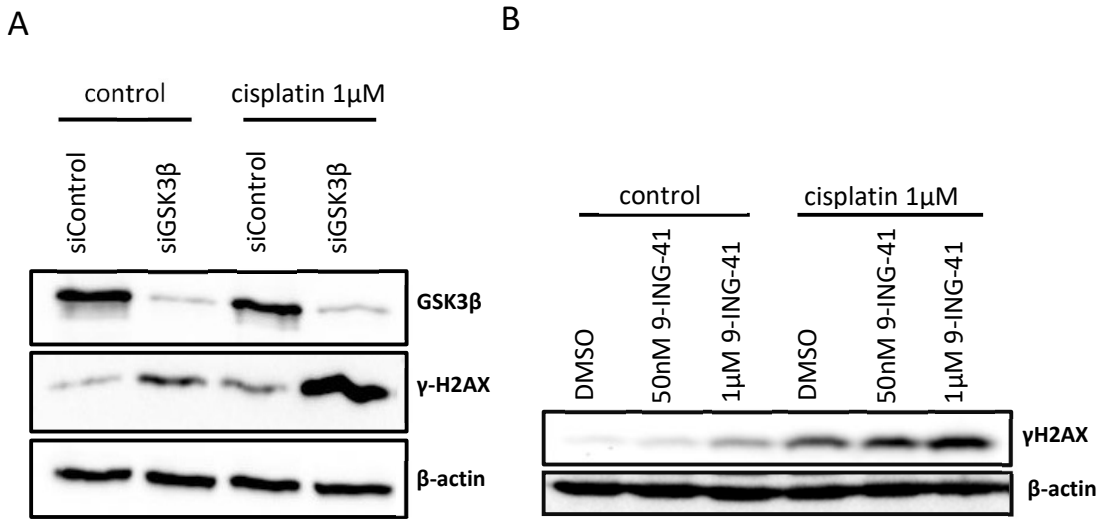

Figure 19: DNA damage is increased by co-treatment with 9-ING-41 or GSK3β knockdown. A) siRNA mediated knockdown of GSK3β was performed for six hours followed by cotreatment with 1 µM cisplatin for 24 h in KPCbl6 cells. B) GSK3β inhibitor 9-ING-41 was combined with cisplatin for 24 h in KPCbl6 cells. DNA damage was evaluated by γH2AX levels. β-actin serves as loading control.

Importantly, GSK3β silencing caused a moderate induction of DNA damage and strongly sensitized pancreatic cancer cells to cisplatin treatment. In fact, we observed a significant and robust increase in DNA damage, as indicated by a strong increase in γH2A.X staining. These results confirmed our pharmacological studies using AR-A and emphasized a critical role of GSK3β inhibition in sensitization of cells towards cisplatin. In line with this conclusion, application of another GSK3β inhibitor, named 9-ING-41, caused a robust increase in DNA damage imposed by cisplatin (Fig. 19B) to a similar extent than AR-A.

3.4.2. GSK3β inhibition induces sensitivity towards various DNA damaging agents

As our hypothesis claims the induction of a BRCAness phenotype through GSK3β inhibition, we sought to verify this effect by testing AR-A treatment in combination with other chemotherapeutic agents, as well as PARP inhibition. For chemotherapy, we decided to treat cells with SN-38, the activated form of irinotecan, part of the FOLFIRINOX treatment regime for pancreatic cancer patients. For inhibition of PARP, we treated cells with Olaparib. The co-treatment of AR-A with SN-38 enhanced the effect of the single drugs on DNA damage levels (Fig. 20A). Also, the combination of AR-A with Olaparib had a beneficial effect in decreasing cell viability (Fig. 20B).

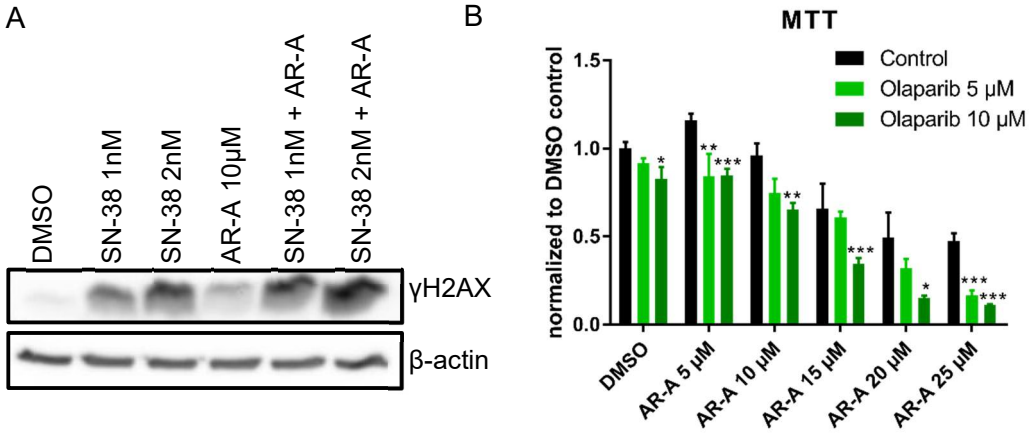

Figure 20: GSK3β inhibition sensitized cells towards treatment with PARP inhibitors and SN38. A) L3.6 were treated with SN38, the activated form of irinotecan, and AR-A for 24 hours. Cells displayed an increase of DNA-damage if cotreated. β-actin serves as loading control. B) KPCbl6 cells were treated with Olaparib, a PARP inhibitor, and AR-A for 48 hours, followed by evaluation of cell viability by MTT assay, whereby co-treatment decreases cell viability. Mean +SD, n=3 (biological replicates with 5 technical replicates), unpaired student t-test, * p≤ 0.05, ** p≤ 0.01, *** p≤ 0.001.

3.4.3. GSK3β inhibition induced DNA damage is dependent on the BRCA mutation status

To test, if the effect we observe on DNA damage levels is based on the downregulation of *BRCA1* and *BRCA2,* we studied other cell lines than KPCbl6 and L3.6pl. As both do not contain known BRCA mutations. Therefore, we compared CAPAN1 and CAPAN2 cells. CAPAN1 cells comprise a *BRCA2* mutation, leading to a truncated protein and a loss a function.[159] This leads for CAPAN1 to display higher sensitivity towards cisplatin treatment. On the other hand, CAPAN2 cells are devoid of a BRCA mutation. We treated both cell lines with AR-A for 48 and 72 hours and compared their DNA damage level. We could observe that AR-A does not affect the DNA-damage levels irrespective of the duration of the treatment in CAPAN1 (Fig. 21). Conversely, we detected an increase of DNA damage under AR-A treatment in CAPAN2 cells further supporting our model that pharmacological inhibition of GSK3β leads to BRCAness-like phenotype that cannot be induced in the already BRCA-mutated CAPAN1.

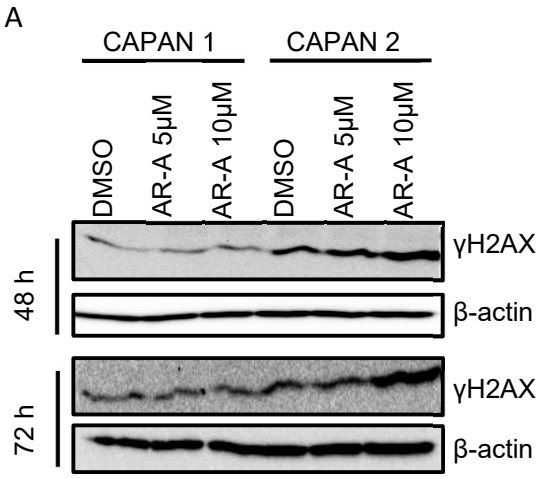

Figure 21: Cell line specific response to GSK3β inhibition. CAPAN1 and CAPAN2 cells were treated for 48 and 72 hours with AR-A (5 and 10 μM). Only in CAPAN2 does AR-A induce DNA damage. β-actin servers as loading control.

3.5. GSK3β accumulates in the nucleus upon cisplatin treatment

Based on our observation that GSK3β inhibition induces DNA-damage and most importantly sensitize the cells to cisplatin treatment, we wanted to test how treatment with cisplatin influences GSK3β. Therefore, we decided to test tumor sections of mice treated with cisplatin or control treatment. These were kindly provided by Katharina Ewers (Institute of Molecular Oncology, University of Göttingen). Prior the treatment, mice have been orthotopically transplanted with KPCbl6 cells. After the development of tumors, mice were treated for two weeks, whereby the group of cisplatin treated mice, received 4 mg/kg two times per week. The sections were stained for GSK3β and as treatment control for γH2AX.

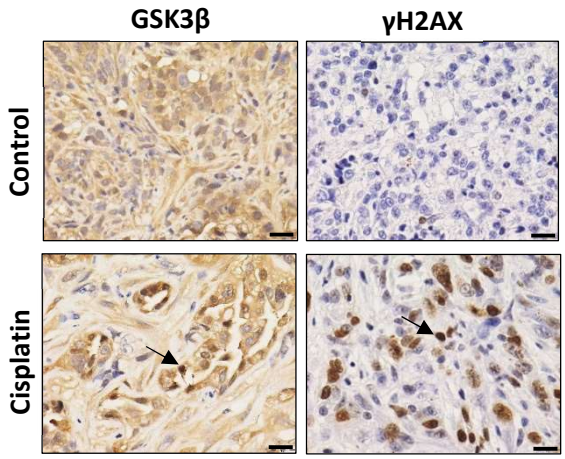

Figure 22: Cisplatin treatment induced GSK3β expression *in vivo*. Orthotopically transplanted KPCbl6 cells (in C57BL6 mice) were treated for two weeks (two injections i.p. [4 mg/kg.] /week) with cisplatin. Pictures show representative staining of control and treated mice. Arrow indicates nuclear localization of GSK3β and γH2AX in cisplatin treated mice. Scale bar indicates 20 µM.

Interestingly, we were able to observe a stronger nuclear localization of GSK3β in cells (Fig. 22). Expectedly, the level of γH2AX increased under cisplatin treatment.

Additionally, we performed immunofluorescence staining of GSK3β in KPCbl6 cells after 24 hours of treatment with 1 µM of cisplatin. The short-term treatment induced nuclear localization of GSK3β, associated with a more aggressive phenotype[77], in comparison with the control cells. (Fig. 23). Thus, confirming the *in vivo* results of orthotopically transplanted KPCbl6 cells.

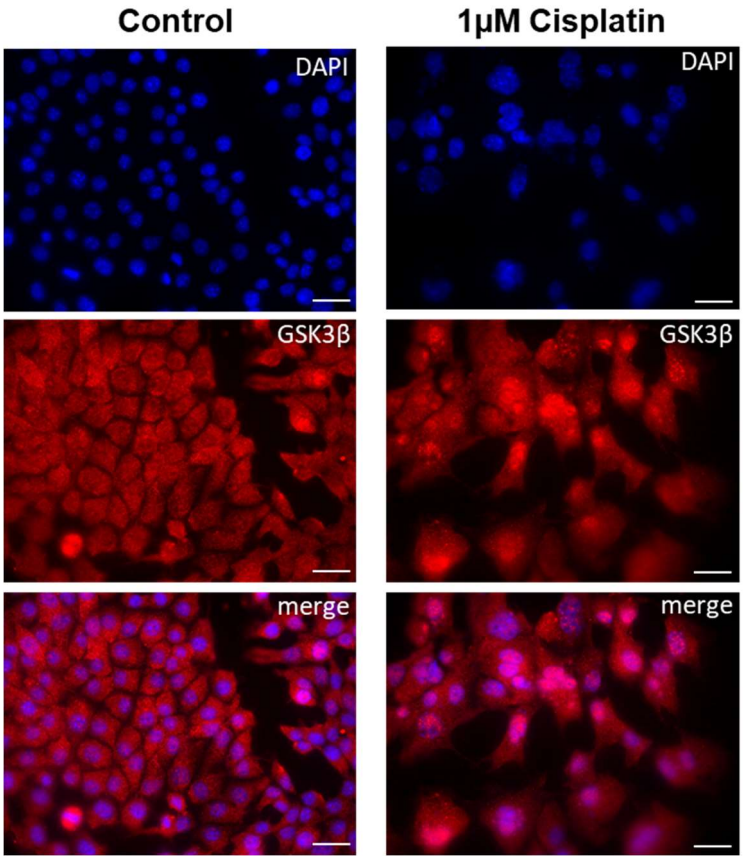

Figure 23: Cisplatin treatment induces nuclear shift of GSK3β *in vitro*. KPCbl6 cells, treated with 1 µM of cisplatin for 24 h and subsequently stained for GSK3β (red) using immunofluorescence. Nucleus was stained with DAPI (blue). Representative pictures showing a nuclear shift of GSK3β induced by cisplatin. Scale bar indicates 25 µm.

Based on the upregulation and most important the nuclear localization of GSK3β observed under cisplatin treatment in tumors and KPCbl6 cells, we aimed to test how increasing levels of GSK3β influence the response to cisplatin.

For this purpose, we overexpressed GSK3β in KPCbl6 cells, followed by cisplatin treatment for 24 hours (Fig. 24). Therefore, we overexpressed a wildtype GSK3β. Interestingly, not only did the overexpression of GSK3β already reduce the basal level of DNA damage, but it also attenuated cisplatin-induced damage. Based on these results, we can conclude that high levels of GSK3β attenuate the DNA damage response induced by cisplatin in KPCbl6 cells.

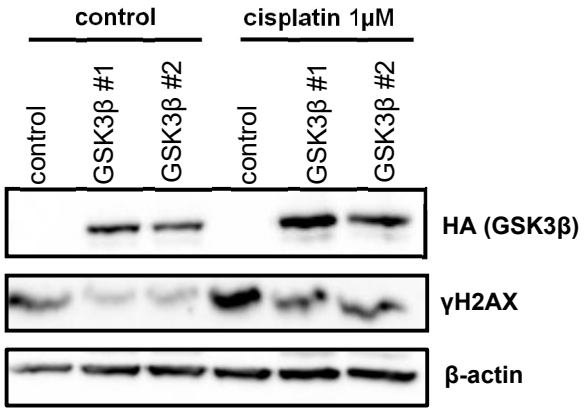

Figure 24: GSK3β overexpression leads to decreased DNA damage under cisplatin treatment. GSK3β construct containing HA-tag were transfected in KPCbl6 cells. After 24 h, they were cotreated with 1µM of cisplatin for 24 h. Transfection efficiency was controlled by HA and DNA damage by γH2AX. β-actin servers as a loading control.

3.6. NFATc1-dependent signatures regulated by GSK3β inhibition

Subsequently, we aimed to identify a possible mechanism which leads to the effects of GSK3β inhibition on DNA damage repair. When analyzing gene signatures regulated by AR-A, we found, beside the already mentioned pathways, ATF2 signatures. ATF2 (Activating Transcription Factor 2) is a member of the AP-1 protein family.[160] Moreover, it has already been shown that ATF2 activation is enhanced after cisplatin treatment and regulates signatures related to cisplatin and genotoxic stress.[161,162] However, when we tested for an alteration of ATF2 levels we did not observe differences after treatment with AR-A. Furthermore, we did not detect a differential interaction of ATF2 with GSK3β after cisplatin treatment via Co-Immunoprecipitation. Therefore, we screened for other potential interaction partners of GSK3β that might lead to a differential transcriptional regulation of DNA damage repair genes. An important interaction partner of AP-1 proteins is the family of NFAT proteins.[163] As previously demonstrated by our group, NFAT is stabilized by and interacts with GSK3β [59] and, thus, we focused on how NFAT might influence the regulation of DNA damage repair.

Therefore, we compared an NKCII data set of our department (MC Hasselluhn, GE Schmidt et al., 2019)[88] with the mRNA-seq data of L3.6pl of this study. NKCII cells have a constitutively active NFATc1 and a *KRAS* mutation. Hereby, we compared the control group with the knockdown of NFATc1 (siNFATc1).

With the purpose of finding genes regulated by AR-A treatment as well as by NFATc1, we performed a comparison of genes downregulated in both experiments (log2 fold change ≤ -0.5, $q < 0.05$). Thus, we found 262 genes downregulated in both treatment groups (Fig. 25). This collection of genes was further processed by GO enrichment analysis (PANTHER, Fisher Exact test, FDR < 0.05). The analysis clearly shows the regulation of DNA damage pathways, including DNA damage repair by homologous recombination and repair of DNA double strand breaks (Fig. 25).

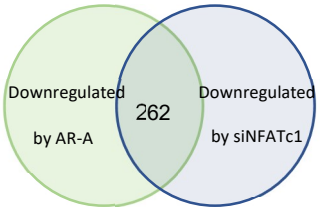

Rank	GO biological process		Fold Enrichment	FDR
1	mitotic DNA replication	GO:1902969	39.34	3.56E-05
2	pyrimidine deoxyribonucleotide biosynthetic process	GO:0009221	29.51	4.45E-02
3	double-strand break repair via break-induced replication	GO:0000727	26.23	8.54E-03
4	DNA replication initiation	GO:0006270	21.46	2.38E-06
5	chromatin remodeling at centromere	GO:0031055	19.07	2.26E-05
6	CENP-A containing nucleosome assembly	GO:0034080	18.36	1.28E-04
7	CENP-A containing chromatin organization	GO:0061641	18.36	1.25E-04
8	centromere complex assembly	GO:0034508	17.01	4.23E-05
9	nuclear DNA replication	GO:0033260	16.56	1.11E-07
10	DNA strand elongation involved in DNA replication	GO:0006271	16.56	2.95E-02
11	cell cycle DNA replication	GO:0044786	16.28	1.17E-07
12	DNA replication-independent nucleosome assembly	GO:0006336	16.14	5.49E-05
13	DNA replication-independent nucleosome organization	GO:0034724	15.74	6.15E-05
14	DNA-dependent DNA replication	GO:0006261	12.06	2.21E-12
15	replication fork processing	GO:0031297	11.57	2.17E-02
17	histone exchange	GO:0043486	11.47	1.56E-03
21	telomere maintenance via semi-conservative replication	GO:0032201	10.35	3.08E-02
22	DNA replication	GO:0006260	9.53	1.94E-13
23	DNA-dependent DNA replication maintenance of fidelity	GO:0045005	9.15	4.77E-02
26	anaphase	GO:0051322	8.02	8.28E-07
27	mitotic anaphase	GO:0000090	8.02	7.64E-07
28	ATP-dependent chromatin remodeling	GO:0043044	7.97	3.47E-03
29	double-strand break repair via homologous recombination	GO:0000724	7.95	3.65E-04

Figure 25: Gene signatures downregulated by AR-A and siNFATc1 are strongly involved in DNA repair. Genes identified by mRNA-seq that are significantly downregulated by AR-A in L3.6 and siNFATc1 in NKCII cells were compared (log2fold ≤ -0.5, q < 0.05). The overlap of 262 genes was used for GO Enrichment Analysis. For this purpose, we utilized the PANTHER tool with Fisher exact test and false discovery rate.

The previously selected DNA repair genes (Fig. 14), were re-analyzed to show the difference between genes regulated by AR-A and siNFATc1 (Fig. 26). These results demonstrate a clear regulation of important genes such as *BRCA1*, *RAD51* or genes of the Fanconi Anemia pathway. Thus, we detected genes commonly regulated by AR-A and NFATc1 which are crucial for homologous recombination. This led to the assumption that NFATc1 is a crucial regulator of observed signatures.

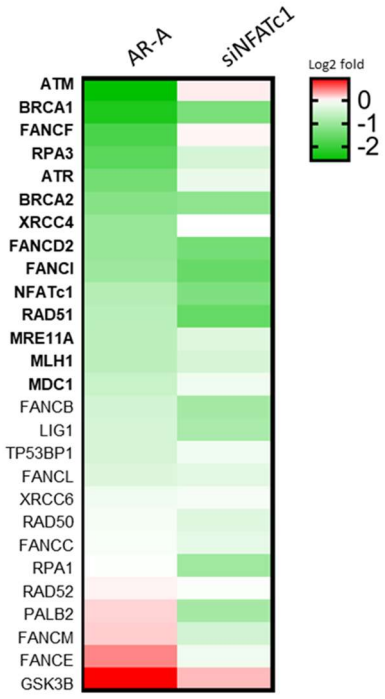

Figure 26: Selected genes involved in DNA repair are also regulated by siNFATc1. Log2 fold changes of selected genes involved in DNA repair, obtained of mRNA-seq of L3.6pl upon AR-A treatment and mRNA-seq of NKCII upon NFATc1 knockdown. Bold marked genes are significantly downregulated under AR-A treatment, displaying a strong regulation of DNA repair genes also under siNFATc1.

3.6.1. NFATc1 regulates DNA damage and sensitize cells to cisplatin treatment

To further focus on the transition into *in vivo* experiments we continued our approach in KPCbl6 cells which can be orthotopically transplanted into immunocompetent mice. Consequently, we performed knockdown of NFATc1 in KPCbl6 cells to evaluate the effect on DNA damage response. Here, we could detect a clear induction of DNA damage after knockdown of NFATc1 (Fig. 27A). Interestingly, knockdown of NFATc1 leads to greater DNA damage than GSK3β inhibition. Thus, the strength of DNA damage with the combination of cisplatin and siNFATc1 was slightly lower, than in the combination with AR-A (Fig. 27B).

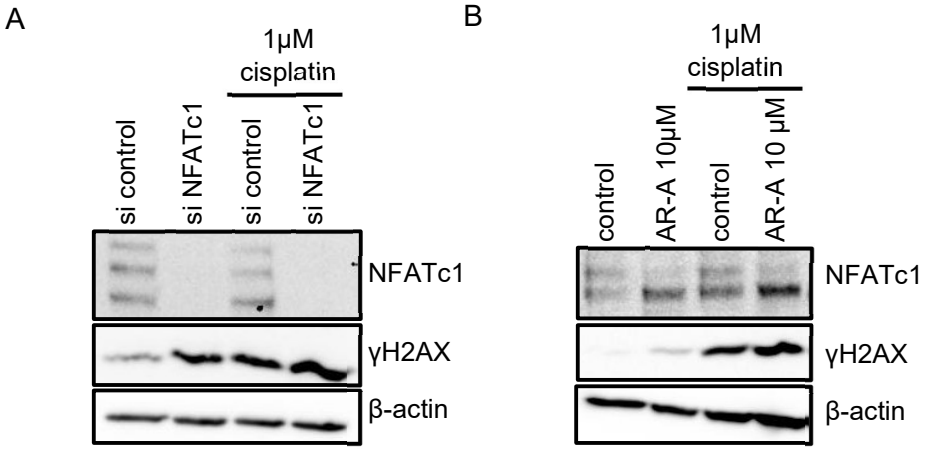

Figure 27: Loss of NFATc1 leads to increased DNA damage under cisplatin. A) KPCbl6 cells were treated with siNFATc1 for 6 h before combined with 1µM cisplatin for 24 h. The DNA damage level was determined via γH2AX, showing a clear induction of DNA damage under siNFATc1 and a beneficial effect, when combining both. B) AR-A treatment (10µM) was combined with 1µM cisplatin for 24 hours, showing the already observed effect in DNA damage and additionally a downregulation of NFATc1 by AR-A. β-actin serves as loading control.

Following the same approach as for GSK3β, we performed an overexpression of NFATc1 in KPCbl6 cells and combined it with cisplatin treatment for 24 hours (Fig. 28). Similarly, we observed decreased basal levels of DNA damage by NFATc1 overexpression. In addition, NFATc1 overexpression was able to reduce the induced damage under cisplatin. Thus, high levels of GSK3β (Fig. 24) and NFATc1 decrease the sensitivity towards cisplatin in KPCbl6 cells.

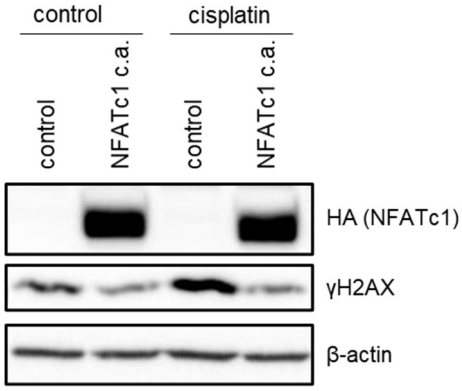

Figure 28: Overexpression of NFATc1 led to reduced levels of DNA damage. Transfection of HA-tagged constitutive active NFATc1 (NFATc1 c.a.) in KPCbl6 cells for 24 hours followed by the combination with 1µM of cisplatin for 24 hours. Transfection effectivity was controlled via HA tag. DNA damage levels were reduced by overexpression of NFATc1 and can reduce effect of cisplatin on DNA damage level. β-actin servers as loading control.

3.6.2. CRISPR/Cas9 mediated knockout of NFATc1 resulted in increased sensitivity to cisplatin

Following the studies investigating a temporary reduction of NFATc1 levels, we used the CRISPR/Cas9 technology to create NFATc1 knockout (k.o.) cell lines. After confirmation of the knockout, we performed cisplatin treatment for 24 and 48 hours. The NFATc1 k.o. cells show a strong increase of DNA damage, especially after 48 hours of treatment (Fig. 29).

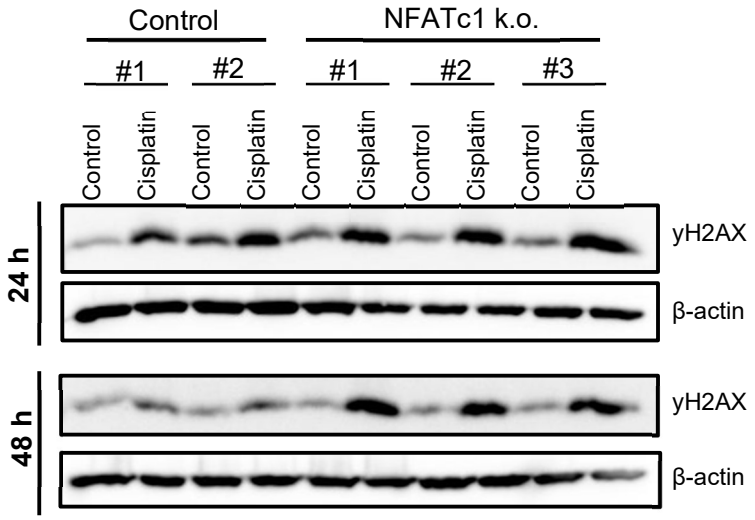

Figure 29: KPCbl6 CRISPR/Cas9 NFATc1 knockout cells showed induction of DNA-damage under cisplatin. KPCbl6 control and NFATc1 knockout clones were treated with 1µM cisplatin for 24 or 48 hours. Numbers indicate independent cell lines generated from single cell clones. NFATc1 knockout clones show a stronger response on DNA damage level towards cisplatin treatment. β-actin serves as loading control.

Consequently, we tested the NFATc1 k.o. cells in comparison to control on their sensitivity towards cisplatin via MTT assay. The results show a significantly higher response of the NFATc1 k.o. cells (Fig. 30A). Importantly, this effect could be observed in all three clones. Additionally, we tested the cisplatin response in KNPC (containing constitutively active NFATc1) cells. Thus, KNPC cells serve as an additional overexpression model of NFATc1 to verify the influence of NFATc1 on the observed cisplatin response. These show a reduced response to cisplatin, although the effect is not significant (Fig. 30B).

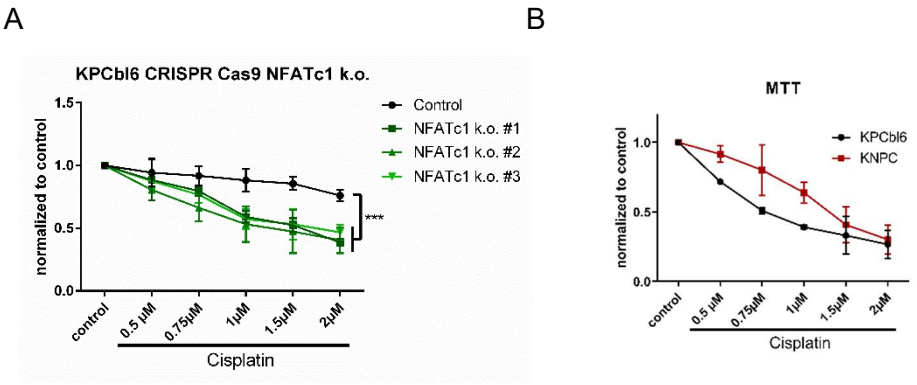

Figure 31: NFATc1-dependent sensitivity to cisplatin on cell viability. A) KPCbl6 cell (control vs NFATc1 k.o.) were treated with increasing concentration of cisplatin for 72 h, whereby NFATc1 k.o. cells displayed a significantly higher sensitivity. B) KPCbl6 cell and KNPC (constitutively active NFATc1) cells were treated with cisplatin for 72h. KNPC are slightly more resistant towards cisplatin treatment then KPCbl6 cells, but not significantly. Mean ±SD, n=3 (biological replicates with 5 technical replicates), unpaired student t-test, *** p≤ 0.001.

To evaluate whether NFATc1 k.o. is sufficient to mimic the effects of AR-A inhibition, we compared them with control cells and treated with AR-A, cisplatin, and the combination. As we already observed via MTT assay a strong response in the NFATc1 k.o. upon cisplatin treatment (Fig. 30), we performed a different method to confirm our results on the proliferation via BrdU assay. The combination treatment induced a strong decrease in cell viability in KPCbl6 control cells by BrdU assay (Fig. 31A).

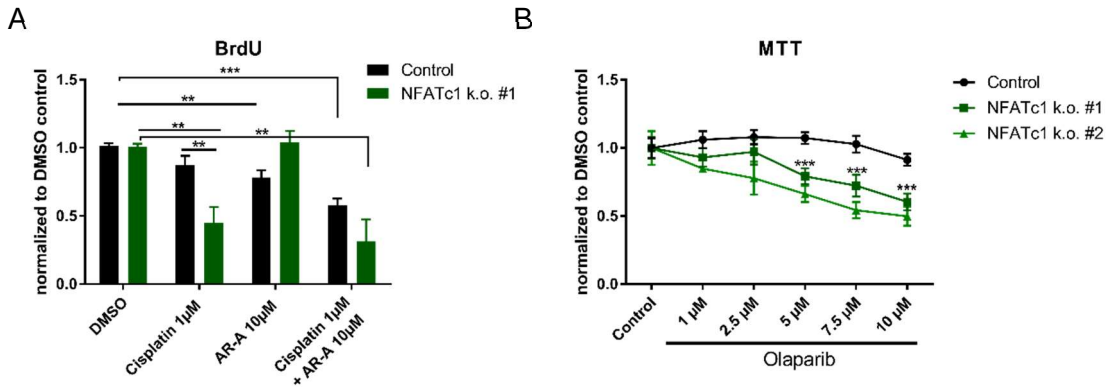

Figure 30: NFATc1 loss leads to higher sensitivity to cisplatin and Olaparib but is not influenced by GSK3β inhibition. A) BrdU assay was performed in KPCbl6 control cells and NFATc1 knockout cells, treated for 48 hours, showing that AR-A and cisplatin is beneficial in control cells but not in NFATc1 knockout. B) MTT assay of KPCbl6 control and NFATc1 k.o. cells were treated for 72 hours with increasing concentrations of Olaparib. NFATc1 k.o. cells are more sensitive to Olaparib treatment. Mean ±SD, n=3 (biological replicates), unpaired student t-test, ** p≤ 0.01, *** p≤ 0.001.

However, the NFATc1 k.o. cells did not show an additive effect when treated with cisplatin and AR-A. This leads to the assumption that the AR-A-driven cisplatin sensitivity is induced by NFATc1 as the loss of NFATc1 prohibits an effect of AR-A on the response to cisplatin.

Based on the previous observation that AR-A caused an enhanced response to Olaparib, we tested Olaparib in KPCbl6 NFATc1 knockout and control cells (Fig. 31B). The loss of NFATc1 led to a significantly stronger decrease in cell viability compared to the control, confirming our assumption. To confirm the effect of NFATc1 on BRCA expression, we further performed a ChIP assay to test the binding capacity of NFATc1 on the TSS (Transcription Start Side) of *BRCA1* and *BRCA2* (Fig. 32). Hereby, we detected a clear difference between NFATc1-bound TSS of *BRCA1* and *BRCA2*, as *BRCA1* was bound more by NFATc1. This result is in line, with our transcription analysis, showing a stronger decrease of BRCA1 after NFATc1 knockdown.

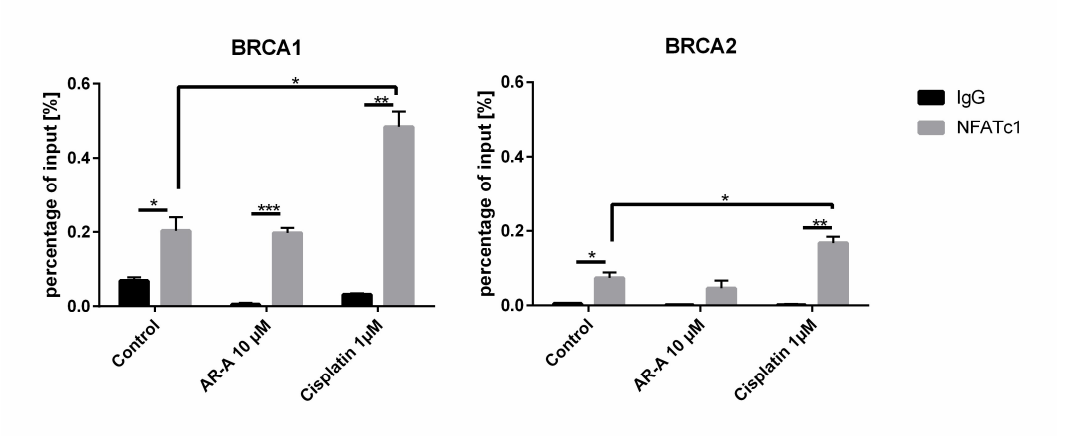

Figure 32 ChIP assay for NFATc1 confirmed binding of NFATc1 on BRCA1 and BRCA2 TSS. ChIP assay was performed in KPCbl6 cells, treated for 24 hours with 10 µM AR-A or 1µM cisplatin. NFATc1 binds to the promoter and its binding is especially increased after cisplatin treatment. n=3 (technical replicates), Mean ±SD, unpaired student t-test, * p≤ 0.05, ** p≤ 0.01, *** p≤ 0.001.

3.6.3.NFATc1 loss impairs repair of cisplatin induced damage

To further test the effect of AR-A and cisplatin on NFATc1 k.o. and control cells, we performed a recovery assay. Cells were treated for 24 hours with AR-A and cisplatin, using concentrations showing additive effects on DNA damage. After 24 hours, the treatment was removed, cells washed with PBS to remove all remaining drug components in the media, followed by adding fresh media. Cells were allowed to recover for 24, 48 or 72 hours. We compared the effects on proliferation (Fig. 33) and cell morphology (Fig. 34).

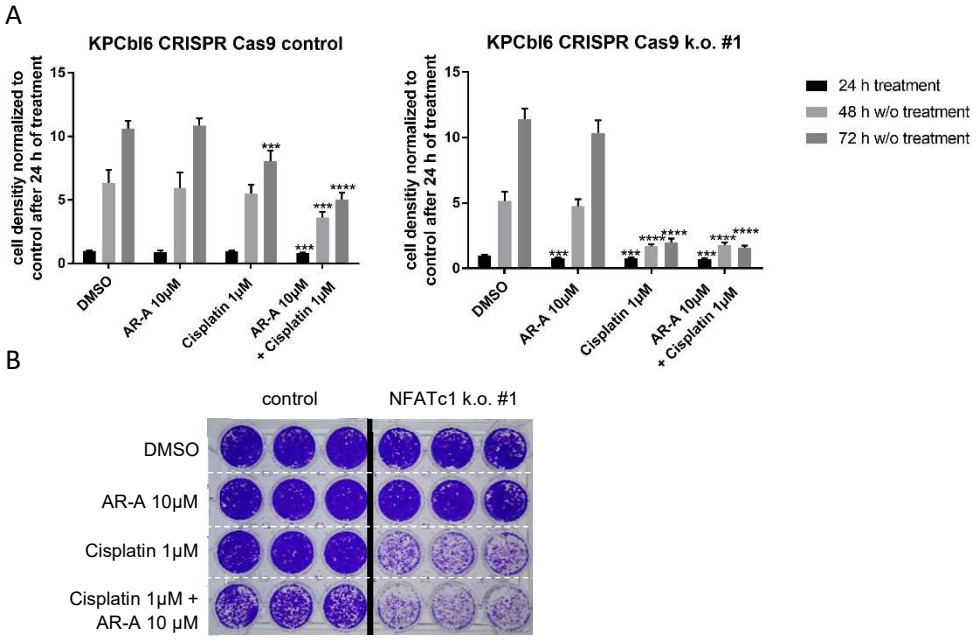

Figure 33: NFATc1 k.o. cells have a delayed recovery from cisplatin treatment. A) Quantification of crystal violet staining. Crystal violet was solubilized and measured photometric. KPCbl6 cells were analyzed after 24 hours of treatment and 48 and 72 hours without treatment. KPCbl6 control cells show a slower recovery of cells after combination treatment of cisplatin and AR-A, then to the single treatment (AR-A 10µM, cisplatin 1µM). In comparison, KPCbl6 NFATc1 k.o. cells do not recover from cisplatin treatment, without an additive effect of AR-A. B) Representative crystal violet staining of cells after a recovery time of 72 hours without treatment. Mean +SD, n=3 (biological replicates with three technical replicates), unpaired student t-test – comparing the treatment with DMSO control for each time point separately, *** $p \leq 0.001$, **** $p \leq 0.0001$.

As shown, by crystal violet staining and its quantification, we detected that KPCbl6 cells were able to recover from AR-A or cisplatin treatment, after treating them for 24 hours (Fig. 33) shown by their increasing cell density. However, when both treatments were compared, we noticed a clear delay of recovery. In contrast to that, KPCbl6 NFATc1 k.o. cells displayed a strong delay in recovering from cisplatin treatment, although this effect could not be altered by the combination with GSK3β inhibition.

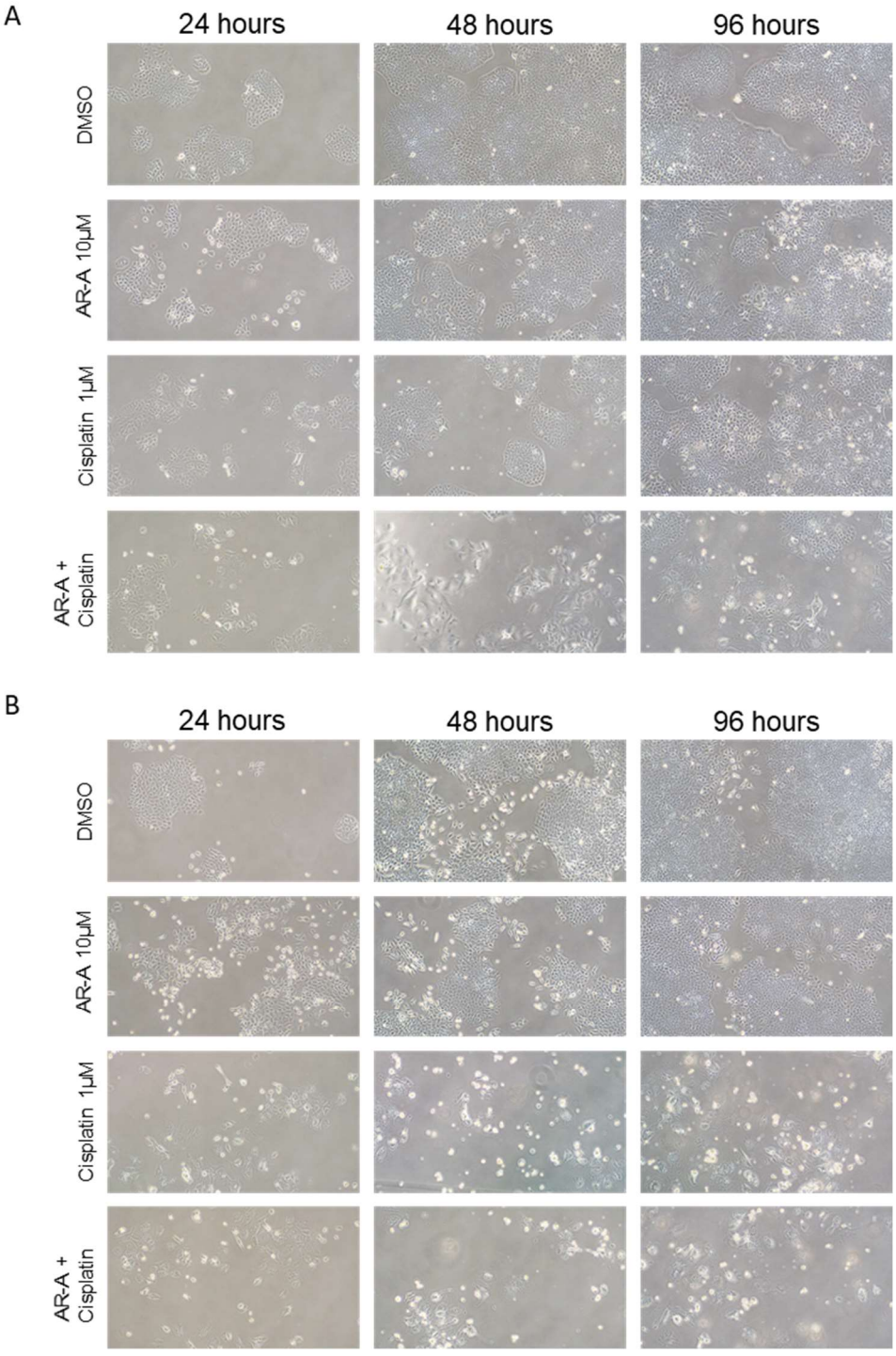

Figure 34: Illustration of KPCbl6 cells after treatment with GSK3β inhibitor and cisplatin. KPCbl6 control (A) and NFATc1 k.o. (B) cells were treated for 24 h (AR-A 10µM, Cisplatin 1µM, Olaparib, 10µM and in combination with AR-A) and then grown in normal growth media for 24, 48 or 72 hours. Representative pictures are displaying the differences in the ability to recover of the treatment. Magnification 20x).

Furthermore, we performed recovery assays by using Olaparib and its combination with AR-A treatment (Fig. 35). However, the effects were not as strong as observed when using cisplatin. The western blot analysis clearly confirmed the results we observed on cell proliferation. After 24 hours, we detected DNA damage in the KPCbl6 control group when treating with all single reagents, which was enriched in their combination with AR-A. After a recovery time of 72 hours, we only observed DNA damage in the conditions that received the combination of cisplatin or Olaparib with AR-A. In comparison, the KPCbl6 NFATc1 k.o. cells revealed a stronger response to cisplatin treatment on DNA damage level, which could not be elevated by the combination with AR-A. Even after 72 hours of recovery, the cells were not able to decrease the level of DNA damage (Fig. 35).

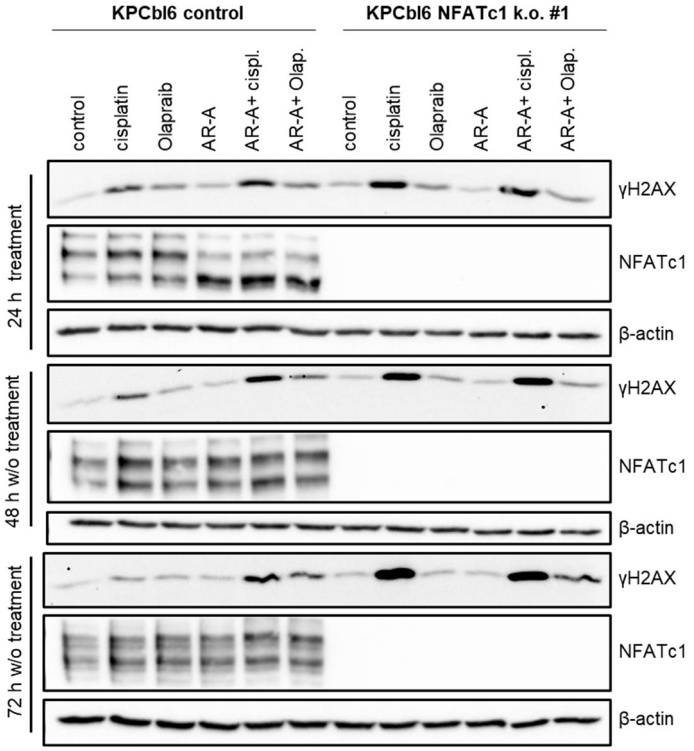

Figure 35: KPCbl6 NFATc1 k.o. cells were not able to repair cisplatin-induced DNA damage. KPCbl6 control and NFATc1 k.o. cells were treated for 24 h (AR-A 10µM, Cisplatin 1µM, Olaparib 10µM and in combination with AR-A) and then grown in normal growth media for 48 or 72 hours. Western-blot analysis showed a delay in recovery for control cells when treated with AR-A in combination with cisplatin or Olaparib, whereas NFATc1 k.o. cells were not able to recover from single cisplatin treatment. β-actin serves as a loading control.

In order to estimate how many patients could fit the criteria of being GSK3β-positive and NFATc1-positive, we compared our TMA data of GSK3β with NFATc1 (Fig. 36). Notably, out of all patients with a GSK3β immunoreactive score of 2 and 3, 80% were also positive for NFATc1. Based on our results, we hypothesized that the remaining 20% which showed no expression for NFATc1 would probably not benefit from an additional treatment with a GSK3β inhibitor.

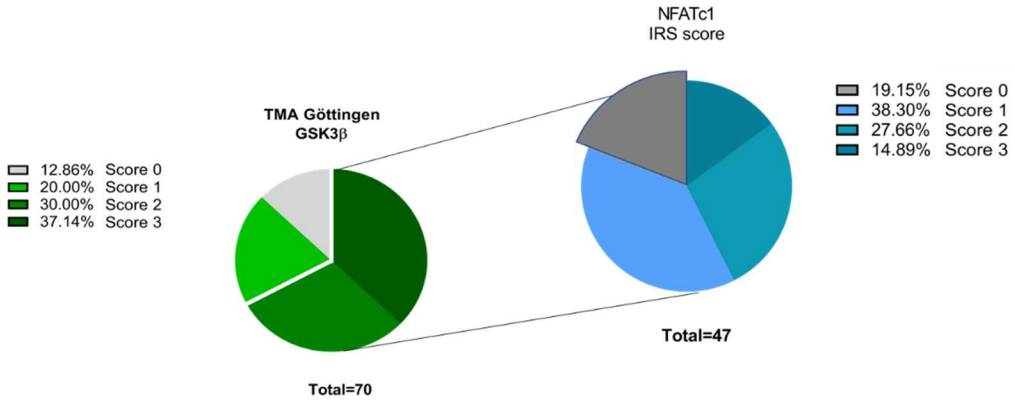

Figure 36: TMA evaluation for GSK3β and NFATc1 reveals that of the GSK3β patients the majority is NFATc1-positive. TMA data analyzed for their immunoreactive score (IRS) revealed that 47 patients showed a high IRS for GSK3β. Out of these individuals, approximately 80 % are NFATc1 positive and might benefit of an additional GSK3β inhibition treatment.

Together, we uncovered a clear regulation of DNA damage repair-related genes under AR-A, which causes a higher responsiveness towards cisplatin and Olaparib. As a potential transcription factor causing the regulation, we identified NFATc1 to play an important role in the regulation and further sensitizing cells for the treatment.

4. Discussion

Pancreatic cancer remains one of the most lethal malignancies, with a devastating prognosis and limited therapeutic options.[1] Novel insights from recent seminal studies significantly increased our understanding of pancreatic cancer biology and most importantly, identified various molecular subtypes in pancreatic cancer that might play a role in the clinical course and therapeutic resistance of patients. These very encouraging findings must now be translated into the development of new therapeutic approaches and molecular treatment strategies.[18] Stratifying patients based on variant DNA damage repair vulnerabilities showed highly promising results in current clinical practice. This led to a recent FDA approval for the use of DNA damage targeting agents, like PARP inhibitors, in BRCA-mutated pancreatic cancer patients.[164] BRCA mutations are not exclusively responsible for DNA damage vulnerabilities and many other factors are known to attenuate DNA damage response.[110] However, this treatment option only accounts for a small portion of patients with certain mutations that could benefit.

Our study uncovers a previously uncharacterized role of GSK3β in regulating the transcription of DNA damage-related genes. Based on our results, we suggest that pharmacological targeting of GSK3β may represent a novel and effective strategy in the treatment of pancreatic cancer, especially in patients with induced DNA damage. We show, that irrespective of germline or somatic mutations in BRCA genes, there is also the possibility to induce a BRCAness subtype at the transcriptional level through inactivation of GSK3β. The inhibition of GSK3β in pancreatic cancer cells can therefore cause an “inducible” BRCAness-like phenotype. As a direct consequence a higher sensitivity towards various DNA damage-related agents, e.g. the PARP inhibitor, Olaparib, cisplatin and irinotecan is achieved. Furthermore, we unraveled the mechanistic link between GSK3β inhibition and “BRCAness” induction and identified NFATc1 as a key transcriptional driver of this central pathway in DNA damage regulation. This is in

line with our observation, that NFTAc1 loss recapitulates the same phenotype as GSK3β inhibition.

4.1. GSK3β in pancreatic cancer

GSK3β plays an important role in numerous malignancies, which is context-specific and reported to be mainly oncogenic in the case of pancreatic cancer.[33] In order to address this characteristic we aimed to verify these reported effects in our system by using both human and murine pancreatic cancer cells, L3.6pl and KPCbl6 cells, respectively. We observed the expected cell cycle arrest and reduced proliferation upon GSK3β inhibition in both systems. Gene expression profiling following GSK3β inhibition further revealed a role for this kinase in transcriptional regulation of DNA damage signatures. Our studies also proposed that GSK3β-driven genes are mainly involved in homologous recombination and repair of DNA double strand breaks. These effects were observed upon pharmacological GSK3β inactivation or in response to its depletion. Notably, GSK3β has a very broad interaction profile.[165] Although our study could demonstrate that GSK3β regulates DNA damage repair it is crucial to further explore these interactions to be able to pinpoint the underlying mechanism of GSK3β-induced BRCAness.

4.1.1. Non-BRCAness mediated chemo sensitization effects of GSK3β inhibition

GSK3β inhibition was reported to exhibit a sensitizing effect on various chemotherapeutic agents.[79,82,83] GSK3β inhibition sensitizes PDAC cells to gemcitabine treatment by stabilizing TOPBP1, which is involved in the activation of the ATR. This will lead to the attenuation of gemcitabine-induced cell cycle arrest.[83] We show in this study, that GSK3β inhibition also leads to decreased expression levels of ATR, which supports previous findings following gemcitabine treatment and is in line with our observation that GSK3β inhibition causes a

significant arrest of pancreatic cancer cells at the G2/M cell cycle phase, as shown in different systems before[75,87]. Pharmacological inhibition of GSK3β was similarly reported to sensitize tumor cells to irradiation in glioblastoma.[82] This sensitization is mediated by inhibiting the phosphorylation of 53BP1 and thus attenuating the process of double-strand break repair. The sensitization to irradiation treatment upon GSK3β inhibition remains to be tested in PDAC.

Alongside the transcriptional regulation of BRCAness phenotype-related genes which we uncover in this study, we observe a moderate but reproducible regulation of the nucleotide excision repair pathway induced following DNA adduct formation precipitated by cisplatin or bulky aromatic lesions. The family of Fanconi Anemia (FA) proteins were observed to be downregulated following GSK3β inhibition. FA proteins have a distinct influence on the regulation repair of DNA crosslinks caused by cisplatin treatment. As the FA and HR pathway share a lot of regulatory proteins and thus being conected[166], an relevant interplay between those two pathways would not be surprising in our system.

It has been shown, that in non-small cell lung cancer (NSCLC) a co-treatment of GSK3 inhibition with paclitaxel is synergistic.[167] Both, paclitaxel and GSK3β inhibition, are known to cause stabilization of microtubule and thereby causing a missegregation of chromosomes.[168–170] A study of Poruchynsky et al. (2015)[171] has shown that microtubules are also important in transporting DNA damage repair proteins. Noteworthy, we observe in our RNA-seq results a downregulation of microtubule based protein transport. Therefore, this mechanism could contribute to the GSK3β inhibition mediated toxicity by prohibiting the transport of remaining DNA damage repair proteins. It still needs to be determined if GSK3β inhibition induces reduced trafficking of DNA damage-related proteins and in which content this process is relevant for the response to DNA damaging agents.

4.1.2. Nuclear localization of GSK3β in the context of chemotherapy

An important observation of our study is the robust nuclear accumulation of GSK3β in cancer cells upon treatment with cisplatin. A similar observation was reported upon irradiation in glioblastoma[82] which could support our hypothesis of the relevance of GSK3β as mediator in the DNA damage response. At this point, it is still unclear how the change of GSK3β localization is regulated in cancer. One known factor with an influence on the localization of GSK3β is AXIN2, which binds to GSK3β and blocks the nuclear localization sequence (NLS).[55] We could not observe a change in the expression of AXIN2 on the transcriptional level following GSK3β inhibition. The counterintuitive results of AXIN2 levels suggest that AXIN2 expression might be controlled on the protein level upon cisplatin treatment leading to increased GSK3β nuclear localization. However, this remains to be tested. Furthermore, no changes of AXIN2 imply an influence of other proteins contributing to the regulation of GSK3β shuttling. If AXIN2 reveals to be relevant in regulating the localization of GSK3β in our system one has to consider, that AXIN2 itself can be upregulated by inactivating mutations of the Ring Finger Protein 43 (*RNF43).*[172] *RNF43* is mutated in about 7% of PDAC patients and its inactivation can increase Wnt signaling activity.[172,173] Thus, RNF43 deregulation might causally be involved in the observed cellular redistribution of GSK3β in pancreatic cancer. The mutation status is not known in the cells used for our study so far.

We could not see a consistent pattern of nuclear accumulation of GSK3β in various PDX tumors treated with gemcitabine and nab-paclitaxel. It has to be tested if this effect is specific to cisplatin and is not translated to other chemotherapeutics. DNA damage repair processes induced by cisplatin are more similar to irradiation compared to gemcitabine and nab-paclitaxel. The next step will be a deeper analysis, tests of different treatments and a comparison of more tumors in order to identify possible factors that influence this process. This is particularly relevant, as the first GSK3β inhibitor has been approved for clinical

trials only recently (NCT03678883). Molecular understanding of GSK3β and its role in PDAC will significantly help in identifying the subgroups of patients that will benefit the most from such inhibitor.

4.1.3. GSK3β inhibition in different subgroups of pancreatic cancer patients

Various molecular subtypes in pancreatic cancer were recently defined with the squamous phenotype, which is considered as the most aggressive type. A recent study by Brunton et. al (2020)[24] showed, that PDAC subtypes are also tightly connected to metabolic plasticity. The lipogenic profile is another indicator for a less aggressive subtypes, while a more glycolytic profile was observed in the squamous subtype.[23] GSK3β is a major driver of glycolysis and therefore is highly connected to the squamous subtype. It has already been shown that metabolism and DNA repair are linked to each other by processes which influence, for example, the chromatin remodeling or synthesis of new nucleotides. Nucleotide synthesis is strongly associated with glycolysis, as an intermediate of pentose-phosphate pathway is mandatory for its occurrence. In line with the observed downregulation of glycolytic genes upon GSK3β inhibition, we also see a downregulation of pathways related to nucleotide metabolism and synthesis. Accordingly, GSK3β inhibition has a high potential in decreasing the aggressiveness when used in patients belonging to more aggressive subtypes.

Another factor is the dependence of the sensitivity towards GSK3β inhibition on chromatin accessibility.[24] A known regulator of chromatin accessibility, ARID1A, is mutated in about 6% of pancreatic cancer patients.[21] It its part of the SWI/SNF chromatin remodeling complex and influences several processes like transcription and DNA replication. ARID1A is recruited to DSBs and contributes to the processing of RPA coating of ssDNA.[174] We observe that pancreatic cancer cells are more sensitive to pharmacological GSK3β inhibition upon loss of ARID1A, probably caused by enhancing the disturbance of DNA damage repair. Based on these results, we suggest that patients with mutated ARID1A mutation

may specifically benefit from GSK3β modulation. However, a detailed analysis of this mechanism needs to be performed.

In summary, we identified a key novel role of GSK3β in pancreatic cancer. The effect can be mainly mediated by an induced “BRCAness” phenotype, but can also be complemented by other mechanisms. Deeper understanding of the molecular mechanisms underlying GSK3β effects will help in identifying the group of patients that will benefit the most from receiving this treatment. One of the major mechanisms of induced-BRCAness identified in this study is the transcription activation of DNA damage genes by NFATc1.

4.2. NFATc1 and pancreatic cancer

As we identified NFATc1 as a mediator of GSK3β-induced BRCAness, we aim to further investigate the role of NFATc1 in this process. We expect tumors with a loss of NFATc1 to be more sensitive to cisplatin or Olaparib treatment. Consistently, we were able to observe an induction of sensitization towards different chemotherapeutics like cisplatin *in vitro* upon loss of NFATc1. Key result of this part of the study was the demonstration of these findings in the case of partial loss (knockdown) in addition to complete loss (knockout) of NFATc1. Based on these results it would be reasonable to treat with an NFATc1 inhbitor rather then targeting GSK3β as upstream protein to avoid massive side effects. However, only pan-NFAT inhibitors, as cyclosporin A (CsA) or tacrolimus, are availble. Unfortunately, targeting the whole family of NFAT proteins causes strong side effects like neuro- and cardiotoxicity, as well as a strong immunosuppressive reaction.[91,106] Thus, the available inhibitors yet do not offer an alternative to GSK3β inhibitors. However, the development of a specific NFATc1 inhibitor would provide an interesting option to target NFATc1-regulated DNA damage response in an GSK3β independent manner.

4.2.1.NFATc1 and chemotherapy

NFATc1 has been shown to drive the transcription of DNA Damage Induced Apoptosis Suppressor (DDIAS), which is an important protein in cisplatin resistance in lung cancer.[175] We do not see a transcriptional regulation of DDIAS upon GSK3β inhibition. However, it is not known if it might be regulated in cisplatin resistant pancreatic cancer. Thus, an upregulation of DDIAS in cisplatin resistant PDAC cell lines or tumors might be mediated by NFATc1 and can be targeted by GSK3β inhibition.

It was shown by Olabisi et al. (2008)[176] that NFAT interacts with PARP where PARP regulates NFAT activity. PARP inhibition leads to reduced ADP-ribosylation of NFAT which causes reduced NFAT-mediated cytokine expression.[176] This effect was only shown on single targets and was not further elucidated on the genome-wide level. It is not yet known, if this also affects DNA damage response genes. Thus, the sensitization that we see when co-treating with PARP and GSK3β inhibitors could be accentuated by a partial effect of PARP inhibition on double-stranded break repair by directly affecting NFATc1 activation.

Cisplatin influences calcium levels by inducing Ca^{+2} efflux from the mitochondria.[177] Calcium is the most important regulatory mechanism of NFAT signaling. While this induction is mediated by mitochondria damage and apoptosis, [177] it may also lead to stronger NFAT induction, thereby further propagating the DNA damage repair response. It cannot be determined if NFATc1 activation is affected by the increased calcium influx, as we cannot see a difference in NFATc1 expression under cisplatin treatment in the orthotopic mouse model so far. Additionally, we failed to observe a consistent nuclear accumulation of NFATc1 at that point of time. It is important to note that the mice in this experiment were sacrificed a day after treatment and the effects of NFATc1 could be time dependent. Further investigation of this response with a time-point study is necessary to address this question.

To further validate the GSK3β-NFATc1 axis, we plan to analyze treated patient cohorts. Those will be evaluated on their GSK3β and NFATc1 levels and if those correspond with responsiveness upon chemotherapy. Thereby, we compare the levels after treatment as well as their basic level of expression and localization. We also plan to test the success of the combination of GSK3β inhibitor with Olaparib or cisplatin *in vivo*.

4.2.2. Transcriptional regulation of DNA damage repair genes by NFATc1

The inhibition of GSK3β leads to the transcriptional regulation of BRCAness associated genes, but GSK3β does not act as a transcription factor itself. It is rather regulating other transcription factors by stabilization or degradation. In order to address this feature, we aimed to understand which factors are most important in regulating gene expression. In a first attempt, we tested ATF2, a protein which is known to be involved the regulation of genes contributing to DNA damage repair.[178] Our RNA-seq showed downregulation of ATF2 gene signatures after GSK3β inhibition, but we could not observe a regulation of mRNA or protein levels after treatment. Based on the induction of DNA damage caused by a knockdown of ATF2, we focused more on determining proteins which might interact with ATF2 and be regulated by GSK3β inhibition. As ATF2 belongs to the group of AP-1 proteins, we were interested in potential interactors of these proteins, namely NFAT.[179] Our analysis of NFATc1 knock-down and knock-out experiments showed a strong sensitization to cisplatin, Olaparib and irinotecan, validated by increased DNA damage levels and growth rate reduction. NFAT-depleted cells were not responsive to GSK3β inhibition in spite of having similar growth rate to control cells. Based on these results, we concluded that NFAT is a major mediator of GSK3β- induced BRCAness (Fig. 37). This effect is specific to NFATc1, as the other proteins of the NFAT group are not affected by the knockdown or they are upregulated in the knockout. Additionally, cells with a loss of NFATc1 are not able to resolve cisplatin-induced DNA damage. Our aim is to identify the general localization pattern of NFATc1 in case of cisplatin treatment next to GSK3β inhibition on a molecular level. We expect that NFATc1 will gain occupancy in proximity to DNA-damage response genes including BRCA1/2 and other. This gain of occupancy is expected to be revered upon GSK3β inhibition further supporting our findings. It remains to be seen if NFATc1 is going to mainly be localized that the transcription starting sites (TSS) of these genes or is going to be localized at associated distal regulating elements. Characterization of these

regions of going to give insight what other transcription and epigenetic factors help NFATc1 driving the transcription of these genes.

In summary, NFATc1 is an important regulator of GSK3β induced-BRCAness and it can be used be used to stratify patients as we do not expect that patients, who express low levels of NFAct1, will not benefit from GSK3β inhibition treatment (Fig. 38).

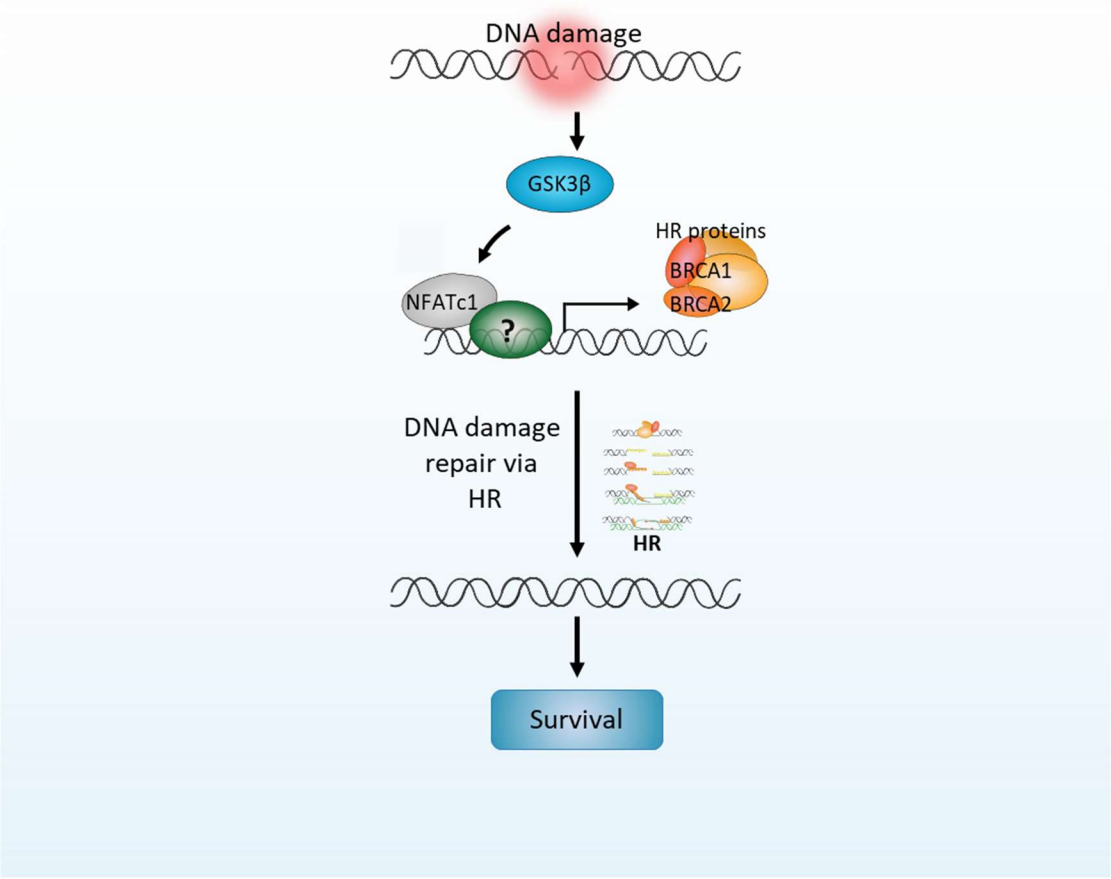

Figure 37: GSK3β is regulating transcription of important genes that take part in HR and thereby contribute to the repair of DNA damage and support the survival. GSK3β is regulating the expression of HR proteins by influencing a major mediator NFATc1. The interaction partner of NFATc1 in this process remains to be identified. The impact of GSK3β in driving the expression of DNA damage repair genes involved in HR the cell supports the repair of DNA DSBs and thus the survival of the cell.

4.3. Conclusion

Within this project, we could highlight the role of GSK3β in regulating DNA damage repair in pancreatic cancer. GSK3β inhibition induces a BRCAness-like phenotype, which precipitates higher sensitivity to cisplatin or PARP inhibition. Our analysis uncovered NFATc1 as key mediator of this process. Thus, a loss of NFATc1 leads to higher sensitivity to DNA damage inducing agents irrespective of GSK3β. Future studies are necessary to further understand the mechanism in order to translate these findings into clinical practice. This will significantly help in optimizing the therapy of pancreatic cancer using mechanism-based translational approaches.

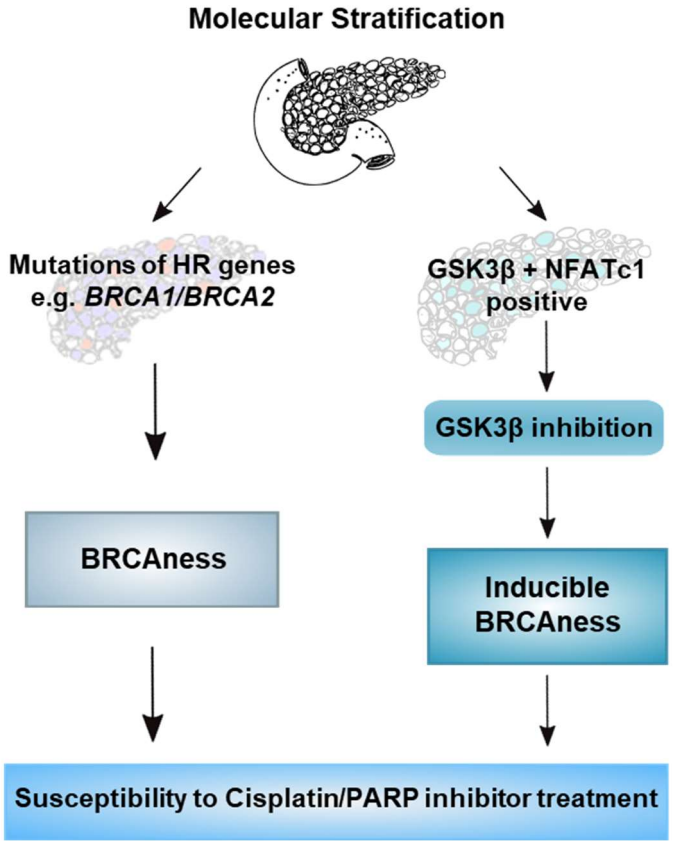

Figure 38: Graphical abstract showing a possible way of stratifying patients based on their mutations of BRCAness genes and their expression of GSK3β and NFATc1. Tumors with BRCAness gene mutations are susceptible for cisplatin or PARP inhibitor treatment. Patients, which are positive for GSK3β and NFATc1, would benefit of a GSK3β inhibition to induce a BRCAness phenotyp.

References

1. Siegel, R. L., Miller, K. D. & Jemal, A. Cancer statistics, 2020. *CA. Cancer J. Clin.* **70**, 7–30 (2020).
2. Zeng, S. *et al.* Chemoresistance in pancreatic cancer. *International Journal of Molecular Sciences* vol. 20 (2019).
3. Cid-Arregui, A. & Juarez, V. Perspectives in the treatment of pancreatic adenocarcinoma. *World J. Gastroenterol.* **21**, 9297–9316 (2015).
4. Hruban, R. H., Goggins, M., Parsons, J. & Kern, S. E. Progression model for pancreatic cancer. *Clin. Cancer Res.* **6**, 2969–2972 (2000).
5. Kamisawa, T., Wood, L. D., Itoi, T. & Takaori, K. Pancreatic cancer. *Lancet* **388**, 73–85 (2016).
6. Hezel, A. F. *et al.* Genetics and biology of pancreatic ductal adenocarcinoma. *Genes Dev.* **20**, 1218–1249 (2006).
7. Morris, J. P., Wang, S. C. & Hebrok, M. KRAS, Hedgehog, Wnt and the twisted developmental biology of pancreatic ductal adenocarcinoma. *Nature Reviews Cancer* vol. 10 683–695 (2010).
8. Almoguera, C. *et al.* Most human carcinomas of the exocrine pancreas contain mutant c-K-ras genes. *Cell* **53**, 549–554 (1988).
9. Löhr, M., Klöppel, G., Maisonneuve, P., Lowenfels, A. B. & Lüttges, J. Frequency of K-ras mutations in pancreatic intraductal neoplasias associated with pancreatic ductal adenocarcinoma and chronic pancreatitis: A meta-analysis. *Neoplasia* **7**, 17–23 (2005).
10. Maitra, A. & Hruban, R. H. Pancreatic cancer. *Annual Review of Pathology: Mechanisms of Disease* vol. 3 157–188 (2008).
11. Roberts, N. J. *et al.* ATM mutations in patients with hereditary pancreatic cancer. *Cancer Discov.* **2**, 41–46 (2012).
12. Hruban, R. H., Canto, M. I., Goggins, M., Schulick, R. & Klein, A. P. Update on familial pancreatic cancer. *Advances in Surgery* vol. 44 293–311 (2010).
13. Schenk, M. *et al.* Familial risk of pancreatic cancer. *J. Natl. Cancer Inst.* **93**, 640–644 (2001).
14. Decker, G. A. *et al.* Risk factors for pancreatic adenocarcinoma and prospects for screening. *Gastroenterology and Hepatology* vol. 6 246–254 (2010).
15. Cid-Arregui, A. & Juarez, V. Perspectives in the treatment of pancreatic adenocarcinoma. *World J. Gastroenterol.* **21**, 9297–9316 (2015).

16. Zeng, S. *et al.* Chemoresistance in pancreatic cancer. *International Journal of Molecular Sciences* vol. 20 (2019).

17. Hidalgo, M. *et al.* Addressing the challenges of pancreatic cancer: Future directions for improving outcomes. *Pancreatology* vol. 15 8–18 (2015).

18. Collisson, E. A., Bailey, P., Chang, D. K. & Biankin, A. V. Molecular subtypes of pancreatic cancer. *Nat. Rev. Gastroenterol. Hepatol.* **16**, 207–220 (2019).

19. Collisson, E. A. *et al.* Subtypes of pancreatic ductal adenocarcinoma and their differing responses to therapy. *Nat. Med.* **17**, 500–503 (2011).

20. Moffitt, R. A. *et al.* Virtual microdissection identifies distinct tumor- and stroma-specific subtypes of pancreatic ductal adenocarcinoma. *Nat. Genet.* **47**, 1168–1178 (2015).

21. Bailey, P. *et al.* Genomic analyses identify molecular subtypes of pancreatic cancer. *Nature* **531**, 47–52 (2016).

22. Puleo, F. *et al.* Stratification of Pancreatic Ductal Adenocarcinomas Based on Tumor and Microenvironment Features. *Gastroenterology* **155**, 1999-2013.e3 (2018).

23. Daemen, A. *et al.* Metabolite profiling stratifies pancreatic ductal adenocarcinomas into subtypes with distinct sensitivities to metabolic inhibitors. *PNAS* (2015) doi:10.1073/pnas.1501605112.

24. Brunton, H. *et al.* HNF4A and GATA6 Loss Reveals Therapeutically Actionable Subtypes in Pancreatic Cancer. *Cell Rep.* **31**, (2020).

25. Hoeflich, K. P. *et al.* Requirement for glycogen synthase kinase-3β in cell survival and NF-κB activation. *Nature* **406**, 86–90 (2000).

26. Ding, L. & Billadeau, D. D. Glycogen synthase kinase-3β: a novel therapeutic target for pancreatic cancer. *Expert Opin. Ther. Targets* **24**, 417–426 (2020).

27. Woodgett, J. R. cDNA cloning and properties of glycogen synthase kinase-3. *Methods Enzymol.* **200**, 564–577 (1991).

28. Soutar, M. P. M. *et al.* Evidence that glycogen synthase kinase-3 isoforms have distinct substrate preference in the brain. *J. Neurochem.* **115**, 974–983 (2010).

29. Hemmings, B. A. & Cohen, P. Glycogen synthase kinase-3 from rabbit skeletal muscle. *Methods Enzymol.* **99**, 337–345 (1983).

30. EMBI, N., RYLATT, D. B. & COHEN, P. Glycogen Synthase Kinase-3 from Rabbit Skeletal Muscle: Separation from Cyclic-AMP-Dependent Protein Kinase and Phosphorylase Kinase. *Eur. J. Biochem.* **107**, 519–527 (1980).

31. Sutherland, C. What are the bona fide GSK3 substrates? *Int. J.*

Alzheimers. Dis. **2011**, (2011).

32. Linding, R. *et al.* Systematic Discovery of In Vivo Phosphorylation Networks. *Cell* **129**, 1415–1426 (2007).

33. Beurel, E., Grieco, S. F. & Jope, R. S. Glycogen synthase kinase-3 (GSK3): Regulation, actions, and diseases. *Pharmacology and Therapeutics* vol. 148 114–131 (2015).

34. Sutherland, C., Leighton, I. A. & Cohen, P. Inactivation of glycogen synthase kinase-3β by phosphorylation: New kinase connections in insulin and growth-factor signalling. *Biochem. J.* **296**, 15–19 (1993).

35. Zhang, H. H., Lipovsky, A. I., Dibble, C. C., Sahin, M. & Manning, B. D. S6K1 Regulates GSK3 under Conditions of mTOR-Dependent Feedback Inhibition of Akt. *Mol. Cell* **24**, 185–197 (2006).

36. An, W.-L. *et al.* Mechanism of zinc-induced phosphorylation of p70 S6 kinase and glycogen synthase kinase 3β in SH-SY5Y neuroblastoma cells. *J. Neurochem.* **92**, 1104–1115 (2005).

37. Krishnankutty, A. *et al.* In vivo regulation of glycogen synthase kinase 3β activity in neurons and brains. *Sci. Rep.* **7**, 1–15 (2017).

38. Lin, L. *et al.* TPA activates LDL receptor-related protein 1-mediated mitogenic signaling involving the p90RSK and GSK3β pathway. *Am. J. Pathol.* **177**, 1687–1696 (2010).

39. Stambolic, V. & Woodgett, J. R. Mitogen inactivation of glycogen synthase kinase-3β in intact cells via serine 9 phosphorylation. *Biochem. J.* **303**, 701–704 (1994).

40. Li, M. *et al.* Cyclic AMP Promotes Neuronal Survival by Phosphorylation of Glycogen Synthase Kinase 3β. *Mol. Cell. Biol.* **20**, 9356–9363 (2000).

41. Moore, S. F. *et al.* Dual regulation of glycogen synthase kinase 3 (GSK3)α/β by protein kinase C (PKC)α and Akt promotes thrombin-mediated integrin α‖bβ3 activation and granule secretion in platelets. *J. Biol. Chem.* **288**, 3918–3928 (2013).

42. Cook, D. *et al.* Wingless inactivates glycogen synthase kinase-3 via an intracellular signalling pathway which involves a protein kinase C. *EMBO J.* **15**, 4526–4536 (1996).

43. Cross, D. A. E., Alessi, D. R., Cohen, P., Andjelkovich, M. & Hemmings, B. A. Inhibition of glycogen synthase kinase-3 by insulin mediated by protein kinase B. *Nature* **378**, 785–789 (1995).

44. Hermida, M. A., Dinesh Kumar, J. & Leslie, N. R. GSK3 and its interactions with the PI3K/AKT/mTOR signalling network. *Adv. Biol. Regul.* **65**, 5–15 (2017).

45. Grimes, C. A. & Jope, R. S. The multifaceted roles of glycogen synthase kinase 3β in cellular signaling. *Prog. Neurobiol.* **65**, 391–426 (2001).

46. Woodgett, J. R. Judging a protein by more than its name: GSK-3. *Science's STKE : signal transduction knowledge environment* vol. 2001 (2001).

47. Patel, P. & Woodgett, J. R. *Glycogen Synthase Kinase 3: A Kinase for All Pathways? Current Topics in Developmental Biology* vol. 123 (Elsevier Inc., 2017).

48. Sutherland, C., Leighton, I. A. & Cohen, P. Inactivation of glycogen synthase kinase-3β by phosphorylation: New kinase connections in insulin and growth-factor signalling. *Biochem. J.* **296**, 15–19 (1993).

49. Wang, Y. *et al.* Cross talk between PI3K-AKT-GSK-3β and PP2A pathways determines tau hyperphosphorylation. *Neurobiol. Aging* **36**, 188–200 (2015).

50. Hernández, F., Langa, E., Cuadros, R., Avila, J. & Villanueva, N. Regulation of GSK3 isoforms by phosphatases PP1 and PP2A. *Mol. Cell. Biochem.* **344**, 211–215 (2010).

51. Kim, L., Liu, J. & Kimmel, A. R. The novel tyrosine kinase ZAK1 activates GSK3 to direct cell fate specification. *Cell* **99**, 399–408 (1999).

52. Doble, B. W. & Woodgett, J. R. GSK-3: Tricks of the trade for a multi-tasking kinase. *Journal of Cell Science* vol. 116 1175–1186 (2003).

53. Hughes, K., Nikolakaki, E., Plyte, S. E., Totty, N. F. & Woodgett, J. R. Modulation of the glycogen synthase kinase-3 family by tyrosine phosphorylation. *EMBO J.* **12**, 803–808 (1993).

54. Bautista, S. *et al.* mTORC1 controls glycogen synthase kinase 3β nuclear localization and function. *bioRxiv* 277657 (2018) doi:10.1101/277657.

55. Meares, G. P. & Jope, R. S. Resolution of the nuclear localization mechanism of glycogen synthase kinase-3: Functional effects in apoptosis. *J. Biol. Chem.* **282**, 16989–17001 (2007).

56. Robertson, H., Hayes, J. D. & Sutherland, C. A partnership with the proteasome; the destructive nature of GSK3. *Biochem. Pharmacol.* **147**, 77–92 (2018).

57. Yost, C. *et al.* The axis-inducing activity, stability, and subcellular distribution of β-catenin is regulated in Xenopus embryos by glycogen synthase kinase 3. *Genes Dev.* **10**, 1443–1454 (1996).

58. Beals, C. R., Sheridan, C. M., Turck, C. W., Gardner, P. & Crabtree, G. R. Nuclear export of NF-ATc enhanced by glycogen synthase kinase-3. *Science (80-.).* **275**, 1930–1933 (1997).

59. Baumgart, S. *et al.* GSK-3 Governs Inflammation-Induced NFATc2 Signaling Hubs to Promote Pancreatic Cancer Progression. *Mol. Cancer Ther.* **15**, 491–502 (2016).

60. Singh, S. K. *et al.* Disruption of a nuclear NFATc2 protein stabilization

loop confers breast and pancreatic cancer growth suppression by zoledronic acid. *J. Biol. Chem.* **286**, 28761–28771 (2011).

61. Boyle, W. J. *et al.* Activation of protein kinase C decreases phosphorylation of c-Jun at sites that negatively regulate its DNA-binding activity. *Cell* **64**, 573–584 (1991).

62. Pulverer, B. J. *et al.* Site-specific modulation of c-Myc cotransformation by residues phosphorylated in vivo. *Oncogene* **9**, 59–70 (1994).

63. Diehl, J. A., Cheng, M., Roussel, M. F. & Sherr, C. J. Glycogen synthase kinase-3β regulates cyclin D1 proteolysis and subcellular localization. *Genes Dev.* **12**, 3499–3511 (1998).

64. Hanger, D. P., Hughes, K., Woodgett, J. R., Brion, J. P. & Anderton, B. H. Glycogen synthase kinase-3 induces Alzheimer's disease-like phosphorylation of tau: Generation of paired helical filament epitopes and neuronal localisation of the kinase. *Neurosci. Lett.* **147**, 58–62 (1992).

65. Lauretti, E., Dincer, O. & Praticò, D. Glycogen synthase kinase-3 signaling in Alzheimer's disease. *Biochim. Biophys. Acta - Mol. Cell Res.* **1867**, 118664 (2020).

66. Jope, R. S. *et al.* Stressed and Inflamed, Can GSK3 Be Blamed? *Trends Biochem. Sci.* **42**, 180–192 (2017).

67. Beurel, E., Michalek, S. M. & Jope, R. S. Innate and adaptive immune responses regulated by glycogen synthase kinase-3 (GSK3). *Trends in Immunology* vol. 31 24–31 (2010).

68. Maixner, D. W. & Weng, H.-R. The Role of Glycogen Synthase Kinase 3 Beta in Neuroinflammation and Pain. *J. Pharm. Pharmacol.* **1**, 001 (2013).

69. Walz, A. *et al.* Molecular pathways: Revisiting glycogen synthase kinase-3β as a target for the treatment of cancer. *Clin. Cancer Res.* **23**, 1891–1897 (2017).

70. McCubrey, J. A. *et al.* Diverse roles of GSK-3: Tumor promoter-tumor suppressor, target in cancer therapy. *Adv. Biol. Regul.* **54**, 176–196 (2014).

71. Ma, C. *et al.* The role of glycogen synthase kinase 3β in the transformation of epidermal cells. *Cancer Res.* **67**, 7756–7764 (2007).

72. Ding, Q. *et al.* Myeloid cell leukemia-1 inversely correlates with glycogen synthase kinase-3β activity and associates with poor prognosis in human breast cancer. *Cancer Res.* **67**, 4564–4571 (2007).

73. Leis, H., Segrelles, C., Ruiz, S., Santos, M. & Paramio, J. M. Expression, localization, and activity of glycogen synthase kinase 3β during mouse skin tumorigenesis. *Mol. Carcinog.* **35**, 180–185 (2002).

74. Farago, M. *et al.* Kinase-inactive glycogen synthase kinase 3β promotes Wnt signaling and mammary tumorigenesis. *Cancer Res.* **65**, 5792–5801

(2005).

75. Lin, J., Song, T., Li, C. & Mao, W. GSK-3β in DNA repair, apoptosis, and resistance of chemotherapy, radiotherapy of cancer. *Biochim. Biophys. Acta - Mol. Cell Res.* **1867**, 118659 (2020).

76. Vijay, G. V. *et al.* GSK3β regulates epithelial-mesenchymal transition and cancer stem cell properties in triple-negative breast cancer. *Breast Cancer Res.* **21**, 37 (2019).

77. Ougolkov, A. V. *et al.* Aberrant nuclear accumulation of glycogen synthase kinase-3β in human pancreatic cancer: Association with kinase activity and tumor dedifferentiation. *Clin. Cancer Res.* **12**, 5074–5081 (2006).

78. Zhou, A. *et al.* Nuclear GSK3β promotes tumorigenesis by phosphorylating KDM1A and inducing its deubiquitylation by USP22. *Nat. Cell Biol.* **18**, 954–966 (2016).

79. Edderkaoui, M. *et al.* An Inhibitor of GSK3B and HDACs Kills Pancreatic Cancer Cells and Slows Pancreatic Tumor Growth and Metastasis in Mice. *Gastroenterology* **155**, 1985-1998.e5 (2018).

80. Taylan, E. *et al.* Dual targeting of GSK3B and HDACs reduces tumor growth and improves survival in an ovarian cancer mouse model. *Gynecol. Oncol.* **0**, (2020).

81. Baehr, C. A., Huntoon, C. J., Hoang, S.-M., Jerde, C. R. & Karnitz, L. M. Glycogen Synthase Kinase 3 (GSK-3)-mediated Phosphorylation of Uracil N-Glycosylase 2 (UNG2) Facilitates the Repair of Floxuridine-induced DNA Lesions and Promotes Cell Survival *. (2016) doi:10.1074/jbc.M116.746081.

82. Yang, Y. *et al.* Nuclear GSK3β induces DNA double-strand break repair by phosphorylating 53BP1 in glioblastoma. *Int. J. Oncol.* **52**, 709–720 (2018).

83. Ding, L. *et al.* Glycogen synthase kinase-3 inhibition sensitizes pancreatic cancer cells to chemotherapy by abrogating the ToPBP1/ATR-mediated DNA damage response. *Clin. Cancer Res.* **25**, 6452–6462 (2019).

84. Medunjanin, S. *et al.* GSK-3β controls NF-kappaB activity via IKKγ/NEMO. *Sci. Rep.* **6**, 38553 (2016).

85. Acikgoz, E., Güler, G., Camlar, M., Oktem, G. & Aktug, H. Glycogen synthase kinase-3 inhibition in glioblastoma multiforme cells induces apoptosis, cell cycle arrest and changing biomolecular structure. *Spectrochim. Acta - Part A Mol. Biomol. Spectrosc.* **209**, 150–164 (2019).

86. Pizarro, J. G. *et al.* A molecular study of pathways involved in the inhibition of cell proliferation in neuroblastoma B65 cells by the GSK-3 inhibitors lithium and SB-415286. *J. Cell. Mol. Med.* **13**, 3906–3917 (2009).

87. Mirlashari, M. R., Randen, I. & Kjeldsen-Kragh, J. Glycogen synthase kinase-3 (GSK-3) inhibition induces apoptosis in leukemic cells through mitochondria-dependent pathway. *Leuk. Res.* **36**, 499–508 (2012).

88. Hasselluhn, M. C., Schmidt, G. E., Ellenrieder, V., Johnsen, S. A. & Hessmann, E. Aberrant NFATc1 signaling counteracts TGFβ-mediated growth arrest and apoptosis induction in pancreatic cancer progression. *Cell Death Dis.* **10**, (2019).

89. Chen, N. M. *et al.* Context-Dependent Epigenetic Regulation of Nuclear Factor of Activated T Cells 1 in Pancreatic Plasticity. *Gastroenterology* **152**, 1507-1520.e15 (2017).

90. Shou, J. *et al.* Nuclear factor of activated T cells in cancer development and treatment. *Cancer Lett.* **361**, 174–184 (2015).

91. Qin, J. J. *et al.* NFAT as cancer target: Mission possible? *Biochimica et Biophysica Acta - Reviews on Cancer* vol. 1846 297–311 (2014).

92. Pan, M.-G., Xiong, Y. & Chen, F. NFAT Gene Family in Inflammation and Cancer. *Curr. Mol. Med.* **13**, 543–554 (2013).

93. Flanagan, M. W., Corthesy, B., Bram, R. J. & Crabtree, G. R. *Nuclear association of aT-cell transcription factor blocked by FK-506 and cyclosporin A*. *Nature* vol. 352 (1991).

94. Hogan, P. G., Chen, L., Nardone, J. & Rao, A. Transcriptional regulation by calcium, calcineurin, and NFAT. *Genes and Development* vol. 17 2205–2232 (2003).

95. Müller, M. R. & Rao, A. NFAT, immunity and cancer: A transcription factor comes of age. *Nat. Rev. Immunol.* **10**, 645–656 (2010).

96. Singh, S. K. *et al.* Antithetical NFAT c1–Sox2 and p53–miR200 signaling networks govern pancreatic cancer cell plasticity. *EMBO J.* **34**, 517–530 (2015).

97. Mognol, G. P., Carneiro, F. R. G., Robbs, B. K., Faget, D. V. & Viola, J. P. B. Cell cycle and apoptosis regulation by NFAT transcription factors: New roles for an old player. *Cell Death and Disease* vol. 7 e2199–e2199 (2016).

98. Lee, J. U., Kim, L. K. & Choi, J. M. Revisiting the concept of targeting NFAT to control T cell immunity and autoimmune diseases. *Frontiers in Immunology* vol. 9 2747 (2018).

99. Yiu, G. K. & Toker, A. NFAT induces breast cancer cell invasion by promoting the induction of cyclooxygenase-2. *J. Biol. Chem.* **281**, 12210–12217 (2006).

100. Tran Quang, C. *et al.* The calcineurin/NFAT pathway is activated in diagnostic breast cancer cases and is essential to survival and metastasis of mammary cancer cells. *Cell Death Dis.* **6**, e1658 (2015).

101. Buchholz, M. *et al.* Overexpression of c-myc in pancreatic cancer caused by ectopic activation of NFATc1 and the Ca2+/calcineurin signaling pathway. *EMBO J.* **25**, 3714–3724 (2006).

102. Köenig, A. *et al.* NFAT-Induced Histone Acetylation Relay Switch Promotes c-Myc-Dependent Growth in Pancreatic Cancer Cells. *Gastroenterology* **138**, (2010).

103. Chen, N.-M. M. *et al.* NFATc1 Links EGFR Signaling to Induction of Sox9 Transcription and Acinar–Ductal Transdifferentiation in the Pancreas. *Gastroenterology* **148**, 1024-1034.e9 (2015).

104. Baumgart, S. *et al.* Inflammation-Induced NFATc1-STAT3 transcription complex promotes pancreatic cancer initiation by KrasG12D. *Cancer Discov.* **4**, 688–701 (2014).

105. Baumgart, S. *et al.* GSK-3 b Governs In fl ammation-Induced NFATc2 Signaling Hubs to Promote Pancreatic Cancer Progression. 491–503 (2016) doi:10.1158/1535-7163.MCT-15-0309.

106. Flores, C., Fouquet, G., Moura, I. C., Maciel, T. T. & Hermine, O. Lessons to Learn From Low-Dose Cyclosporin-A: A New Approach for Unexpected Clinical Applications. *Front. Immunol.* **10**, 588 (2019).

107. Ellenrieder, V., König, A. & Seufferlein, T. Current Standard and Future Perspectives in First- and Second-Line Treatment of Metastatic Pancreatic Adenocarcinoma. *Digestion* **94**, 44–49 (2016).

108. Von Hoff, D. D. *et al.* Increased survival in pancreatic cancer with nab-paclitaxel plus gemcitabine. *N. Engl. J. Med.* **369**, 1691–1703 (2013).

109. Conroy, T. *et al.* FOLFIRINOX versus gemcitabine for metastatic pancreatic cancer. *N. Engl. J. Med.* **364**, 1817–1825 (2011).

110. Golan, T. *et al.* Maintenance Olaparib for Germline *BRCA* -Mutated Metastatic Pancreatic Cancer. *N. Engl. J. Med.* **381**, 317–327 (2019).

111. Ciccia, A. & Elledge, S. J. The DNA Damage Response: Making It Safe to Play with Knives. *Mol. Cell* **40**, 179–204 (2010).

112. Valko, M., Rhodes, C. J., Moncol, J., Izakovic, M. & Mazur, M. Free radicals, metals and antioxidants in oxidative stress-induced cancer. *Chemico-Biological Interactions* vol. 160 1–40 (2006).

113. Jackson, S. P. & Bartek, J. The DNA-damage response in human biology and disease. *Nature* vol. 461 1071–1078 (2009).

114. Hoeijmakers, J. H. J. DNA Damage, Aging, and Cancer. *N. Engl. J. Med.* **361**, 1475–1485 (2009).

115. De Sousa Cavalcante, L. & Monteiro, G. Gemcitabine: Metabolism and molecular mechanisms of action, sensitivity and chemoresistance in pancreatic cancer. *Eur. J. Pharmacol.* **741**, 8–16 (2014).

116. Sampath, D., Rao, V. A. & Plunkett, W. Mechanisms of apoptosis induction by nucleoside analogs. *Oncogene* vol. 22 9063–9074 (2003).

117. Longley, D. B., Harkin, D. P. & Johnston, P. G. 5-Fluorouracil: Mechanisms of action and clinical strategies. *Nature Reviews Cancer* vol. 3 330–338 (2003).

118. Grogan, L., Sotos, G. A. & Allegra, C. J. Leucovorin modulation of fluorouracil. *Oncology (Williston Park).* **7**, 63–66 (1993).

119. Bao, X., Wu, J., Kim, S., LoRusso, P. & Li, J. Pharmacometabolomics Reveals Irinotecan Mechanism of Action in Cancer Patients. *J. Clin. Pharmacol.* **59**, 20–34 (2019).

120. Stahley, M. R. & Stivers, J. T. Mechanism and Specificity of DNA Strand Exchange Catalyzed by Vaccinia DNA Topoisomerase Type i. *Biochemistry* **49**, 2786–2795 (2010).

121. Bruno, P. M. *et al.* A subset of platinum-containing chemotherapeutic agents kills cells by inducing ribosome biogenesis stress. *Nat. Med.* **23**, 461–471 (2017).

122. Wang, D. & Lippard, S. J. Cellular processing of platinum anticancer drugs. *Nature Reviews Drug Discovery* vol. 4 307–320 (2005).

123. Rocha, C. R. R., Silva, M. M., Quinet, A., Cabral-Neto, J. B. & Menck, C. F. M. DNA repair pathways and cisplatin resistance: An intimate relationship. *Clinics* vol. 73 (2018).

124. Hoeijmakers, J. H. J. Genome maintenance mechanisms for preventing cancer. *Nature* vol. 411 366–374 (2001).

125. Scully, R., Panday, A., Elango, R. & Willis, N. A. DNA double-strand break repair-pathway choice in somatic mammalian cells. *Nat. Rev. Mol. Cell Biol.* **20**, 698–714 (2019).

126. Chang, H. H. Y., Pannunzio, N. R., Adachi, N. & Lieber, M. R. Non-homologous DNA end joining and alternative pathways to double-strand break repair. *Nat. Rev. Mol. Cell Biol.* **18**, 495–506 (2017).

127. Davis, A. J. & Chen, D. J. DNA double strand break repair via non-homologous end-joining. *Translational Cancer Research* vol. 2 130–143 (2013).

128. Lieber, M. R. The mechanism of double-strand DNA break repair by the nonhomologous DNA end-joining pathway. *Annual Review of Biochemistry* vol. 79 181–211 (2010).

129. Vítor, A. C., Huertas, P., Legube, G. & de Almeida, S. F. Studying DNA Double-Strand Break Repair: An Ever-Growing Toolbox. *Frontiers in Molecular Biosciences* vol. 7 24 (2020).

130. Makharashvili, N. & Paull, T. T. CtIP: A DNA damage response protein at the intersection of DNA metabolism. *DNA Repair (Amst).* **32**, 75–81

(2015).

131. Lamarche, B. J., Orazio, N. I. & Weitzman, M. D. The MRN complex in double-strand break repair and telomere maintenance. *FEBS Letters* vol. 584 3682–3695 (2010).

132. Liu, Y. & West, S. C. Distinct functions of BRCA1 and BRCA2 in double-strand break repair. *Breast Cancer Res.* **4**, 9–13 (2002).

133. Her, J. & Bunting, S. F. How cells ensure correct repair of DNA double-strand breaks. *Journal of Biological Chemistry* vol. 293 10502–10511 (2018).

134. Li, X. & Heyer, W. D. Homologous recombination in DNA repair and DNA damage tolerance. *Cell Research* vol. 18 99–113 (2008).

135. Schwertman, P., Bekker-Jensen, S. & Mailand, N. Regulation of DNA double-strand break repair by ubiquitin and ubiquitin-like modifiers. *Nat. Rev. Mol. Cell Biol.* **17**, 379–394 (2016).

136. Lord, C. J. & Ashworth, A. BRCAness revisited. *Nat. Rev. Cancer* **16**, 110–120 (2016).

137. FDA approves olaparib for gBRCAm metastatic pancreatic adenocarcinoma | FDA. https://www.fda.gov/drugs/resources-information-approved-drugs/fda-approves-olaparib-gbrcam-metastatic-pancreatic-adenocarcinoma.

138. Turner, N., Tutt, A. & Ashworth, A. Hallmarks of 'BRCAness' in sporadic cancers. *Nature Reviews Cancer* vol. 4 814–819 (2004).

139. Waddell, N. *et al.* Whole genomes redefine the mutational landscape of pancreatic cancer. *Nature* **518**, 495–501 (2015).

140. Love, M. I., Huber, W. & Anders, S. Moderated estimation of fold change and dispersion for RNA-seq data with DESeq2. *Genome Biol.* **15**, 550 (2014).

141. Andrews, S. A quality control tool for high throughput sequence data.

142. Blankenberg, D. *et al.* Manipulation of FASTQ data with galaxy. *Bioinformatics* **26**, 1783–1785 (2010).

143. Anders, S., Pyl, P. T. & Huber, W. HTSeq-A Python framework to work with high-throughput sequencing data. *Bioinformatics* **31**, 166–169 (2015).

144. Institute, B. Picard. *Broad Institute, GitHub Repos.*

145. Kim, D. *et al.* TopHat2: Accurate alignment of transcriptomes in the presence of insertions, deletions and gene fusions. *Genome Biol.* **14**, R36 (2013).

146. Hingorani, S. R. *et al.* Trp53R172H and KrasG12D cooperate to promote

chromosomal instability and widely metastatic pancreatic ductal adenocarcinoma in mice. *Cancer Cell* **7**, 469–483 (2005).

147. He, X., Saint-Jeannet, J. P., Woodgett, J. R., Varmus, H. E. & Dawid, I. B. Glycogen synthase kinase-3 and dorsoventral patterning in Xenopus embryos. *Nature* **374**, 617–622 (1995).

148. Najafova, Z. *et al.* BRD4 localization to lineage-specific enhancers is associated with a distinct transcription factor repertoire. *Nucleic Acids Res.* **45**, 127–141 (2017).

149. Afgan, E. *et al.* The Galaxy platform for accessible, reproducible and collaborative biomedical analyses: 2018 update. *Nucleic Acids Res.* **46**, W537–W544 (2018).

150. SortSam.

151. Subramanian, A. *et al.* Gene set enrichment analysis: A knowledge-based approach for interpreting genome-wide expression profiles. *Proc. Natl. Acad. Sci.* **102**, 15545–15550 (2005).

152. Mootha, V. K. *et al.* PGC-1α-responsive genes involved in oxidative phosphorylation are coordinately downregulated in human diabetes. *Nat. Genet.* **34**, 267–273 (2003).

153. Hamdan, F. H. & Johnsen, S. A. DeltaNp63-dependent super enhancers define molecular identity in pancreatic cancer by an interconnected transcription factor network. *Proc. Natl. Acad. Sci. U. S. A.* **115**, E12343–E12352 (2018).

154. Bhat, R. *et al.* Structural Insights and Biological Effects of Glycogen Synthase Kinase 3-specific Inhibitor AR-A014418. *J. Biol. Chem.* **278**, 45937–45945 (2003).

155. Sun, T., Rodriguez, M. & Kim, L. Glycogen synthase kinase 3 in the world of cell migration. *Dev. Growth Differ.* **51**, 735–742 (2009).

156. Wong, W., Raufi, A. G., Safyan, R. A., Bates, S. E. & Manji, G. A. Brca mutations in pancreas cancer: Spectrum, current management, challenges and future prospects. *Cancer Management and Research* vol. 12 2731–2742 (2020).

157. Golan, T. *et al.* Overall survival and clinical characteristics of pancreatic cancer in BRCA mutation carriers. *Br. J. Cancer* **111**, 1132–1138 (2014).

158. Rogakou, E. P., Boon, C., Redon, C. & Bonner, W. M. Megabase chromatin domains involved in DNA double-strand breaks in vivo. *J. Cell Biol.* **146**, 905–915 (1999).

159. McCabe, N. *et al.* BRCA2-deficient CAPAN-1 cells are extremely sensitive to the inhibition of Poly (ADP-Ribose) polymerase: an issue of potency. *Cancer Biol. Ther.* **4**, 934–936 (2005).

160. Lopez-Bergami, P., Lau, E. & Ronai, Z. Emerging roles of ATF2 and the

dynamic AP1 network in cancer. *Nature Reviews Cancer* vol. 10 65–76 (2010).

161. Hayakawa, J. *et al.* Identification of Promoters Bound by c-Jun / ATF2 during Rapid Large-Scale Gene Activation following Genotoxic Stress. **16**, 521–535 (2004).

162. Chen, J., Solomides, C., Simpkins, F. & Simpkins, H. The role of Nrf2 and ATF2 in resistance to platinum-based chemotherapy. *Cancer Chemother. Pharmacol.* **79**, 369–380 (2017).

163. Boise, L. H. *et al.* The NFAT-1 DNA binding complex in activated T cells contains Fra-1 and JunB. *Mol. Cell. Biol.* **13**, 1911–1919 (1993).

164. FDA. FDA Briefing Document Oncologic Drugs Advisory Committee Meeting NDA 206162 Olaparib (Lynparza ®) AstraZeneca. 1–31 (2019).

165. Jope, R. S. & Johnson, G. V. W. The glamour and gloom of glycogen synthase kinase-3. **29**, (2004).

166. Michl, J., Zimmer, J. & Tarsounas, M. Interplay between Fanconi anemia and homologous recombination pathways in genome integrity. *EMBO J.* **35**, 909–923 (2016).

167. O'Flaherty, L. *et al.* Tumor growth suppression using a combination of taxol-based therapy and GSK3 inhibition in non-small cell lung cancer. *PLoS One* **14**, (2019).

168. Duda, P. *et al.* Targeting GSK3 and Associated Signaling Pathways Involved in Cancer. *Cells* **9**, (2020).

169. Wakefield, J. G., Stephens, D. J. & Tavaré, J. M. A role for glycogen synthase kinase-3 in mitotic spindle dynamics and chromosome alignment. *Journal of Cell Science* vol. 116 637–646 (2003).

170. Yardley, D. A. Nab-Paclitaxel mechanisms of action and delivery. *J. Control. Release* **170**, 365–372 (2013).

171. Poruchynsky, M. S. *et al.* Microtubule-targeting agents augment the toxicity of DNA-damaging agents by disrupting intracellular trafficking of DNA repair proteins. *Proc. Natl. Acad. Sci. U. S. A.* **112**, 1571–1576 (2015).

172. Jiang, X. *et al.* Inactivating mutations of RNF43 confer Wnt dependency in pancreatic ductal adenocarcinoma. *Proc. Natl. Acad. Sci. U. S. A.* **110**, 12649–12654 (2013).

173. Raphael, B. J. & The Cancer Genome Atlas Research, N. Integrated Genomic Characterization of Pancreatic Ductal Adenocarcinoma. *Cancer Cell* **32**, 185-203.e13 (2017).

174. Shen, J. *et al.* ARID1A Deficiency Impairs the DNA Damage Checkpoint and Sensitizes Cells to PARP Inhibitors. *Cancer Discov.* **5**, 752–767 (2015).

175. Im, J. Y. *et al.* DNA damage-induced apoptosis suppressor (DDIAS), a novel target of NFATc1, is associated with cisplatin resistance in lung cancer. *Biochim. Biophys. Acta - Mol. Cell Res.* **1863**, 40–49 (2016).

176. Olabisi, O. A. *et al.* Regulation of Transcription Factor NFAT by ADP-Ribosylation. *Mol. Cell. Biol.* **28**, 2860–2871 (2008).

177. Shaloam, D. & Tchounwou, P. B. Cisplatin in cancer therapy: Molecular mechanisms of action. *Eur. J. Pharmacol.* **740**, 364–378 (2014).

178. Lo Iacono, M. *et al.* ATF2 contributes to cisplatin resistance in non-small cell lung cancer and celastrol induces cisplatin resensitization through inhibition of JNK/ATF2 pathway. *Int. J. Cancer* **136**, 2598–2609 (2015).

179. Lo, C., Rao, A. & Macia, F. Partners in transcription : NFAT and AP-1. **1**, 2476–2489 (2001).

Acknowledgement

Most importantly, I would like to thank my supervisor Prof. Volker Ellenrieder for giving me the opportunity to work in his lab and perform my thesis. Your discussions, critical reviewing my data, motivation and ideas helped me to develop my skills and all of the projects. I really appreciate the freedom of following my own thoughts and interests. Furthermore, I'm grateful being involved in processes like grant writing and learning how to build up a project.

Furthermore, I would like to thank my thesis committee Prof. Bernd Wollnik, Prof. Steven Johnsen and Prof. Argyris Papantonis for the valuable input, as well as I thank all my collaboration partners. First, I would like to thank the KFO 5002, for providing PDX and CDX material, the Institute of Pathology for the TMAs and Prof. Dobbelstein and Katharina Ewers for tumor samples. Importantly, I would like to thank Elisabeth Hessmann for her support throughout my PhD whenever problems occurred and helping me with constructive discussions, as well as providing the RNA-seq data of NKCII cells. From the Hessmann group, I would like to thank Marie for designing the guide RNAs and project discussions. I really appreciate the collaboration with Steven Johnsen and Feda Hamdan which fortunately continued. I really enjoy the discussion which always helped me a lot and encouraged me to continue my work and I'm looking forward to the upcoming data. I would like to thank Oliver Hahn for the valuable discussions and input whenever needed no matter what project it was about.

On my way to the PhD a had the chance to work with and learn from so many great scientists. Especially I want to thank Eva Benito, for being such a great supervisor. I really appreciate the chance of learning from you so much. I also would like to thank Florian Wegwitz for the chance of writing my master thesis and still having great discussions with you.

This work would not be the same without Kristina Reutlinger. Together we managed the up and downs of this project and many more projects which did not find the way into this. I do not know how much I can thank you for all your support

during the last years. Thank you for your valuable friendship and all the encouragement!

The PhD would be a lonely journey without a great lab. I would like to thank all members of the Department for such a pleasant working environment and all your support. Firstly, I would like to thank Shiv Singh for his input. I thank Jessica, Rieke, Christin, Waltraut and Sercan for their technical assistance. Waltraut and Sercan as well for the generation of and support with the PDX and CDX. I would like to thank the PhD students for discussions and fun moments: Lukas, Laura, Mengyu, Alice, Shilpa, Lennart, Marie and Iswarya. I really thank Umair for his support and discussions throughout the PhD. Especially, I want to thank Nina, Melanie and Lisa for not only scientific discussions but importantly also their friendship. Furthermore, I really appreciate all the work and contributions of my students, in particular the work of Pascal on the KDM project.

A very special thank you for all the great people who helped with proofreading my thesis and their useful discussions: Feda, Robyn, Oliver, Hauke, Amanda, Nina and Elisa!

I want to thank all my friends for their support, their patients when I was lost in research and barely found a way out of my data and making life much more enjoyable. Therefore, I would like to thank beside so many more people, Feda, Oliver, Kristina and Lisa. Most importantly I would like thank Elisa and Amanda. It is an honor to find friends like you and I have to thank you so much for your friendship, your support and just being such amazing.

I would not be at this point without my family! I cannot thank you enough for being always there if needed, my save harbor and source of energy. It means a lot for me to have such a wonderful family. Especially, I want to thank my parents and my brother, for all their support, not only during the PhD. I would not have been able to manage it without you. You are there whenever needed, understand whatever it is about, encourage me in any decision I take and bring so much positivity and happiness into my life. Thank you!